

DOE/NASA/0117-80/1
NASA CR-159803
AIRESEARCH 80-16762

DESIGN STUDY OF TOROIDAL TRACTION CVT FOR ELECTRIC VEHICLES

A. E. Raynard, J. H. Kraus, and D. D. Bell
AiResearch Manufacturing Company of California
The Garrett Corporation

(NASA-CR-159803) DESIGN STUDY OF TOROIDAL
TRACTION CVT FOR ELECTRIC VEHICLES Final
Report (AiResearch Mfg. Co., Torrance,
Calif.) 161 p HC A08/MF A01 CSCL 13I

N80-25661

Unclas
G3/37 23502

January 1980

Prepared for
NATIONAL AERONAUTICS AND SPACE ADMINISTRATION
Lewis Research Center
Cleveland, Ohio 44135
Under Contract DEN 3-117

for

U.S. DEPARTMENT OF ENERGY
Conservation and Solar Applications
Office of Transportation Programs



TABLE OF CONTENTS

	<u>Page</u>
EXECUTIVE SUMMARY	1
INTRODUCTION	4
Purpose	4
Background	4
PROGRAM SCOPE AND PROCEDURES	7
Task I, Design Methodology	7
Task II, Identification of Required Technology	8
Task III, Suitability for Alternate Applications	8
Task IV, Design and Technical Assessment Report	9
DESIGN REQUIREMENTS	10
DESIGN CONFIGURATIONS	12
Baseline Drive	12
Series Drive	12
Two-Speed Shifted Drive	12
Inverse Regenerated Drive	16
Regenerated Drive	16
TRANSMISSION RATIO CONTROL	20
Motor Control	20
CVT Control	20
Flywheel Starting	22
Alternate Control System	24
CVT Power Roller Actuation	30
TRACTION DRIVE DESCRIPTION	30
Operation	30
Traction Characteristics	33

	<u>Page</u>
TASK I, CONFIGURATION ANALYSIS AND SELECTION	47
Computer Simulation	47
Analysis Step 1, Parametric Study	56
Analysis Step 2, Configuration Selection	65
Analysis Step 3, Design Optimization	67
Analysis Step 4, Roller Control System Analysis	77
Roller Control System Analytical Results	84
Selected Design Description	95
TASK II, IDENTIFICATION OF REQUIRED TECHNOLOGY ADVANCEMENTS	112
Control System Development	112
Traction Fluid Development	112
Traction Coefficient Verification	114
Contact Loss Verification	115
TASK III, SUITABILITY FOR ALTERNATE APPLICATIONS	116
Electric Motor Powered Vehicle	116
Hybrid Electric Vehicle with an Internal Combustion Engine	119
Scalability to Alternate Weight Vehicles and Torque Levels	124
APPENDIX A: DETERMINATION OF CONTACT AREA DIMENSIONS	128
APPENDIX B: PARAMETRIC STUDY DATA	130
APPENDIX C: WEIGHT CALCULATIONS	140
APPENDIX D: CVT DRAWING AND PARTS LIST	149
REFERENCES	155
DISTRIBUTION	157

EXECUTIVE SUMMARY

This report describes the design study program of a toroidal traction CVT for electric vehicles. The work was performed by Garrett-AIRsearch as part of the Electric and Hybrid Vehicle Program for the U.S. Department of Energy. The work was managed by the Bearing, Gearing, and Transmission Section of the NASA Lewis Research Center. It was performed under Contract DEN 3-117.

The objectives of this study were: (1) develop, evaluate, and optimize, a preliminary design concept for a continuously variable transmission (CVT) to couple the high-speed output shaft of an energy storage flywheel to the drive train of an electric vehicle, (2) identify technological advancements required to develop the CVT design concept, and (3) determine the suitability of the CVT design concept for alternate electric and hybrid vehicle applications.

The program effort was directed toward evaluating and comparing five different full toroidal cavity, traction drive CVT configurations, selecting one design configuration, and optimizing that design with respect to the specification requirements. Program activity was separated into four tasks that were performed according to the following schedule:

Task	1979								1980	
	M	J	J	A	S	O	N	D	J	
I Design study	████████████████									
II Required technical advancements					████████████████					
III Alternate applications						██████████████				
IV Design and technical assessment						████████████████				

S-48832

The purpose of Task I was to conduct engineering analyses to select and optimize a CVT design configuration and develop a preliminary CVT design to meet the design requirements. During this task five CVT design configurations were compared using the following design criteria: efficiency, cost, size, weight, reliability, noise, controls, and maintainability. Each design consisted of one or two full toroidal cavity traction drive elements connected to various reduction gearing arrangements. A computer simulation was used to compare the performance of the five CVT design configurations. Based on this analysis, a dual-cavity full toroidal traction drive with regenerative gearing was selected for the CVT design configuration. The design was then optimized to obtain estimated operational efficiencies up to 95 percent and a 98.3 percent probability of achieving the specified 2600-hr operating life.

The final design selected during Task I is illustrated in figure 1. The dual-cavity toroidal traction drive and the regenerative gearing are shown in the figure. The CVT will meet all the design requirements specified in the statement of work. A striking feature of the design is that it is infinitely variable, so that the input shaft can be operated at full speed when attached

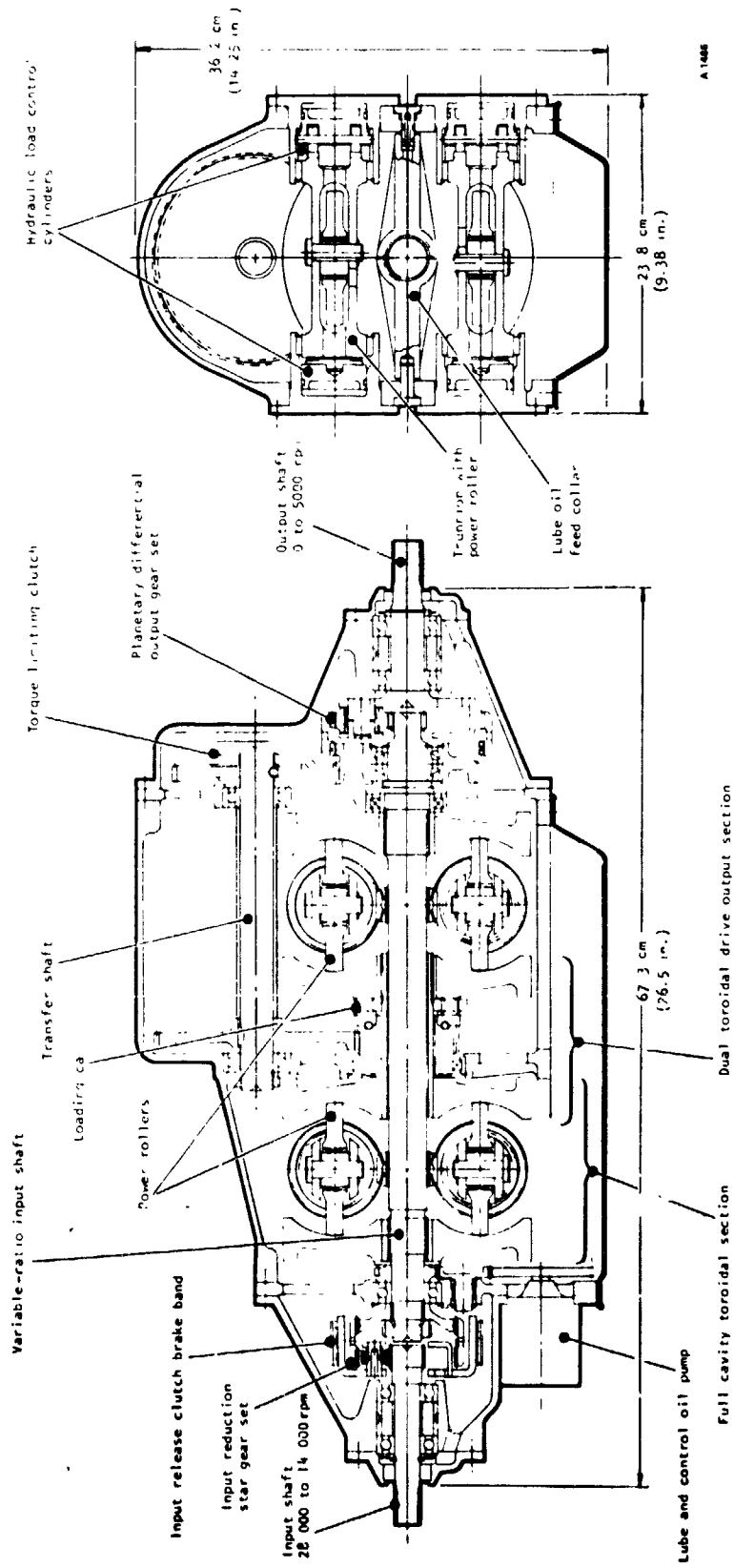


Figure 1.--Toroidal traction CVT for electric vehicles.

to a flywheel or to an electric motor; and the output shaft can be brought to zero speed, which eliminates the need for a clutching device. The design encompasses conventional materials and manufacturing techniques, and the CVT is comparable in weight and size to a present day automotive automatic transmission.

During Task II technological advancements required for developing the CVT to production status were identified. This included defining the problem areas and estimating the means and efforts required to solve the problems. Although no technical problems are expected with the basic CVT design, three areas were identified that will require some development. They are the ratio control system, the traction fluid properties, and evaluation of the traction contact performance.

The control system dynamics must be evaluated in detail to ensure that a smooth transfer of power takes place both ways between the flywheel and vehicle and that the CVT is responsive to the driver command. This can be accomplished by a combination of analog computer analysis and dynamometer testing.

Present traction fluids exhibit two properties that limit the operational envelope of a traction drive: a rather high viscosity index and a tendency to entrain air. Traction fluid manufacturers are conducting development work to solve these problems, and the traction fluid properties may change with each new development. Test verification of the actual traction fluid properties operating in a CVT is needed to obtain the best traction contact performance analysis.

In Task III the suitability of the selected CVT design concept for alternate electric and hybrid vehicle applications and alternate vehicle sizes and maximum output torques was determined. In all cases the toroidal traction drive design concept was applicable to the vehicle system. The regenerative gearing could be eliminated in the electric-powered vehicle because of the reduced ratio range requirements. In the other cases the CVT with regenerative gearing would meet the design requirements after appropriate adjustments in size and reduction gearing ratios.

Task IV consisted of preparing a design report and discussing the design criteria and tradeoffs. The report presents the results of the engineering analyses conducted on the CVT during the design process; these included stress, critical speed, life, reliability, weight, and performance.

INTRODUCTION

Purpose

The program described in this report was initiated to evaluate, optimize, and develop a preliminary design concept for a continuously variable transmission (CVT) to couple the high-speed output shaft of an energy storage flywheel to the drive train of an electric vehicle (shown in fig. 2), identify the technology advancements required to develop the CVT, and determine the suitability of the CVT design concept for alternate electric and hybrid vehicle applications.

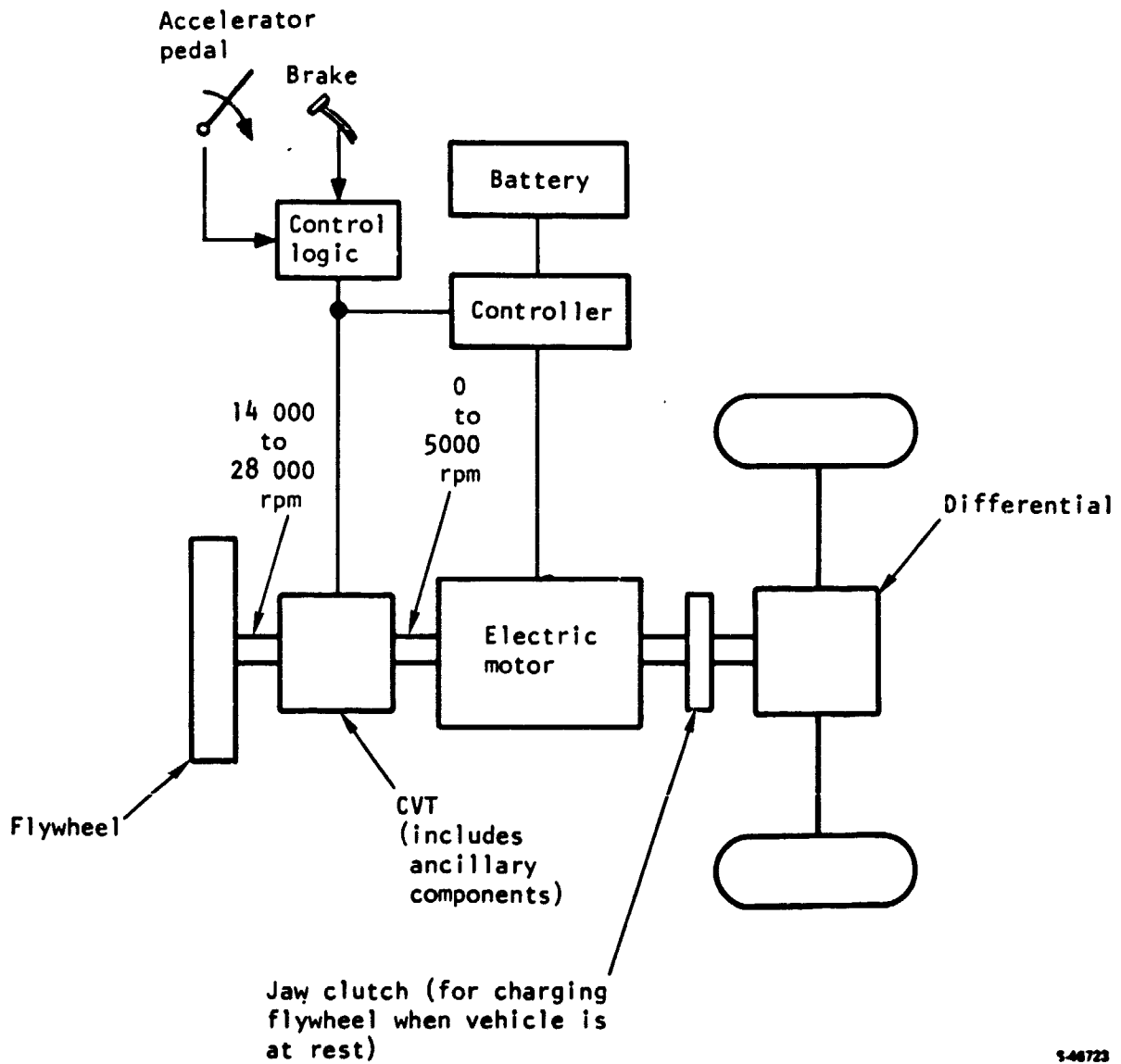
This work was part of the Electric and Hybrid Vehicle Program of the U.S. Department of Energy. It was performed under Contract DEN 3-117 and managed by the Bearing, Gearing, and Transmission Section of the NASA Lewis Research Center.

Background

In a traction drive, torque is transmitted from one smooth rolling element to another by the resistance to shearing of a fluid pad separating the two elements. This traction phenomenon is discussed in detail in the Operation Description subsection. A large variety of different traction drive mechanisms have been attempted, some successfully and some not. Some of the more common types of traction drives are shown schematically in figure 3. Of the variable ratio traction drive configurations conceived, the toroidal type has shown the best combination of power, speed, and efficiency.

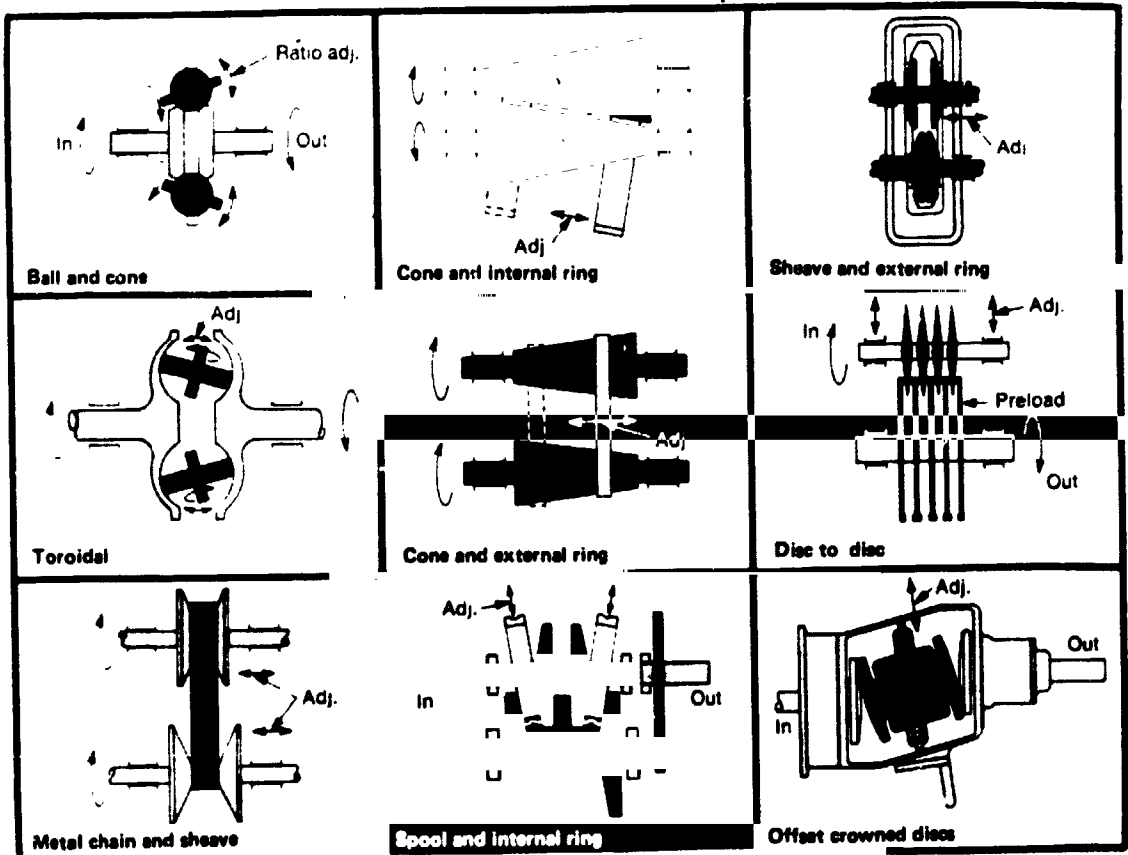
The first toroidal drive patent was issued in 1877. Since that time several variations of the toroidal drive design concept have been manufactured and tested by various individuals. Today over two dozen companies throughout the world manufacture various types of traction drives that are primarily used in industrial applications. They are generally used in light-duty service. Steel and traction fluid developments in recent years, however, allow the design of higher power traction drives as a result of increased material strength and improved fluid traction properties.

This report presents the toroidal traction drive resulting from an engineering design study and supporting analyses. The design study included the latest traction fluid properties data and available empirical data from traction contact experiments.



1-46723

Figure 2.--Schematic of CVT drive train of flywheel-equipped electric vehicle.



F-31286

Figure 3.--Some common types of traction drives.

PROGRAM SCOPE AND PROCEDURES

The program effort was directed toward evaluating and comparing five different full toroidal cavity, traction drive CVT configurations, selecting one design configuration, and optimizing that design with respect to the specification requirements. These requirements are described in the following Design Requirements section.

In this report, Task IV of the program, activity is discussed in terms of the three principal tasks:

- Task I--Conduct an engineering analysis to select and optimize a CVT configuration to meet the design requirements, and develop a preliminary CVT design.
- Task II--Identify technology advancements required for developing the CVT to production status. This includes defining the problem areas and estimating the means and efforts required to solve the problems.
- Task III--Determine the suitability of the CVT concept for alternate electric and hybrid vehicle applications and the suitability of the selected CVT design for alternate vehicle sizes and maximum output torques.

These tasks were performed according to the following schedule:

Task	1979								1980	
	M	J	J	A	S	O	N	D	J	
I Design study	████████████████									
II Required technical advancements					████████	████████	████████			
III Alternate applications						████████	████████	████████		
IV Design and technical assessment						████████	████████	████████	████████	

S-46832

Task I, Design Methodology

A digital computer program was developed to analyze the performance of the CVT. The details of the program are discussed in the Task I, Configuration Analysis and Selection section. The computer program was used to select the optimal toroidal cavity and roller dimensions, compare the performance of different design configurations, and predict the performance of the final CVT design configuration.

A parametric study was conducted to select the optimal toroidal cavity and roller dimensions. The study consisted of optimizing preselected CVT performance parameters while varying the toroid and roller dimensions, holding all other operating conditions constant. The toroid and roller geometry that yielded optimal performance were then selected.

The selected toroid/roller geometry was then used to compare five candidate CVT design configurations. These five CVT design configurations are described in the Design Configurations subsection. To compare the performance of the design configurations, a mathematical model of each was made and input into the computer program. The performance of each was then evaluated at preselected operating conditions. The final design configuration was selected using specific, ranked design criteria. These design criteria, starting with the most important, are:

- (1) Efficiency
- (2) Cost
- (3) Size and weight
- (4) Reliability
- (5) Noise
- (6) Controls
- (7) Maintainability

Task II, Identification of Required Technology

The operation of the selected CVT design configuration was analyzed with respect to potential technological problems. This analysis included identifying the problems and discussing the effort required to solve the problem. All aspects of the design were included in the analysis, the control system, the traction fluid performance requirements, and all the mechanical components.

Task III, Suitability for Alternate Applications

The suitability and scalability of the toroidal cavity traction drive CVT concept for electric and hybrid vehicles and alternate vehicle weights and output torques were determined by comparing the mechanical requirements of the alternate applications to the initial conditions. This included ratio range, speeds, torques, and size. The alternate application design configurations included an electric vehicle powered by an electric motor, and a hybrid vehicle with an electric motor and internal combustion engine. The alternate vehicle weights were 790 kg (1750 lb) and 10 000 kg (22 000 lb), and respective output torques were 210 N-m (155 lb-ft) and 2600 N-m (1900 lb-ft). These configurations were evaluated in accordance with the specified operating conditions. The computer program was used to verify the analysis when necessary.

Task IV, Design and Technical Assessment Report

Information relating to the CVT design selection and analysis of Task I is presented. A full description and layout of the selected CVT design configuration, including performance maps, are presented as well. The selected CVT design is described in the Selected Design Description subsection.

A discussion of the design approach covers the design tradeoffs, the strengths and weaknesses of the five candidate design configurations, and the ability of each to achieve the design specifications.

Detailed engineering analyses of the selected CVT configuration were performed. The results are presented in the Configuration Analysis and Selection subsection. These analyses included stress, critical speed, life, reliability, weight, and geartrain.

Engineering consultants were employed as necessary to guide the engineering analyses in the areas of stress, life, traction fluid properties, and configuration design. These consultants included Dr. Alston Gu and Byron Heath, AiResearch Manufacturing Company; and Milton Scheiter, General Motors, retired.

Discussions of the required technological advancements identified in Task II and the suitability of the CVT design for the alternate vehicle applications specified in Task III are included.

DESIGN REQUIREMENTS

The design requirements are specified in the statement of work and apply in the performance of all three tasks. The design requirements are outlined in this section. The purpose of the design requirements is to describe a CVT that has both a wide ratio range and high efficiency, with reliability, size, weight, and cost comparable to those of present day automotive transmissions.

The CVT performance requirements are as follows:

- Input flywheel speed: 14 000 to 28 000 rpm
- Output shaft speed: 0 to 5000 rpm
- Maximum delivered torque: 450 N-m (330 lb-ft)
- Maximum delivered power: 75 kW (100 hp) for 5 s
- Ratio change rate: full ratio 2 s (increasing or decreasing)
- Bi-direction power flow
- Startup and driving smoothness of conventional automatic transmission
- High efficiency over its entire operating spectrum
- Overall size and weight comparable to those of present automotive transmissions of equal power
- Maintainability equal to or better than present automotive automatic transmissions

The design features of the vehicle are as follows:

- Vehicle curb weight: 1700 kg (3750 lb)
- Extracted flywheel energy: 1.8 MJ (0.5 kWh)
- CVT controls to provide "feel" of conventional automatic transmission
- Reverse drive by electric motor or CVT
- Electric motor to charge flywheel from rest
- Design life:

10 percent life, 2600 hr

Weighted average power: 16.5 kW (22 hp)

Average speed: 21 000 rpm input/3000 rpm output

The initial effort was directed toward determining the CVT ratio range requirements specified by the design requirements and creating the preliminary CVT design configurations to meet these requirements.

Establishing a ratio of the input and output speed requirements will yield the ratio range necessary for meeting the design requirements. Therefore, the CVT must have an infinite ratio range if a zero output speed is to be achieved. This can be accomplished with the addition of regenerative gearing to the toroidal drive. All the configurations discussed here are described in detail in the Design Configurations subsection.

The statement of work, however, indicates that a minimum CVT output speed of up to 850 rpm is acceptable if the CVT is not continuously controllable down to zero output speed. This would require the addition of a slipping clutch to the driveline to allow the differential input speed to go to zero. The minimum output speed would be dictated by the slipping clutch performance.

The minimum CVT ratio range necessary to achieve an 850 rpm minimum CVT output speed is 11.7:1. Because the full cavity toroidal drive has a maximum usable ratio range of about 8:1, the design must expand this ratio. Five CVT design configurations were considered that could attain the required ratio range, and each was evaluated to determine the advantages and disadvantages during the selection process.

DESIGN CONFIGURATIONS

Each of the five CVT design configurations evaluated during this study include toroidal traction elements coupled in various ways to another toroidal traction element and/or reduction gear sets. These design configurations are described below.

Baseline Drive

The baseline drive (fig. 4) incorporates smooth rollers in both the single-stage fixed-ratio planetary drive system and in the variable toroidal roller section that provides the variable output speed and can provide a reverse function. Power is transmitted to the input shaft, which drives the sun element of the fixed-ratio planetary drive at input speed. Torque from the sun is reacted by the planet rollers and is transferred to the ring element and planet carrier. The planet carrier is attached to the output shaft of the drive and transmits all of the output power. It should be noted that the sun element is operating in a direction opposite to the ring and is feeding power back into the toroid system by the reactive torque required to deliver power to the output shaft. When the speed of the ring element through the toroidal system is modulated so that the surface speed of the ring approaches that of the sun, the output shaft speed will approach zero speed. Any surface speed of the ring that is higher than the sun produces a reverse rotation of the output shaft. Variable speeds are obtained by inclining the toroidal rollers with respect to the input and output discs, thereby increasing or decreasing the respective speeds of the discs.

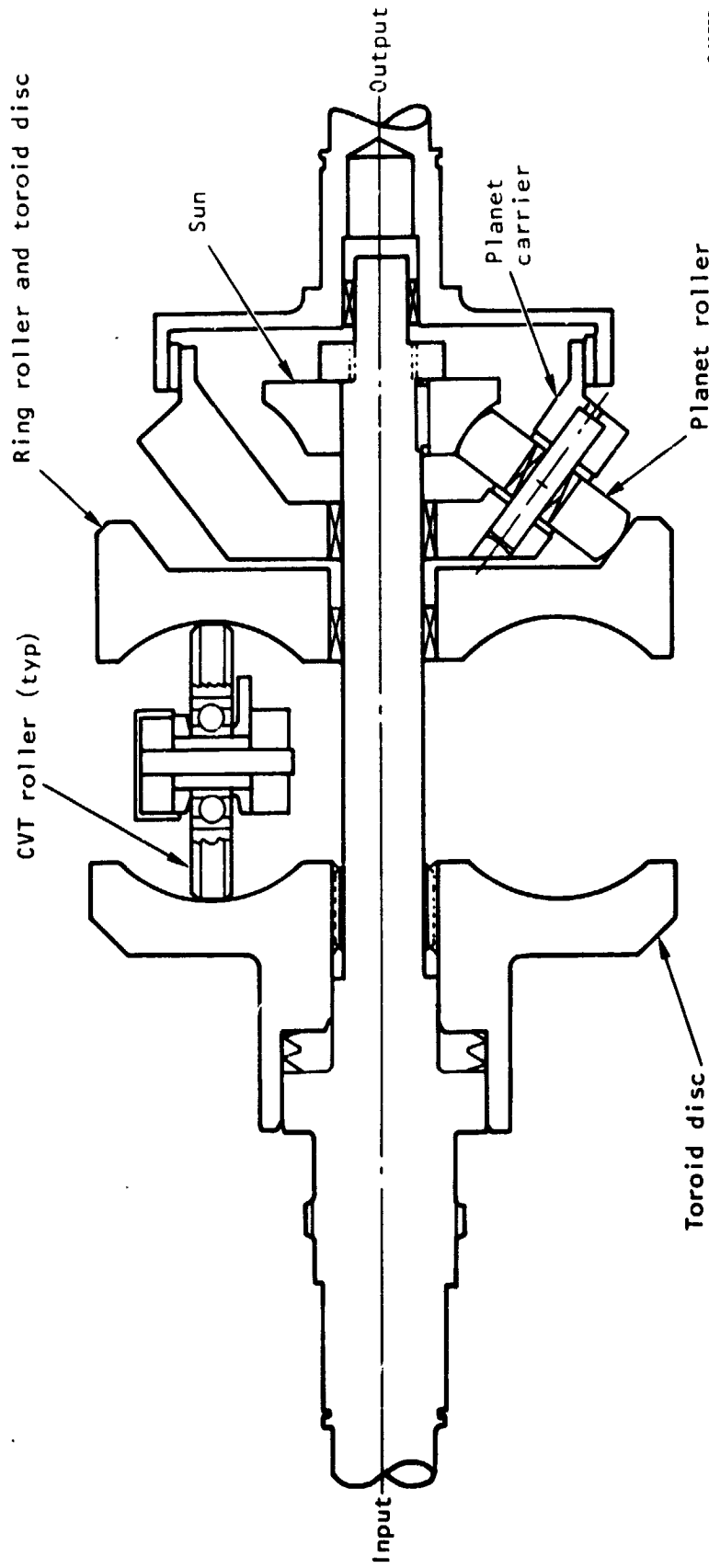
The roller control system is described in the Transmission Ratio Control subsection.

Series Drive

This configuration consists of two toroidal cavities in series with the output of the first connected to the input of the second as shown in figure 5. Power is transmitted to the input shaft, which drives the input disc. Torque from the disc is reacted by the rollers and transmitted to the output disc. The output disc is connected to the input disc of the second cavity. Again the torque is reacted by the rollers and transmitted to the output disc. Variable speeds are obtained by varying the angle of inclination of the rollers with respect to the input and output discs. Independent roller controls are required for each cavity. The minimum output speed can be achieved by additional reduction gearing, as required.

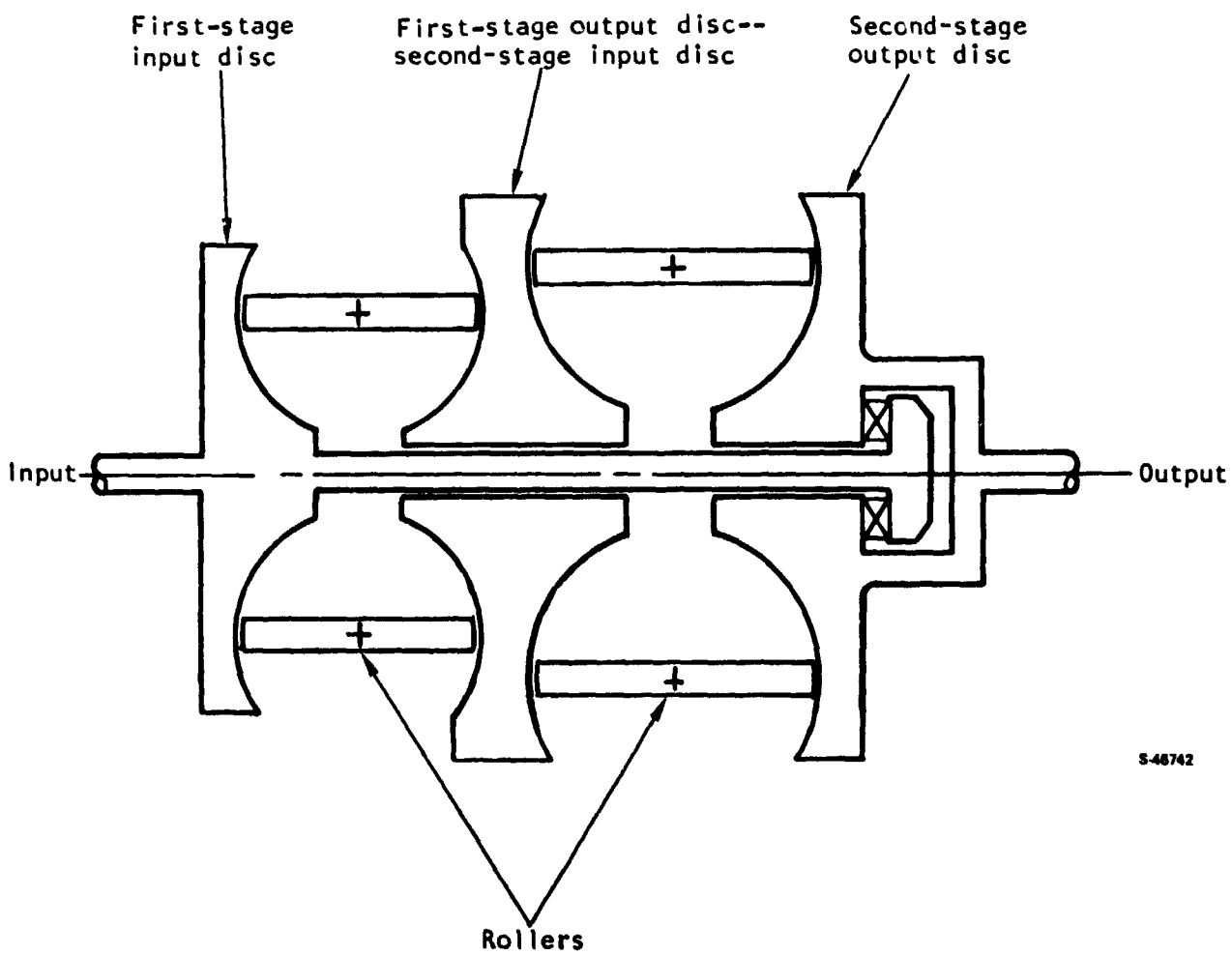
Two-Speed Shifted Drive

The two-speed concept incorporates two toroidal cavities in parallel with the output discs connected to a reduction planetary gearset as shown in figure 6. Power is transmitted to the input discs. The input discs are tied together and are located in the center of the transmission. Torque from the discs is



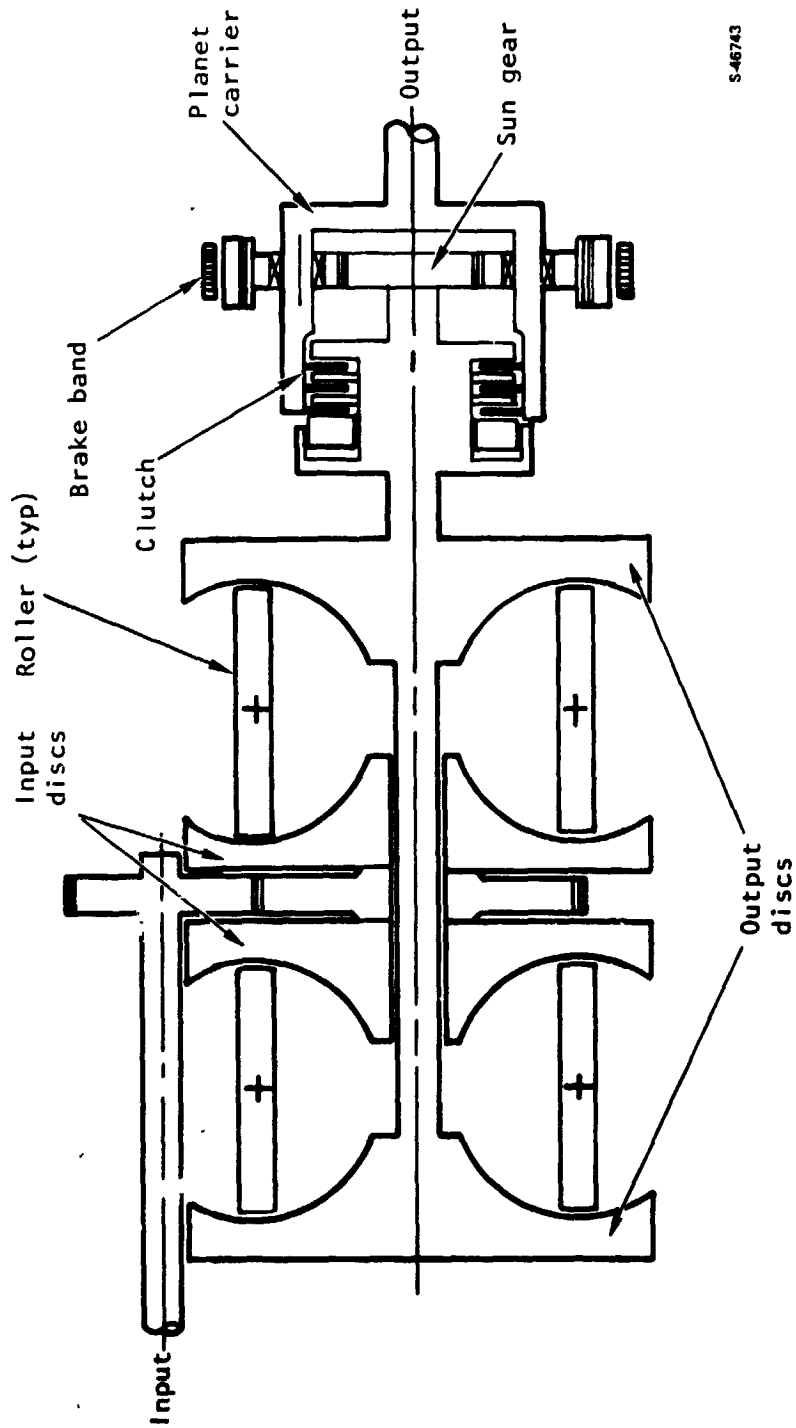
S-46736

Figure 4.---Baseline drive.



548742

Figure 5.--Series drive.



S-46743

Figure 6.--Two-speed shifted drive.

reacted by the rollers and transmitted to the output discs. The output discs, which are connected together, drive the planetary sun element. The planet carrier is attached to the output shaft of the drive. A brake band is positioned around the planetary ring element, and a clutch is positioned to connect the sun element directly to the planet carrier.

When the maximum gear reduction is desired, the output discs drive the output shaft through the planetary reduction with the clutch released and the brake band applied to the ring element. The output discs drive the sun element. Torque from the sun is reacted by the planet gears against the stationary ring element. The output shaft is attached to the planet carrier and rotates as the planets are driven by the sun gear.

The planetary reduction can be bypassed by releasing the brake band and applying the clutch. The output discs then drive the planet carrier directly through the clutch.

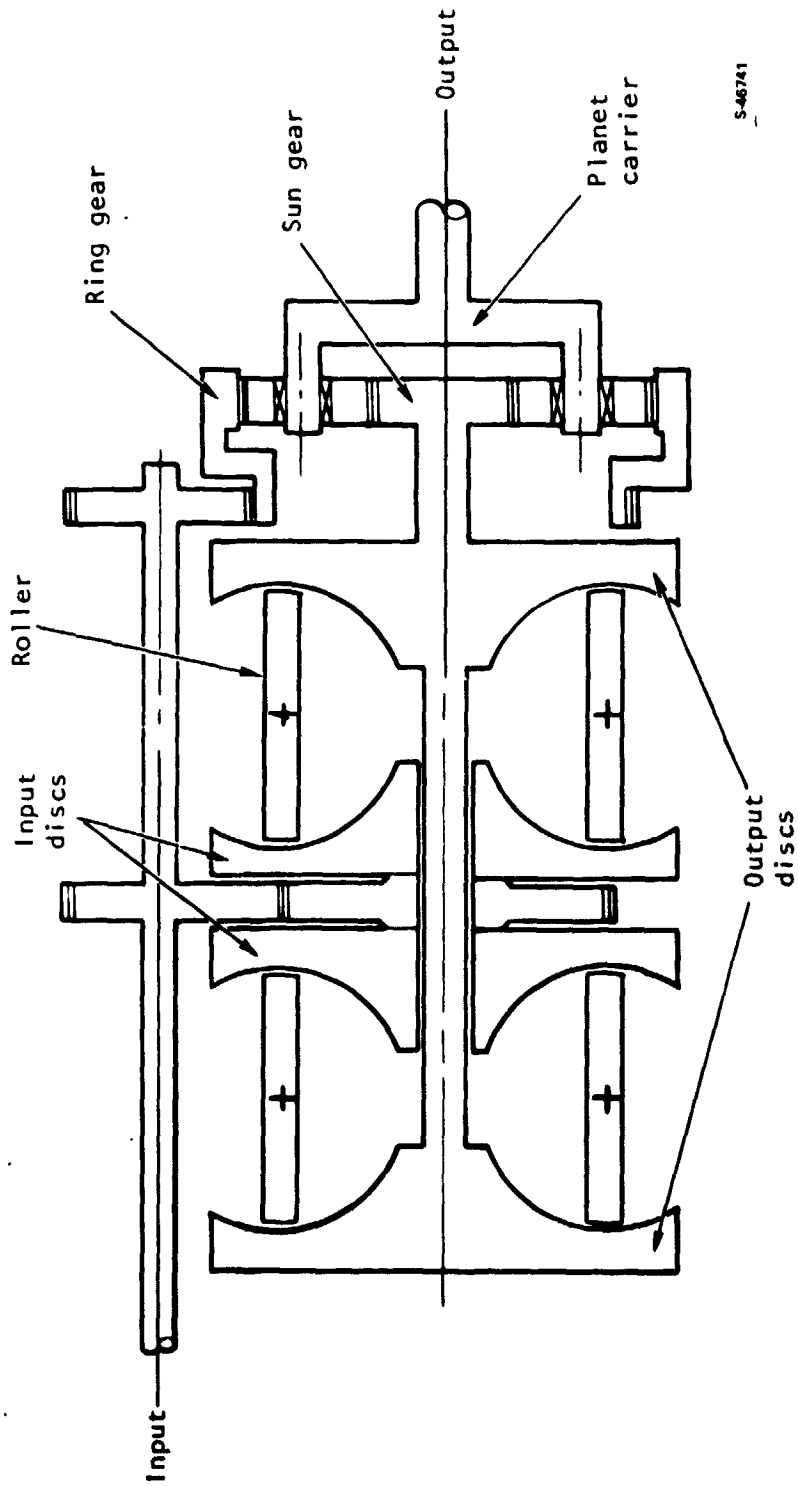
The shift occurs as the toroidal cavity reaches the ratio extremes. During acceleration, the planetary would be in reduction. When the toroid rollers move to the maximum overdrive position, the shift would occur. Simultaneously, the brake band would be released, the clutch would be activated, and the rollers would be driven to a predetermined position to match the new overall transmission ratio to the ratio prior to the shift.

Inverse Regenerated Drive

The inverse regenerated drive (fig. 7) incorporates a single-stage fixed-ratio planetary drive system and a variable toroidal roller section that provides the variable output speed and can provide a reverse function. The design utilizes two toroid cavities, in parallel, with the input discs and output discs connected together. Power is transmitted to the input shaft, which drives the input discs and the planetary ring element at a speed that is proportional to the input speed. Torque from the ring is reacted by the planet gears and is transferred to the sun gear. The planet carrier is attached to the output shaft of the drive and transmits all of the output power. The sun gear operates in a direction opposite to the ring and is feeding back power into the toroid system by the reactive torque required to deliver power to the output shaft. By modulating the speed of the sun gear through the toroidal system so that the surface speed of the sun approaches that of the ring, the output shaft speed will approach zero speed. Any surface speed of the sun that is higher than the ring produces a reverse rotation of the output shaft. Variable speeds are obtained by varying the angle of inclination of the toroid rollers in the toroid cavity.

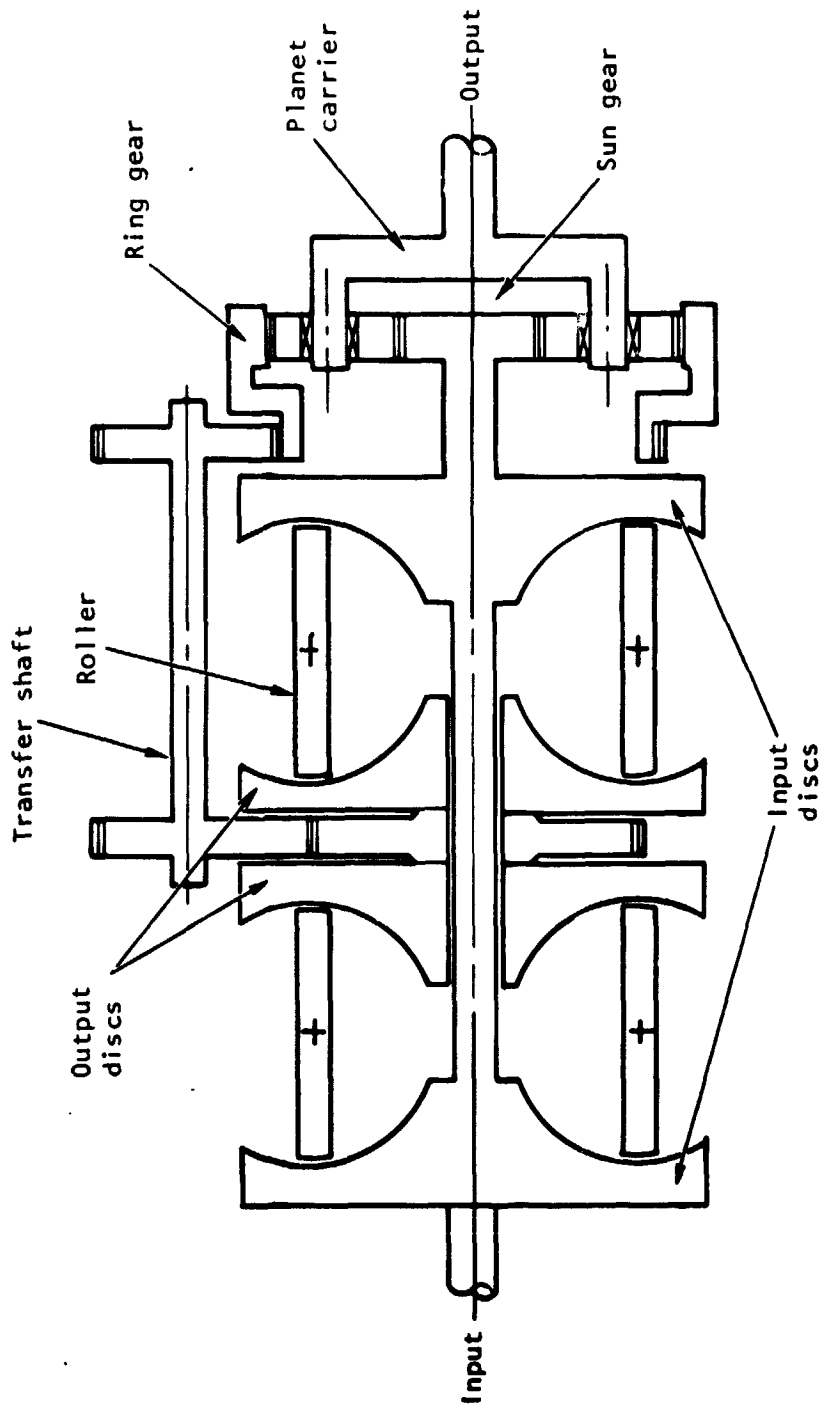
Regenerated Drive

The regenerated drive concept (fig. 8) is similar to the inverse regenerative concept described above. The sun gear speed in the regenerated drive is proportional to the input speed. Output shaft speed is zero when the ring gear surface speed is equal to the sun gear surface speed. As the ring gear speed is increased, the output shaft speed also increases.



S-46741

Figure 7.--Inverse regenerated drive.



S-46740

Figure 8.--Regenerated drive.

The principal difference between the regenerated drive and the inverse regenerated drive is that the rotational speed of the reacting member (sun gear) decreases as the output shaft speed increases for the inverse regenerated drive and the rotational speed of the sun gear increases as the output shaft speed increases for the regenerated drive.

TRANSMISSION RATIO CONTROL

The combination of two power sources, namely the electric motor and the flywheel/CVT, in the same vehicle drive system requires control logic that will sum the power sources to produce the desired driver command. The greatest benefit to the propulsion system will occur when the electric motor power demands are load-leveled, which results in a reduction in electric motor and controller sizes and an increase in the utilization of battery energy.

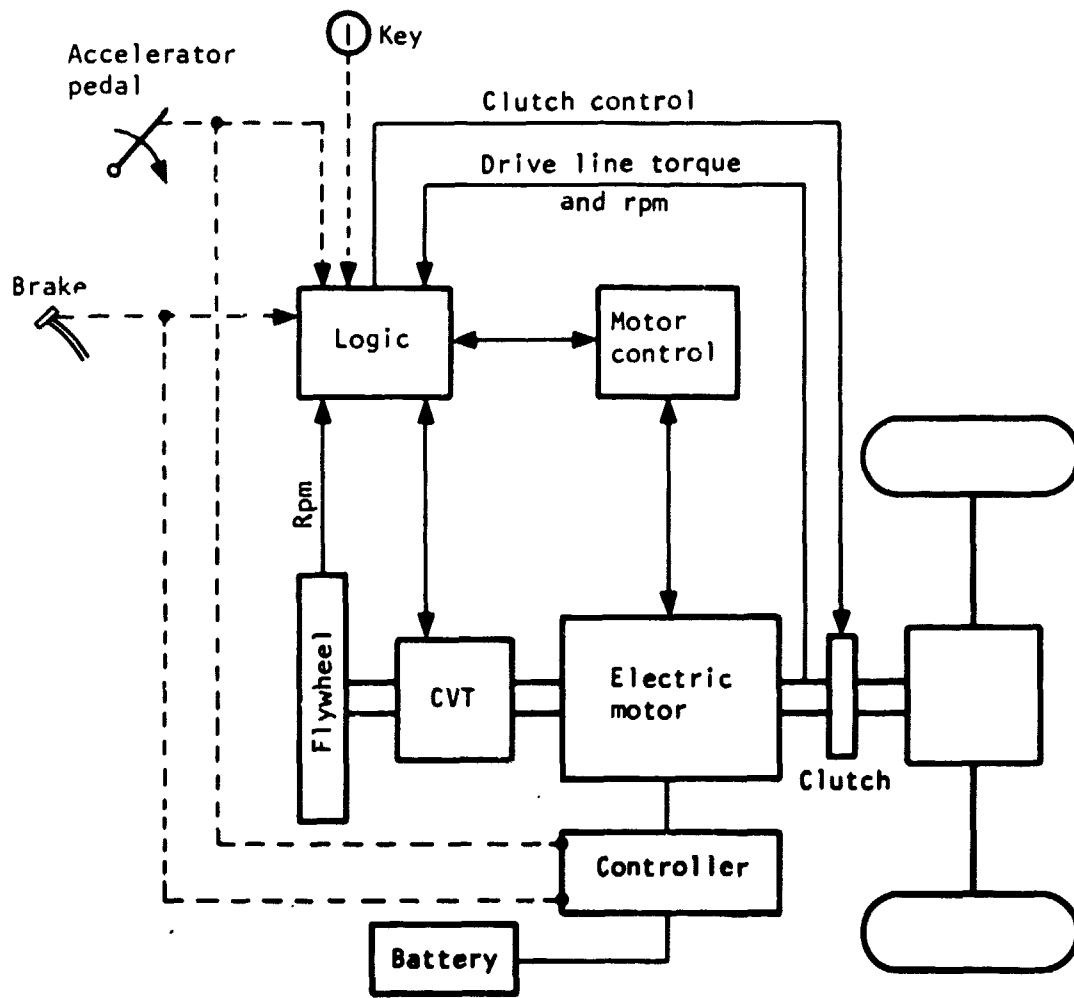
To provide the required control strategy, two control loops are needed. One control loop is used to manage the flywheel energy level by comparing the flywheel speed and the vehicle speed so that the flywheel energy can be maintained as desired for a given vehicle operating cycle. The flywheel speed is held within prescribed limits by the addition of electric motor power or the extraction of vehicle kinetic energy through the use of the motor as a generator during portions of the vehicle operation such as hill descent. The second control loop is used to change the CVT ratio so that combined flywheel and electric motor power sources provide a vehicle output power as commanded by the inputs from the accelerator and brake pedals. A schematic of the vehicle control system is shown in figure 9.

Motor Control

The motor control is separate from the CVT control system. However, the control function must be correlated with the flywheel/CVT control system as described in the operation of the roller position control logic. The motor controller responds to the command to maintain flywheel speed at the required value, and it does this by adjusting motor current to the required power level. A current limit can be selected which provides sufficient power to maintain a maximum steady-state driving condition, such as a hill climb at some prescribed value of vehicle speed. In a typical dc mechanically commutated motor, the current limit is established by an armature chopper when the motor is below its base speed, or the speed where the motor back EMF is less than the supply voltage. The current limit is established by field weakening when the motor speed is above base speed. An attempt should be made to control the motor operation in a range that results in the lowest level of source current that produces maximum battery energy capability.

CVT Control

The CVT control of power flow into and out of the flywheel must provide for the added power source supplied by the electric motor. Since this power source is located between the CVT and the vehicle wheels, the CVT control will be biased by the added power so that the CVT control reflects the net power to satisfy the accelerator and brake pedal commands. The bias signal can be proportional to the electric motor current.



6-46722

Figure 9.--Schematic of vehicle controls for a CVT-equipped flywheel electric vehicle.

The CVT control is accomplished by a ratio change between the input and output shafts to control the flow of power to and from the flywheel. The ratio change is accomplished by applying a force to the power rollers so that the rollers move to the rolling path that produces the commanded ratio change. This is a force-feedback actuation system that is hydraulically powered with pressure-balanced hydraulic actuators. A schematic of the CVT hydraulic control is shown in figure 10; a list of the control valves is given below.

- (1) Forward, neutral, and reverse valve selects:
 - (a) Pump pressure to Valve 2 for forward
 - (b) Both outputs to sump for neutral
 - (c) Pump pressure to Valve 3 for reverse
- (2) The flywheel charge command valve is solenoid activated for flywheel charging when the vehicle is stopped and in neutral.
- (3) The power command valve proportions roller position control pressures to accelerator pedal position.
- (4) The flywheel charge control solenoid valve proportions the roller position control pressures to charge the flywheel-solenoid. Force and direction are controlled by flywheel speed control logic.
- (5) The roller position ratio limit valve reverses roller position control pressures when roller tilt reaches maximum in either direction.
- (6) The maximum power limit valve limits the roller position control system maximum pressure for maximum load limit on the transmission.
- (7) The demand pressure valve sets pump discharge pressure to a fixed amount over maximum control system pressure.
- (8) The maximum pressure valve limits system pressure.
- (9) The shuttle valve selects maximum control system pressure for pump pressure control.

Flywheel Starting

To start or to charge the flywheel using the electric motor when the vehicle is stopped is performed by an automatic sequence as a result of turning on the ignition key:

- (1) The jaw clutch between the motor and the vehicle is disengaged.
- (2) The CVT ratio is controlled towards overdrive so that flywheel speed can be increased with a motor speed that rapidly approaches base speed or above.

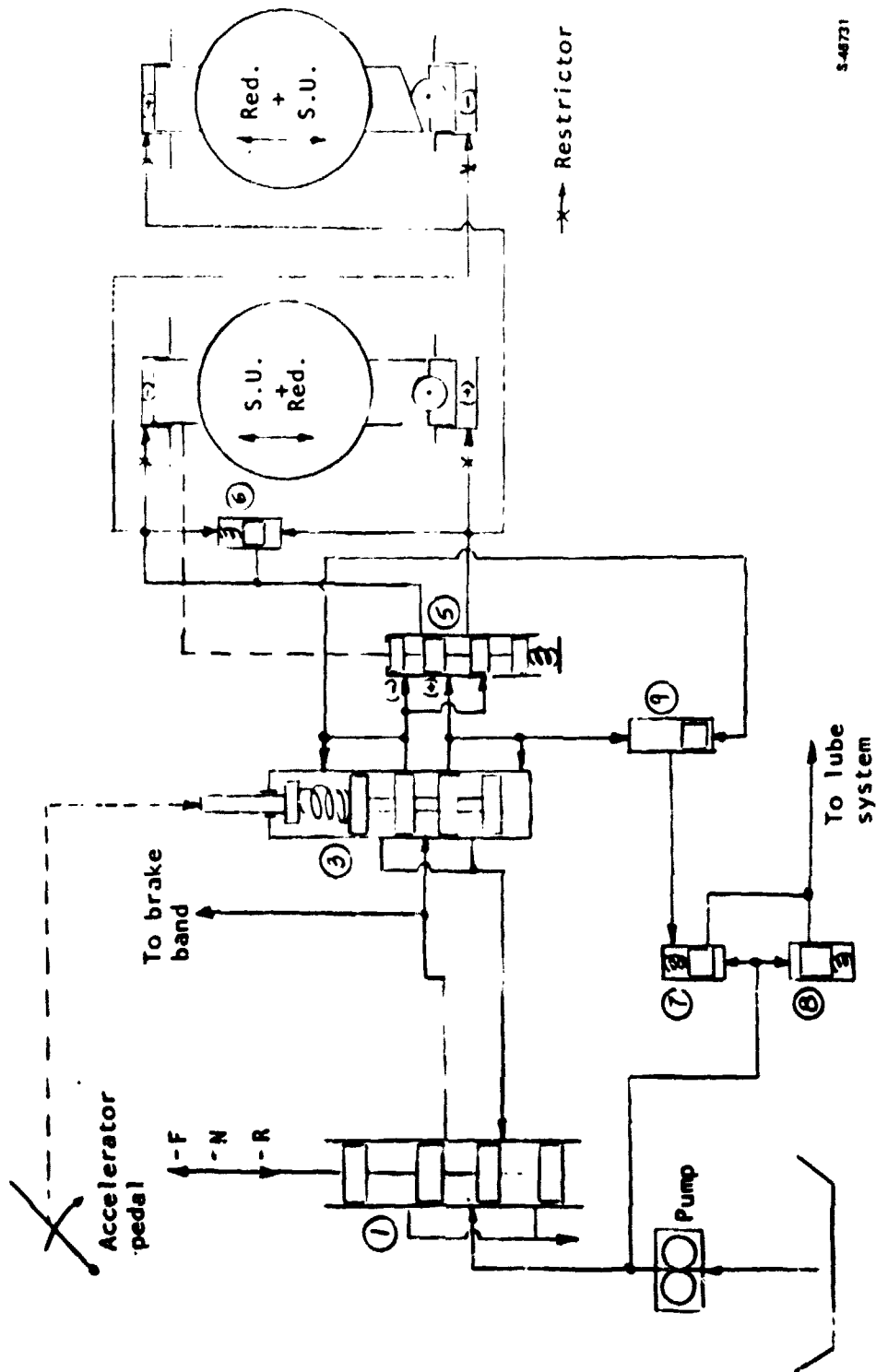


Figure 10.--CVT control hydraulic schematic

- (3) When the key is turned off, the jaw clutch is again disengaged, and the CVT ratio is controlled towards overdrive so that the flywheel can be restarted by the motor.

Alternate Control System

A simplified alternate vehicular drive train and control system is shown in figure 11. This configuration has the electric motor connected directly to the flywheel with a fixed ratio speed increaser. The motor control becomes a function of flywheel speed. Motor efficiency can be maximized because the motor operates within a 2:1 speed range (the same as the flywheel) rather than from zero to 5000 rpm. All vehicle power goes through the CVT, which has direct power control regardless of whether the power comes from the flywheel or the motor. The CVT hydraulic control schematic for this configuration is shown in figure 12.

The flywheel starting system is simplified since the CVT ratio can remain in maximum reduction when the vehicle is stopped and the flywheel coasts down below its normal operating range. Starting is provided by applying power to the electric motor, which speeds up and charges the flywheel.

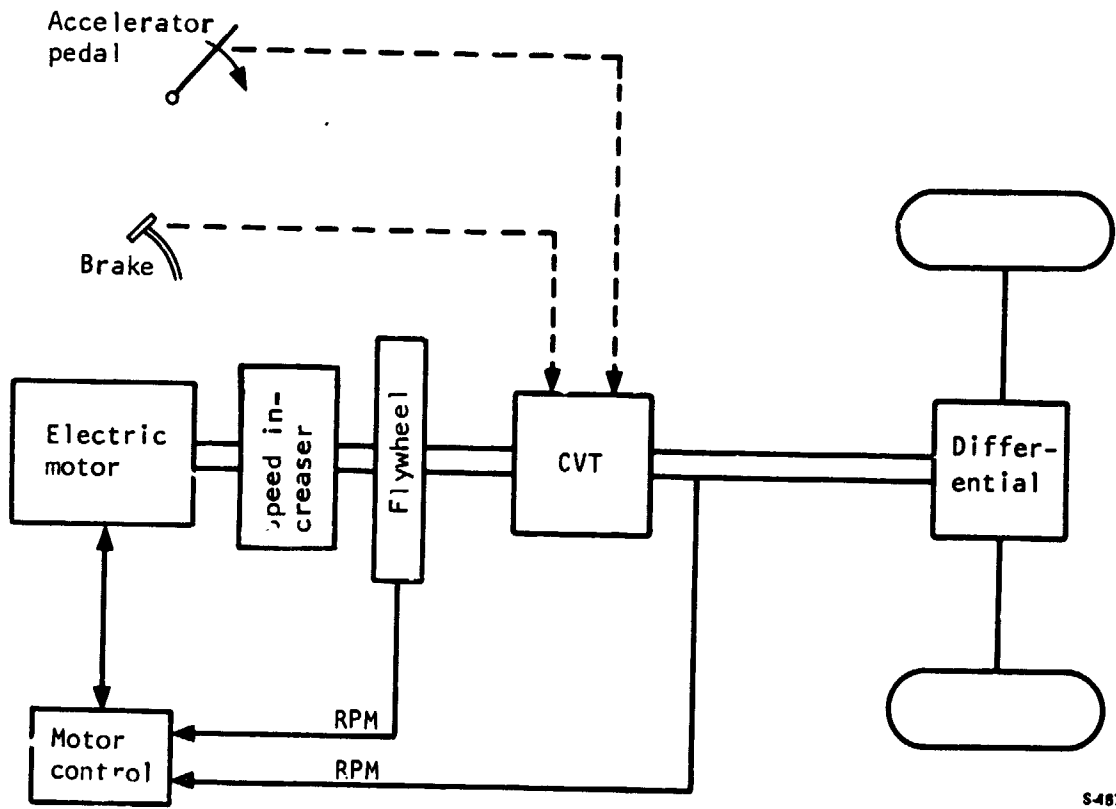
CVT Power Roller Actuation

With a toroidal type traction CVT, there have traditionally been two different types of control systems used to position the power rollers--a position control type and a load control type.

Position control system.--The position control system controls the drive ratio by adjusting the actual geometric tilt of the power rollers. This is usually done by manipulating the roller rotational axis to cause the roller to steer and roll to a new position.

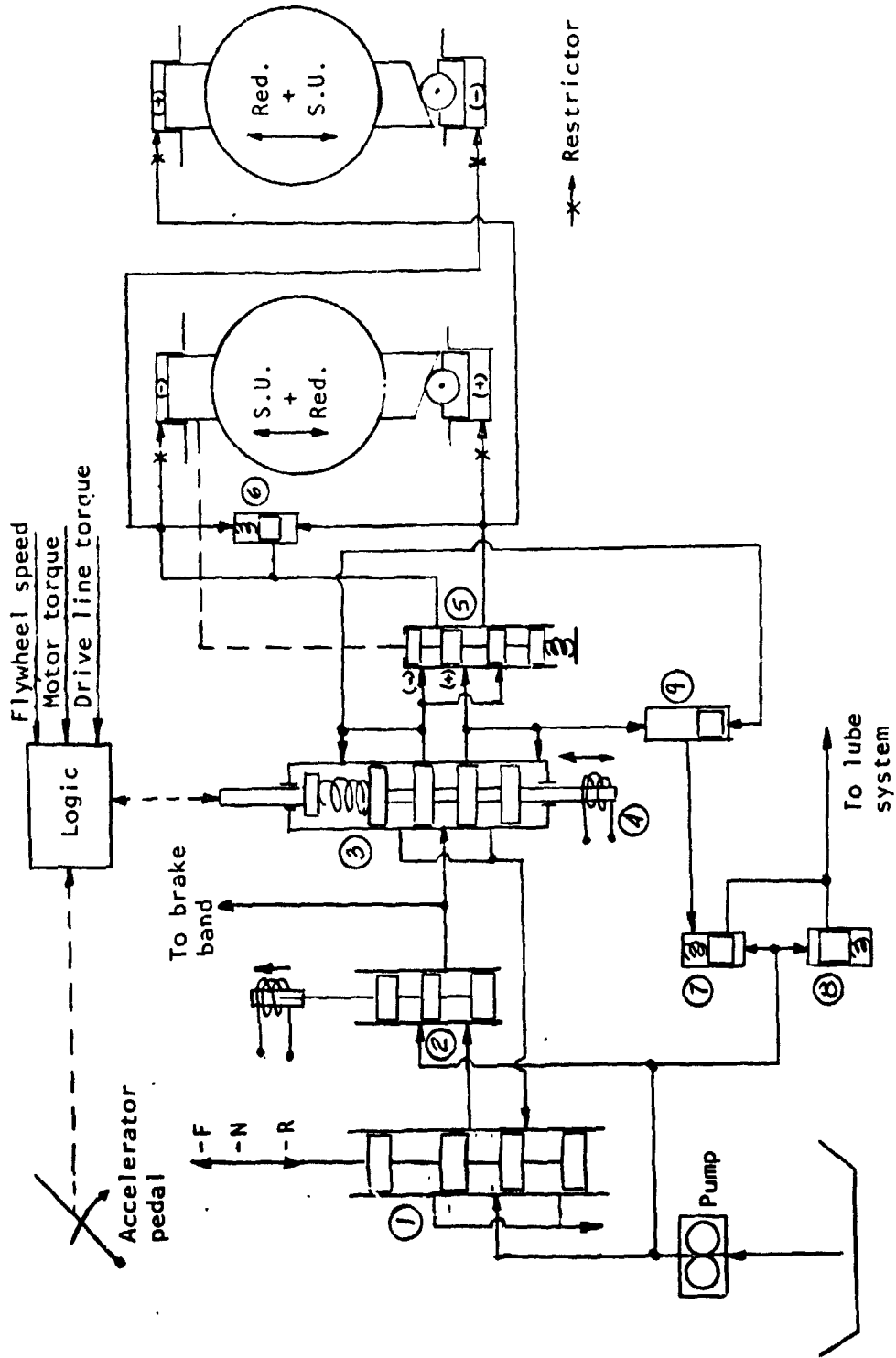
As normally used a position control system is insensitive to the power carried by the drive and will not respond to changes in power levels. This lack of feedback makes it very difficult to cause all the power rollers to share the load equally, especially with a dual cavity drive configuration. Each roller must be held in a true geometric position to within a very small tolerance while the drive is subjected to load and thermal stresses. Any backlash, out-of-tolerance, misalignment, etc., will allow the rollers to vary from true position and induce roller-to-roller interaction and fighting.

Because of the insensitivity to drive loads, a position type system was not judged acceptable for this CVT application, where a load responsive control system is required.



S-48726

Figure 11.--Schematic of alternate vehicle controls for a CVT-equipped flywheel electric vehicle.



S-46730

Figure 12.--CVT alternate control hydraulic schematic.

Load control system.--The load (force-feedback power roller) control system ideally fits load responsive control requirements of an automotive application. With this system, the controls adjust the tangential forces carried by the power roller, not the roller tilt. The system is shown schematically in figure 13. The rotating input disc imparts a tangential force (a) on the power roller causing it to rotate and impart an equal tangential force (d) on the output disc. A reaction force (b) is imparted on the power roller. The sum of forces (a) and (b) is balanced by the force (c) from the hydraulic pressure in a support cylinder. While these forces are in balance, the roller stays on the tangential point of roll on the traction discs, and remains stable. When there is a difference between the sum of the tangential forces and the support force, the roller moves to either lead or lag the tangent point, and generate a roller steering action, as shown in figure 14.

In figure 14 the rolling contact is shown at point (b). That contact rolls on the traction disc along the circular pathway (a-b-c) as the disc rotates about center C. The contact also rolls on the power roller, but in a straight line represented by (d-b-e). As long as the contact remains at tangent point (b), there is no vectorial error between the roll paths on the disc and power roller.

Steering action occurs when the sum of the tangential forces is different from the force from the hydraulic cylinder. Fig. 14 shows the rolling contact between the input disc and the power roller. When the sum of the tangential forces exceeds the hydraulic cylinder force, the rolling contact will move to point (f) to lag the tangent point. At point (f), the roller roll path (d-f-b) has a vectorial difference from the new traction disc roll path (shown dashed). This vectorial error causes the power roller to roll down a spiral path, bringing the contact inward towards the center C.

On the output disc, the same action occurs except that the direction of the roll paths are reversed, and the contact point spirals outward away from center C. Thus, when the sum of the tangential forces exceeds the hydraulic force, the contact on the input disc is steered towards the disc center while the contact on the output disc is steered away from the center; the power roller then moves toward reduction. The opposite action occurs when the sum of the tangential forces is less than the hydraulic force, and the roller moves towards speed-up.

Each power roller is therefore controlled independently by its own hydraulic cylinder. With all the cylinders connected in parallel, all the rollers must find a roll path where they will have equal tangential forces and thus equal loads. If one roller is moved slightly towards speed-up in relation to the others, it will have higher tangential forces (by carrying more than its share of the load) and will undergo the move towards reduction as described above. The load sharing between rollers is as accurate as the force of the separate hydraulic cylinders. No other critical parts or dimensions are involved.

By controlling the hydraulic pressure in the cylinders, the vehicle control system commands the tangential forces on the power rollers and, therefore, the power transmitted by the CVT. The specific ratio of the CVT is not controlled and will assume any value required between the flywheel and vehicle speeds. The CVT can transmit power to and from the flywheel as commanded by

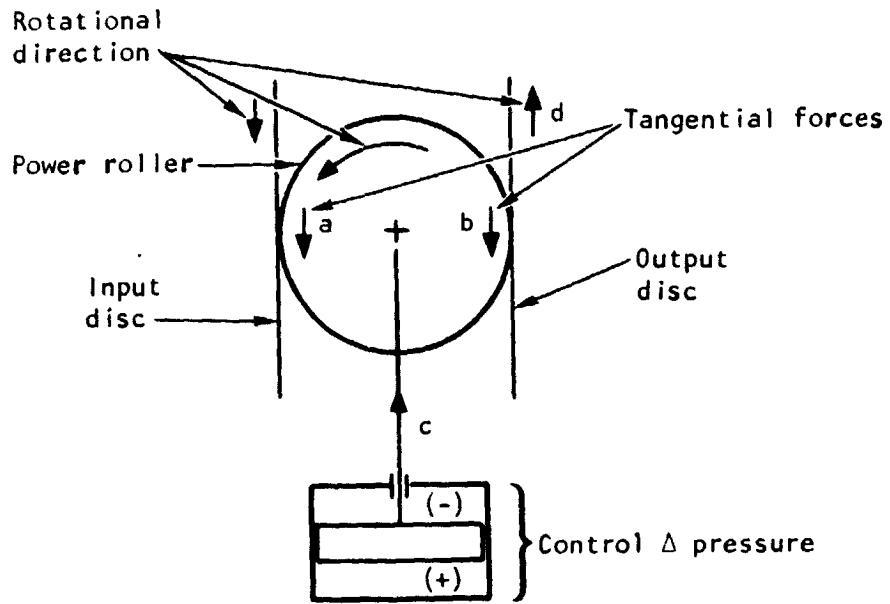


Figure 13.--Load control schematic.

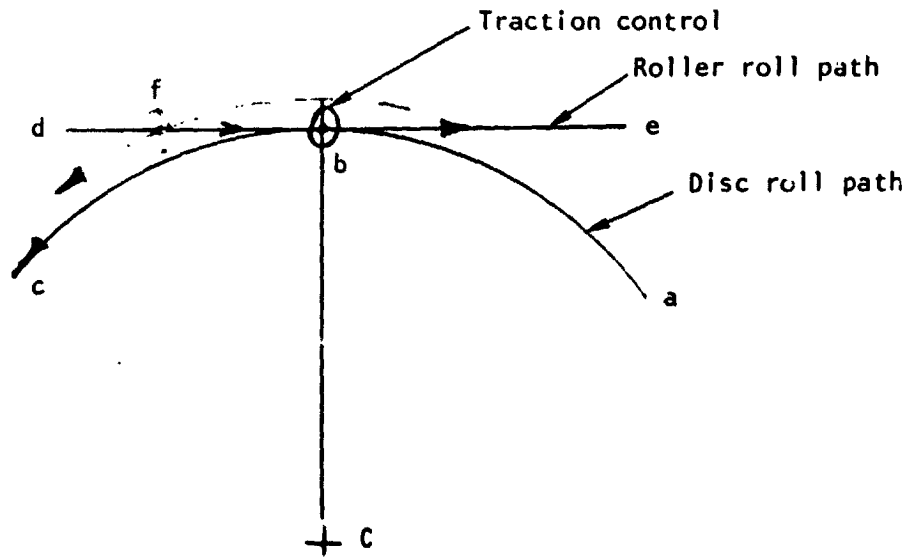


Figure 14.--Roller steering action.

8-46732

increasing, decreasing, or reversing these hydraulic pressures. When the hydraulic pressures are set equal (or both to zero), the rollers will not carry a load and will find a roll path where no load is transmitted. That path will be at the exact CVT ratio of the flywheel speed to the vehicle drive shaft speed. Any variation from this ratio will produce positive or negative tangential forces. When the vehicle is stopped, the CVT ratio will be at zero output speed.

To control the rate at which the roller tilts or changes ratio, the hydraulic cylinder must be connected to the roller assembly in such a way that there is a stroke or displacement of oil as a function of the tilt. The flow rate of the oil entering and leaving the cylinder is restricted by orifices.

In the optimized design configuration, the hydraulic cylinder is split in half with each half pushing on one end of the roller carrier or trunion. One end of the trunion has an integral cam surface. The piston on that end pushes against these cam surfaces through a pair of cam followers. The trunion rotates as the roller tilts within the toroidal cavity, and the piston is forced to move up or down the cam ramps.

This configuration has been built and tested on numerous drive configurations and will have no difficulty in meeting the specified requirement of running from maximum ratio to minimum ratio in 2 s. As designed, a sustained displacement of less than 0.05 mm (0.002 in.) from the true tangent point of roll will produce this rate of ratio change.

TRACTION DRIVE DESCRIPTION

Operation

This section describes the basic principle behind the operation of a traction drive and defines some of the important parameters used in the analysis of the traction contact between two rolling surfaces.

In a traction drive, torque is transmitted across two smooth rolling surfaces; not by metal-to-metal contact, but by the resistance to shearing of a fluid pad separating the two surfaces.

A simplified sketch showing the basic principle of traction drives is shown in figure 15. The rotation of the driving member causes shearing in the traction fluid between the two surfaces. This creates a tangential force that drives the driven member. The amount of shearing in the traction fluid is a function of the normal force (F_N) and the fluid traction coefficient (μ) which is defined as:

$$\mu = \frac{F_T}{F_N} \quad (1)$$

therefore,

$$F_T = \mu F_N \quad (1a)$$

The fluid film between the rolling surfaces resists shear and minimizes slippage while operating in the elastohydrodynamic region of lubrication. The fluid actually becomes a semi-solid under the high momentary contact pressure in a traction drive.

The fixed ratio arrangement shown in figure 15 is representative of a simple single stage speed reducer, and the power (kW) transmitted can be expressed as:

$$P_{out} = \eta P_{in} = \frac{2\pi R_1 N_1 F_N \mu \eta}{33\,000} \times 0.746 \quad (2)$$

where

η = efficiency

R_1 = radius of input disc, m (ft)

N_1 = speed of input disc, rpm

F_N = normal forces, kg (lb)

μ = traction coefficient

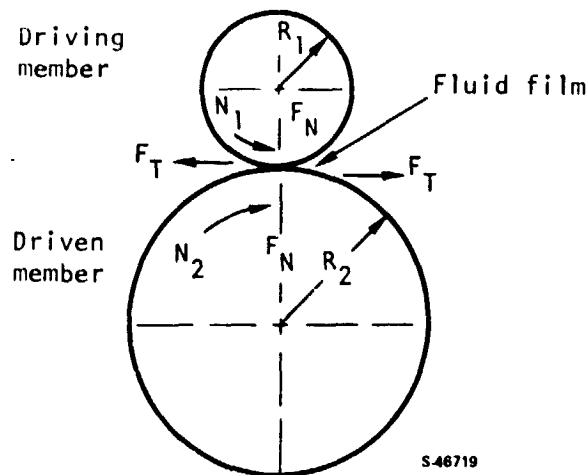


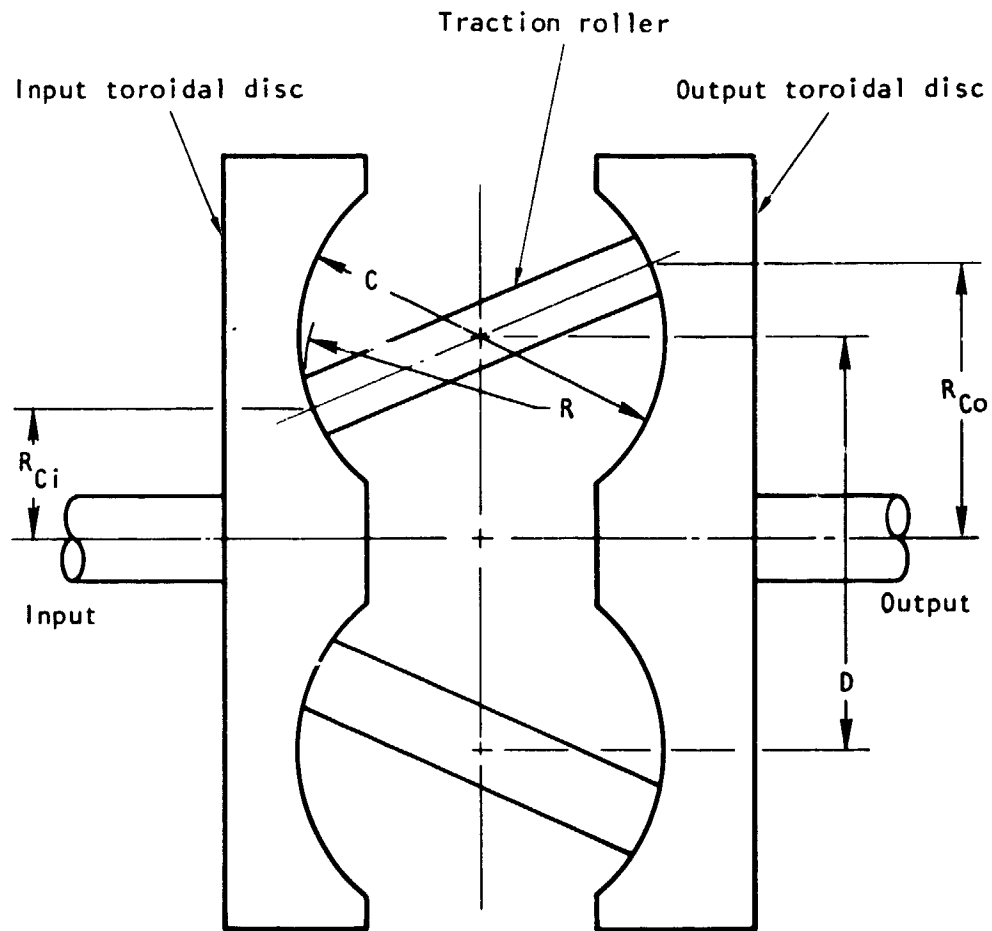
Figure 15.--Basic principle of traction drives.

A variable ratio traction drive arrangement would use a toroidal cavity formed by separate input and output discs on a common center and a number of traction rollers positioned equidistant around the center of the toroidal cavity (fig. 16). The effective speed ratio across the toroidal cavity would be the ratio of the input and output radii:

$$\text{Ratio} = \frac{R_{CI}}{R_{CO}} \quad (3)$$

For highest drive efficiency, the normal forces between the discs and the rollers need to be varied in accordance with varying torque and ratio conditions. An initial preload force is applied by springs to prevent any initial slip between the discs and rollers during startup. Upon rotation and torque application, load cams attached to the output shaft increase the preload between the rollers and discs.

The rollers are steered to change ratio and are held in position by means of hydraulic control pistons. The hydraulic force balances the tangential forces on the rollers. When a new ratio position is desired, hydraulic pressure is changed in the control pistons causing the rollers to move from the tangent position of roll to a new position where the forces are again balanced. There the rollers again return to the tangent point of roll. Parallel hydraulic connections between the roller control cylinders enable all rollers to share the same loads (in each cavity) so that all rollers are equally loaded.



D = Toroidal pitch diameter

C = Toroidal cavity diameter

R = Power roller contact radius, transverse to rolling direction

R_C = Contact rolling radius; i = input; o = output

Aspect ratio = C/D

Conformity = $2 R/C$

Drive ratio, input speed/output speed = R_{Co}/R_{Ci}

8-48730

Figure 16.--CVT toroid cavity arrangement.

In the toroidal cavity design concept (fig. 16) the axial thrust force created by the load cam is balanced through the tension shaft connecting the discs. This results in the elimination of axial bearing loads and minimizes the reaction forces in the housing.

Traction Characteristics

Many factors influence the traction phenomenon within the fluid pad separating the two traction surfaces. Several of these factors are defined below.

Contact area.--When two elements such as a sphere and a plate (fig. 17) are held together by a force normal to the plane of contact, an area develops because the pressure deforms both the sphere and the plate. This flattening is a function of the modulus of elasticity of the materials, the normal or contact force, and the curvature of the sphere and plate. The contact area is a circle or an ellipse depending on the geometry of the two bodies in contact. The contact area dimensions are found using the general case of two bodies in contact, reference 1, which is presented in detail in Appendix A.

Axial force.--The axial force is the force on the toroid discs parallel to the centerline of the toroid. As mentioned above, the axial force is varied by the use of a load cam mechanism attached to the output disc. Therefore, the axial force is proportional to the torque on the output disc and the loading cam lead:

$$F_{AX} = \frac{4 \pi T N_{ROLL}}{L} + F_i \quad (4)$$

where

T = torque

N_{ROLL} = number of rollers

L = cam lead

F_i = preload

Normal force.--The force normal to the plane of contact between the disc and roller is the contact force, as shown in figure 18. The contact force is a function of the axial force, roller position, and number of rollers:

$$F_N = \frac{F_{AX}}{\cos(\alpha) N_{ROLL}} \quad (5)$$

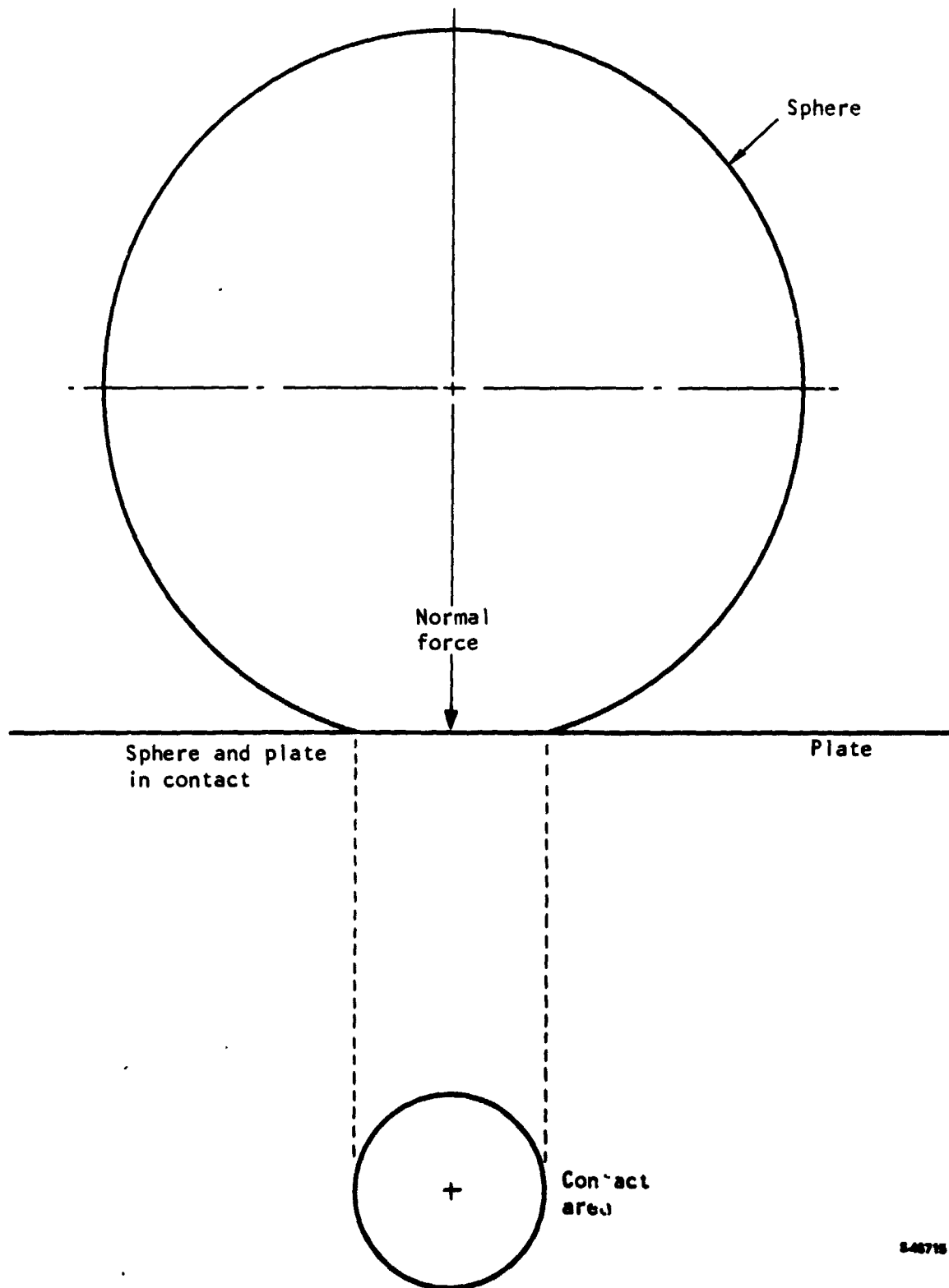
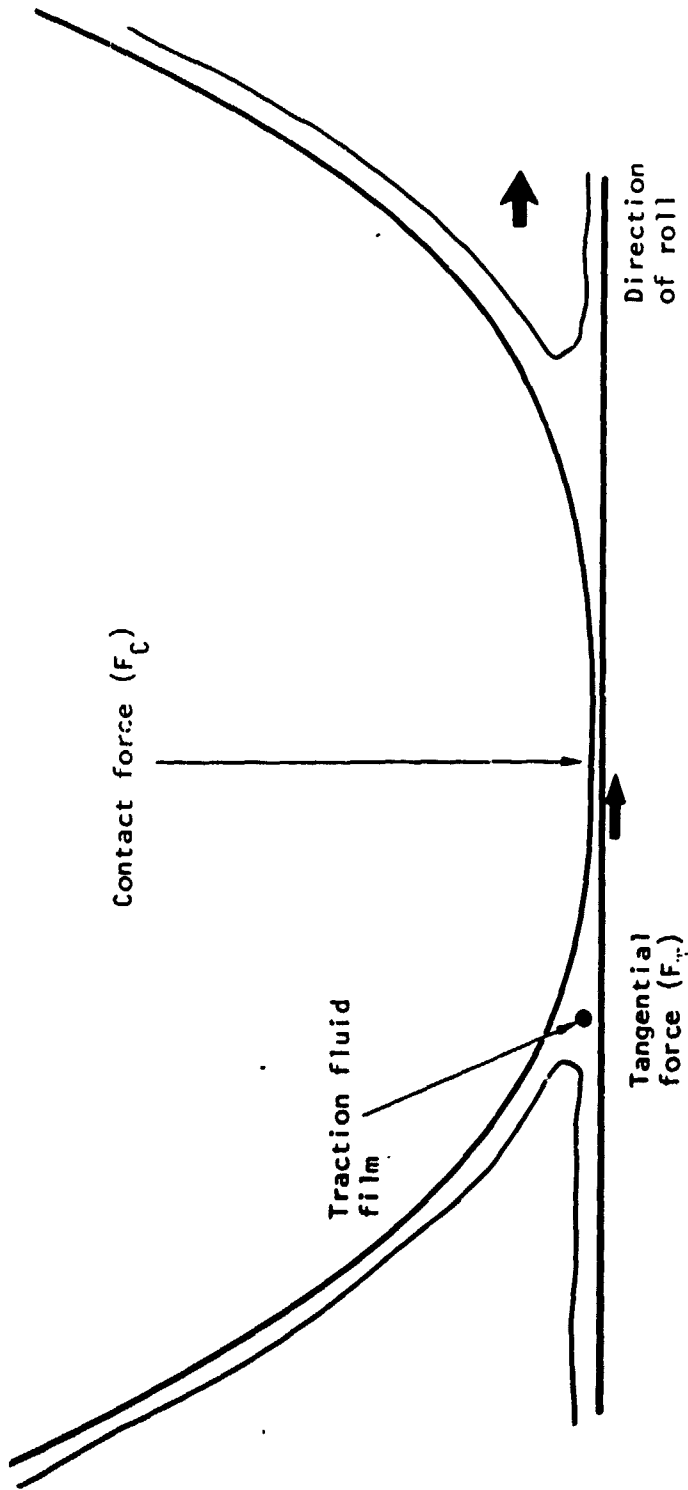


Figure 17.--Sphere and plate in contact.



$$\text{Traction coefficient } \mu = \frac{\text{Tangential force}}{\text{Contact force}}$$

The traction coefficient must be determined experimentally for the parametric conditions rolling speed, Hertz pressure, temperature, spin, curvatures, etc., as are used in the drive design.

S-46738

Figure 18.--Contact force.

where

F_{AX} = axial force

α = angular position of the roller with respect to the horizontal

N_{ROLL} = number of rollers

Hertzian pressure.--The Hertzian pressure is the compressive stress at any point in the contact area. The Hertzian pressure is assumed to have a parabolic distribution over the contact area, with the maximum Hertz pressure being at the center of the contact area and going to zero at the edge of the contact area (fig. 19). The Hertz pressure distribution is defined as (ref. 2):

$$\sigma = \frac{3 F_N}{2\pi ab} \left[1 - \left(\frac{x}{a}\right)^2 - \left(\frac{y}{b}\right)^2 \right]^{1/2} \quad (6)$$

where

F_N = normal force

a = half the major axis

b = half the minor axis

x and y = point coordinates

Film thickness.--When a fluid is present between the two surfaces, they are separated by a pad of fluid, as shown in figure 20. The thickness of this fluid pad is a function of the fluid viscosity, contact force, contact area, equivalent diameter of rolling, and the rolling speed of the contact. The equivalent diameter of rolling is the spherical diameter that will yield the same contact area; this is used for comparative purposes when the actual contact area is an ellipse. The film thickness is (ref. 3):

$$t_{FILM} = 1.6\alpha^{.6} E^{.03} \left[\frac{v}{V} \right]^{.7} D_R^{.43} \left[\frac{F_N}{\sqrt{D_{MAJ}}} \right]^{-.13} \quad (7)$$

where

α = viscosity pressure component

E = material modulus of elasticity

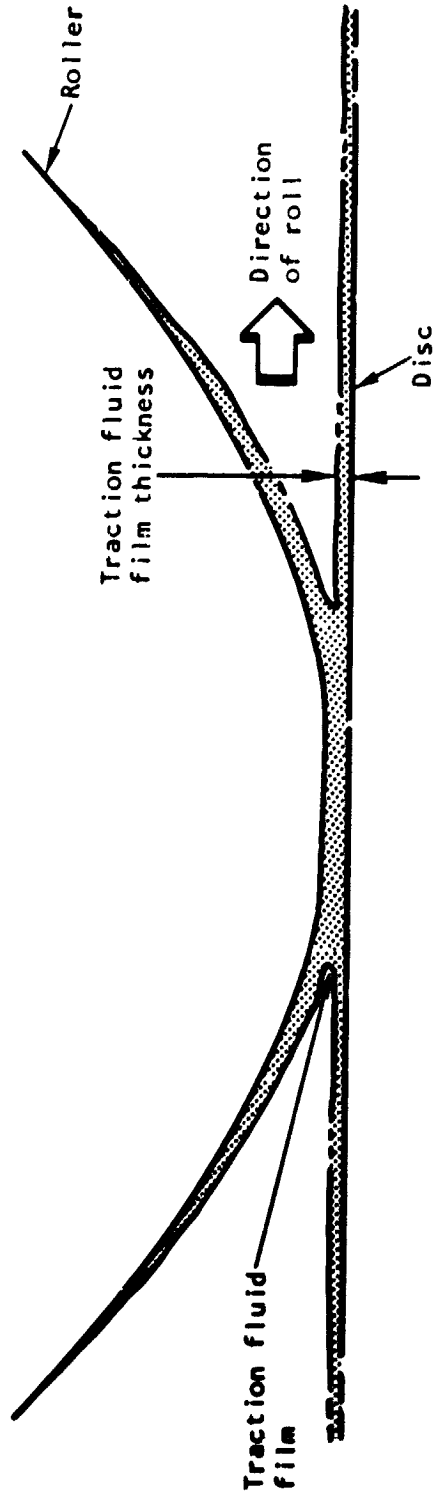
v = fluid viscosity

V = rolling speed, m/s (ft/s)

D_R = equivalent diameter of rolling

F_N = normal force

D_{MAJ} = major diameter of contact area



S-48734

Figure 20.--Fiim thickness

Tangential force.--This is the power carrying force along the plane of the traction contact; the force that transmits torque from one traction part to another part (see fig. 18). The tangential force is transmitted between the traction parts through the resistance to shear of the fluid within the traction contact.

$$T_F = \frac{T}{R_C N_{ROLL}} \quad (8)$$

where

T = the torque on the disc

R_C = the contact radius

N_{ROLL} = number of rollers

Traction coefficient.--The traction coefficient is defined as the ratio of the tangential force to the contact force. It is a measure of the ability of the fluid to sustain shear.

Spin.--In a traction drive, the roller rolls on the disc in a curved path; therefore, for an elliptical contact area oriented with its major axis perpendicular to the direction of roll, the outer edge must traverse a larger distance than the inner edge as it rolls over this curved path (fig. 21). This rotation, superimposed on the rolling contact due to a curved roll path, is called spin. The rotation is about an axis normal to the contact plane.

Creep.--Creep is defined as the motion of one traction surface relative to the other traction surface due to the shearing in the traction fluid. In a traction drive, a torque is transmitted to the roller through the fluid film. As the disc rotates, shearing occurs in the traction fluid, resulting in the disc moving a greater distance than the roller (fig. 22). The difference in relative motion is called creep:

$$C_R = \frac{\tau_{ROLL}}{12 V} \quad (9)$$

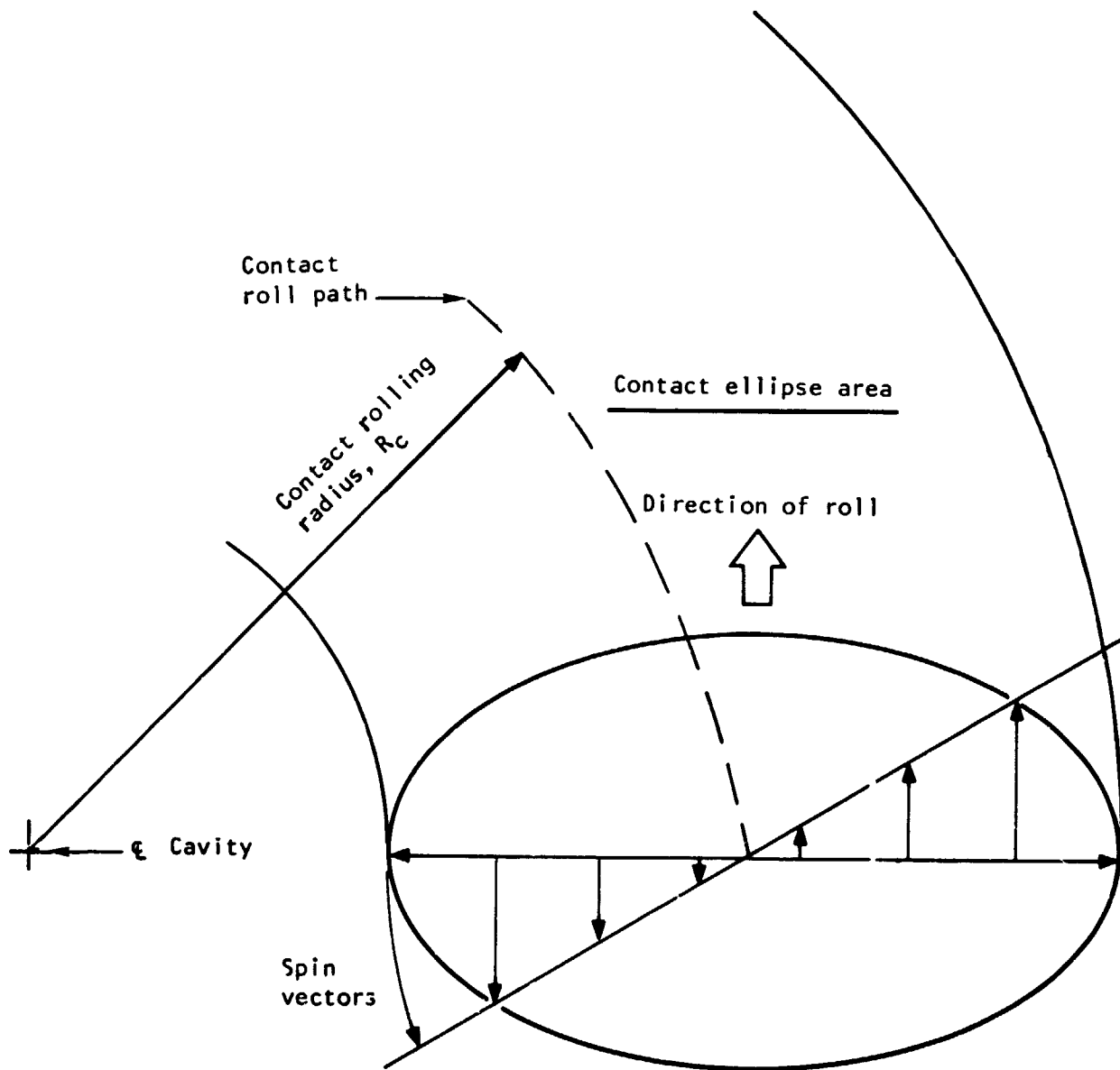
where

τ_{ROLL} = the shear rate in the direction of roll

V = rolling speed

It is often more convenient to express creep as a percentage. It can then be related to most other contact parameters:

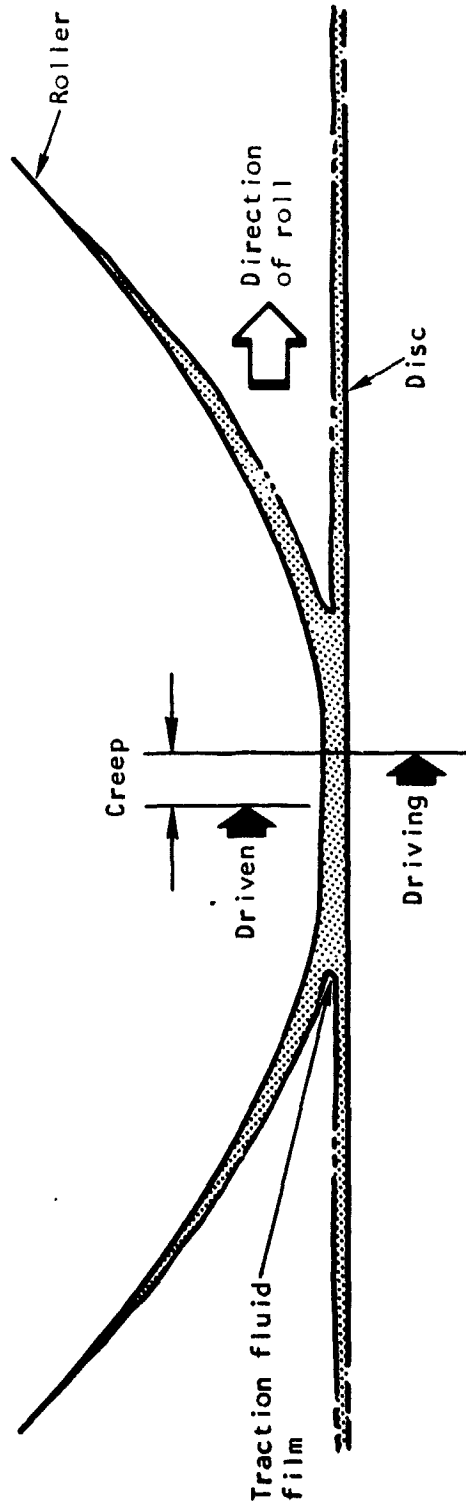
$$\text{Percent } C_R = 100 C_R \quad (9a)$$



Spin--Rotation superimposed on the rolling
 contact due to a curved roll path;
 the rotation is about an axis normal
 to the contact plane

Figure 21.--Spin.

8-46737



S-46735

Creep--Motion of traction surface relative to the contacting surface due to shear in the traction fluid and strain of the roller contact ellipse

Figure 22.--Creep.

Traction drive life.--The life analysis is performed on the toroidal cavity traction components, the discs and rollers. The analysis uses the standard Lundberg-Palmgren theory for fatigue failure of two bodies in contact (ref. 4).

The total traction drive life is given by the following equations:

$$L_{10} = \left[(L_{10})_i^{-10/9} + (L_{10})_o^{-10/9} \right]^{-0.9} (BANK)^{(-1/3)}_B \quad (10)$$

where

L_{10i} , L_{10o} are the L_{10} fatigue lives of the rolling contacts subjected to a normal load Q . This may be estimated by:

$$(L_{10})_k = \left(\frac{Q_c}{Q} \right)^3 \quad (11)$$

where

$$k = i, o$$

and

i refers to the input contact and o the output contact

The basic dynamic capacity (Q_c) for each of the traction drive contacts is defined as the contact load that the contact can endure for one million revolutions with a survival probability of 90 percent. According to reference 4 the basic dynamic capacity for a rolling element contact can be written as

$$Q_c = A_1 \phi D^{1.4**} \quad (12)$$

where

$$\phi = \left(\frac{T_i}{T} \right)^{3.1} \left(\frac{\xi}{\xi_1} \right)^{0.4} \frac{(a^*)^{2.8} (b^*)^{3.5} (D)^{0.3}}{(D \Sigma \rho)^{2.1} \left(\frac{D}{d} \right)^{0.3}} u^{-1/3} \quad (13)$$

(Symbol definitions are presented at the end of this subsection.)

Power input disc and roller Contact: Let the contact point be defined by r_i as shown in figure 23. The curvature sum of the surfaces at the input contact is

$$\begin{aligned} \Sigma \rho_i &= \frac{1}{r_c} + \frac{1}{r_r} + \frac{\sin(\alpha)}{r_i} - \frac{1}{r_c} \\ &= \frac{1}{r_r} + \frac{\sin(\alpha)}{r_i} \end{aligned} \quad (14)$$

(**For $D < 1$ in., the exponent 1.8 is recommended.)

and the ratio of the curvature difference to the curvature sum is

$$F(\rho)_i = \frac{\left(\frac{1}{r_c} - \frac{1}{r_r}\right) + \left(\frac{\sin(\alpha)}{r_i} + \frac{1}{r_c}\right)}{\Sigma \rho_i} \quad (15)$$

The angle α can be determined when the contact between the roller and the power output disc, defined by the radius r_o , is known. Let $r_o/r_i = n$. One obtains from figure 23

$$\alpha = \sin^{-1} \left[\frac{(n-1)r_i}{2r_c} \right] \quad (16)$$

With $F(\rho)$ calculated, a^* and b^* in eq. (13) can be obtained from ref. 4.

$$\frac{b^*}{a^*} = \sqrt{(t^2 - 1)(2t - 1)} \quad (17)$$

And ζ and T are:

$$\zeta = \frac{1}{(t+1)\sqrt{2t-1}} \quad (18)$$

$$T = \frac{\sqrt{2t-1}}{2t(t+1)} \quad (\text{ref. 4}) \quad (19)$$

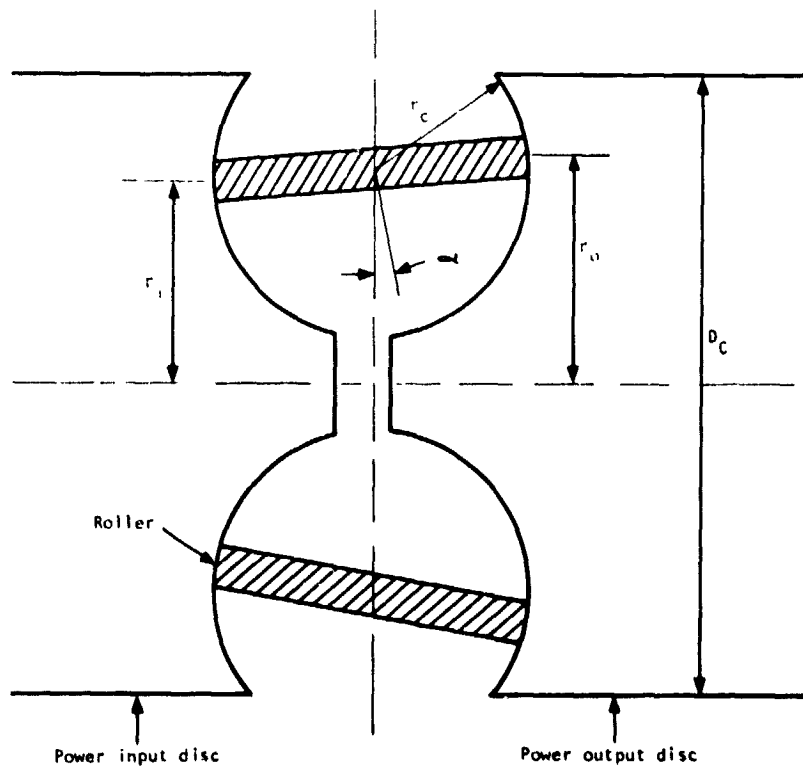


Figure 23.--Roller geometry.

For the special case of a circular contact, i.e., $b^*/a^* = 1$, one obtains

$$\zeta_1 = 0.3509$$

and

$$T_1 = 0.2139$$

The roller diameter at the contact is

$$D = 2r_c$$

and the raceway diameter of the input disc is

$$d = 2r_i$$

When the disc is rotating, a point on its contact track line is alternately stressed and unstressed twice per revolution. The number of stress cycles per revolution of the input disc is therefore

$$u = 2$$

Power output disc and roller contact: The output contact point as shown in figure 23 is defined by r_o , which is related to r_i by

$$r_o = r_i + 2r_c \sin \alpha \quad (20)$$

The curvature sum of the surfaces at the output contact is

$$\begin{aligned} \Sigma \rho_o &= \frac{1}{r_c} + \frac{1}{r_r} - \frac{\sin(\alpha)}{r_o} - \frac{1}{r_c} \\ &= \frac{1}{r_r} - \frac{\sin(\alpha)}{r_o} \end{aligned} \quad (21)$$

and

$$F(\rho)_o = \frac{\frac{1}{r_c} - \frac{1}{r_r} + \frac{\sin(\alpha)}{r_o} + \frac{1}{r_c}}{\Sigma \rho_o} \quad (22)$$

The raceway diameter of the output disc is

$$d = 2r_o$$

When the input disc revolves one revolution, the number of stress cycles on the output disc is

$$u = \frac{2r_i}{r_o} \quad (23)$$

A_1 and B in equations (10) and (12) are constants.

For bearings fabricated on 52100 steel, through-hardened to Rockwell C = 61.7 to 64.5, test data of Lundberg et al. (refs. 2 and 4) indicate $A_1 = A/0.0706$ with $A = 7450$ in inch-pound units, i.e., $A_1 = 105, 524$.

B is a life adjustment factor (ref. 5). It includes adjustment factors for material, processing, lubrication, speed effects, and misalignment. The expected traction drive life equals the rated L_{10} life times this life adjustment factor.

B = 5 in this analysis.

It may be noted that the Lundberg-Palmgren theory assumes that the risks of fatigue failure of the bodies in contact are both equally great. Because the contact track line on the rollers is constant, while on the raceways of the discs it varies with the angle α , it is likely that roller failure may be more frequent than disc failures. The L_{10} life predicted by equation (10) is therefore conservative if all parameters are accurately estimated.

Nomenclature:

A_1	material constant for the basic dynamic capacity
a^*, b^*	coefficients for determination of the major and minor semi-axes of the pressure ellipse
B	life adjustment factor
BANK	number of toroidal cavities in parallel
d	raceway diam
D	rolling element diam
L	fatigue life in millions of revolutions
Q_c	basic dynamic capacity
Q	constant load
r_c	radius of cavity
r_r	radius of roller crown
T	ratio of max. shear stress amplitude to max. Hertz stress
u	number of stress cycles per revolution of driving unit

ρ curvature

ζ ratio of depth where max. shear stress amplitude occurs to semi-minor axis of contact ellipse

Subscripts:

i input disc

o output disc

r roller

TASK I, CONFIGURATION ANALYSIS AND SELECTION

CVT design configuration analysis, selection, and optimization were divided into four steps. Each step was directed towards optimizing one aspect of the CVT design.

The first step consisted of performing a parametric study wherein changes in preselected CVT performance parameters were observed with respect to variations in the toroid and roller geometry. The purpose of this parametric study was to establish the optimal toroid geometry.

Having established the toroid geometry, the second step of the analysis, selection of the optimal CVT design configuration, was begun. The final CVT design configuration was selected from the five candidates based on the ranked design criteria presented in the statement of work. In order of their overall importance they are: efficiency, cost, size and weight, reliability, noise, controls, and maintainability.

The third step consisted of optimizing the final CVT design configuration.

A fourth and final step consisted of studying the transient load and motion characteristics of the CVT roller control system. To perform this study, an analog computer simulation was generated from a math model describing a vehicle containing a CVT.

Computer Simulation

A digital computer simulation was developed from an existing AiResearch program, and the program output data were used in the decision making process of each of the steps outlined above. The purpose of the computer simulation was to model each CVT design configuration and evaluate the traction contact and overall CVT performance under various operating conditions.

Because of the complex interrelationship between the traction contact parameters, creating an analytical model of the traction contact was difficult. The traction coefficient is affected by several contact parameters, including spin, temperature, creep, rolling speed, Hertz pressure, film thickness, the curvatures of the two elements, and the surface finish of the elements. Similarly, creep and spin are affected by some, or all, of the parameters mentioned above. The digital computer program was written to include both empirical data and analytical expressions.

The simulation uses analytical methods to determine the speeds and loads through the CVT and empirical data to evaluate the traction contact for the given operating conditions. It is constructed to be flexible using a modular form. The fluid properties and empirical data are input as data maps that can be modified as additional data become available. Independent subroutines are used to interpolate within the data maps. A mathematical model of each CVT design configuration is included in the program and uses standardized variable names. Any configuration can be selected for evaluation by setting an indicator flag.

Logic diagrams of the computer program and contact analysis subroutine are presented in figures 24 and 25, respectively.

Data inputs to the program are made through data cards and include the following:

- (1) Speed and power into the CVT
- (2) Output torque and power limits
- (3) Toroid and roller dimensions
- (4) CVT configuration, including
 - (a) Number of toroid cavities
 - (b) Number of rollers per cavity
- (5) Ratios of additional gear sets, including the planetary gear ratio
- (6) Finite toroid cavity speed ratios, up to eight possible

A first approximation is performed in which the initial gearing and bearing, traction contact, and oil pump losses are each estimated to be 2 percent of the input power. The program then proceeds through each ratio of the CVT and calculates the input and output speeds and torques, subtracting the losses as applicable. The final output power and torque are compared to the maximum allowable values specified in the input and set equal to the maximum values if they exceed the maximum value.

The contact and tangential forces are calculated using the axial force on the discs, the torque and the roller geometry. The traction coefficient is found by:

$$\mu = \frac{F_T}{F_N} \quad (24)$$

The contact area is calculated using the general formula for two bodies in contact (Appendix A), and the mean Hertz pressure is calculated by dividing the contact force by the contact area.

The average spin is calculated using the roller geometry and speeds.

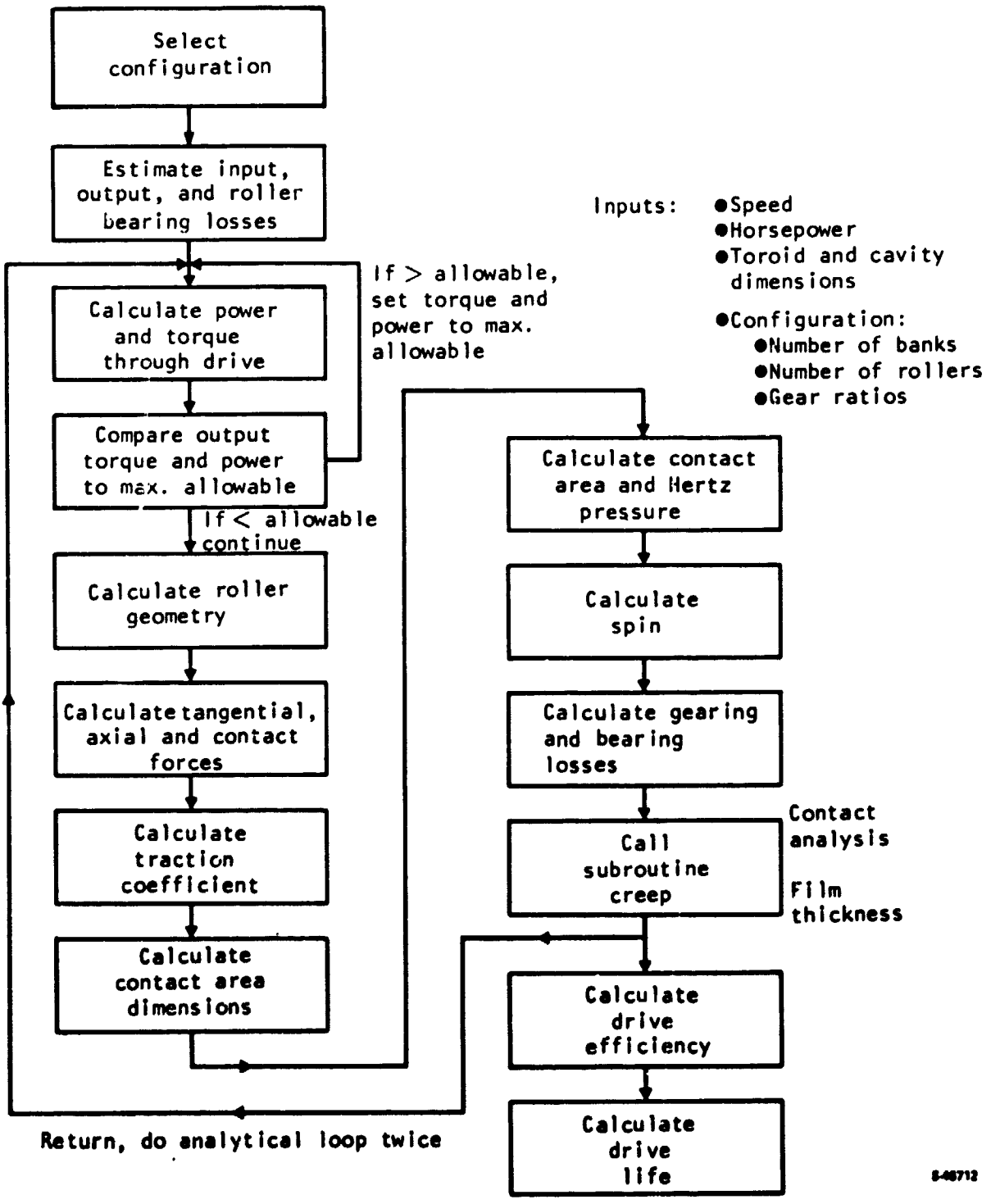


Figure 24.--Computer program.

8-48712

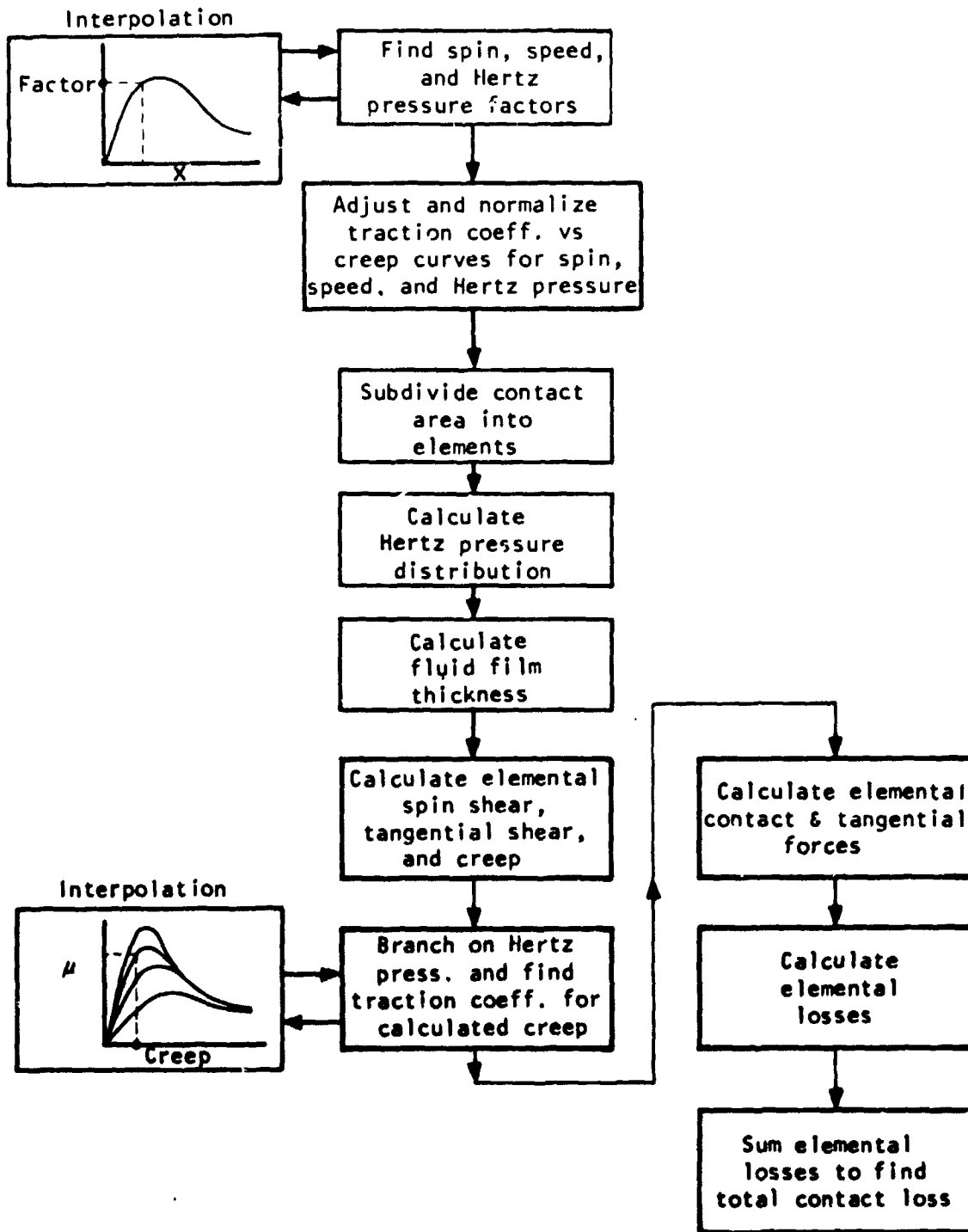


Figure 25.--Contact analysis subroutine.

848716

The final gearing and bearing losses are calculated using the loads, speed, and sizes of the elements.

The traction contact losses are calculated, and the program repeats the analysis using the actual loss values. To determine the contact loss, the total percent creep must be found. The total percent creep is the sum of the percent creep due to spin and the percent creep due to the tangential force.

Percent creep is also a function of the traction coefficient, Hertz pressure, and spin as well as other variables. The procedure used to calculate the traction loss is described below.

Research has been done using traction machines to determine the traction coefficient characteristics with respect to percent creep. The procedure is to set a Hertz pressure and percent creep and then find the traction coefficient. A typical family of traction coefficient vs percent creep curves for various Hertz pressures is shown in figure 26. As used in the program, these curves are normalized to unity and then multiplied by other correction factors.

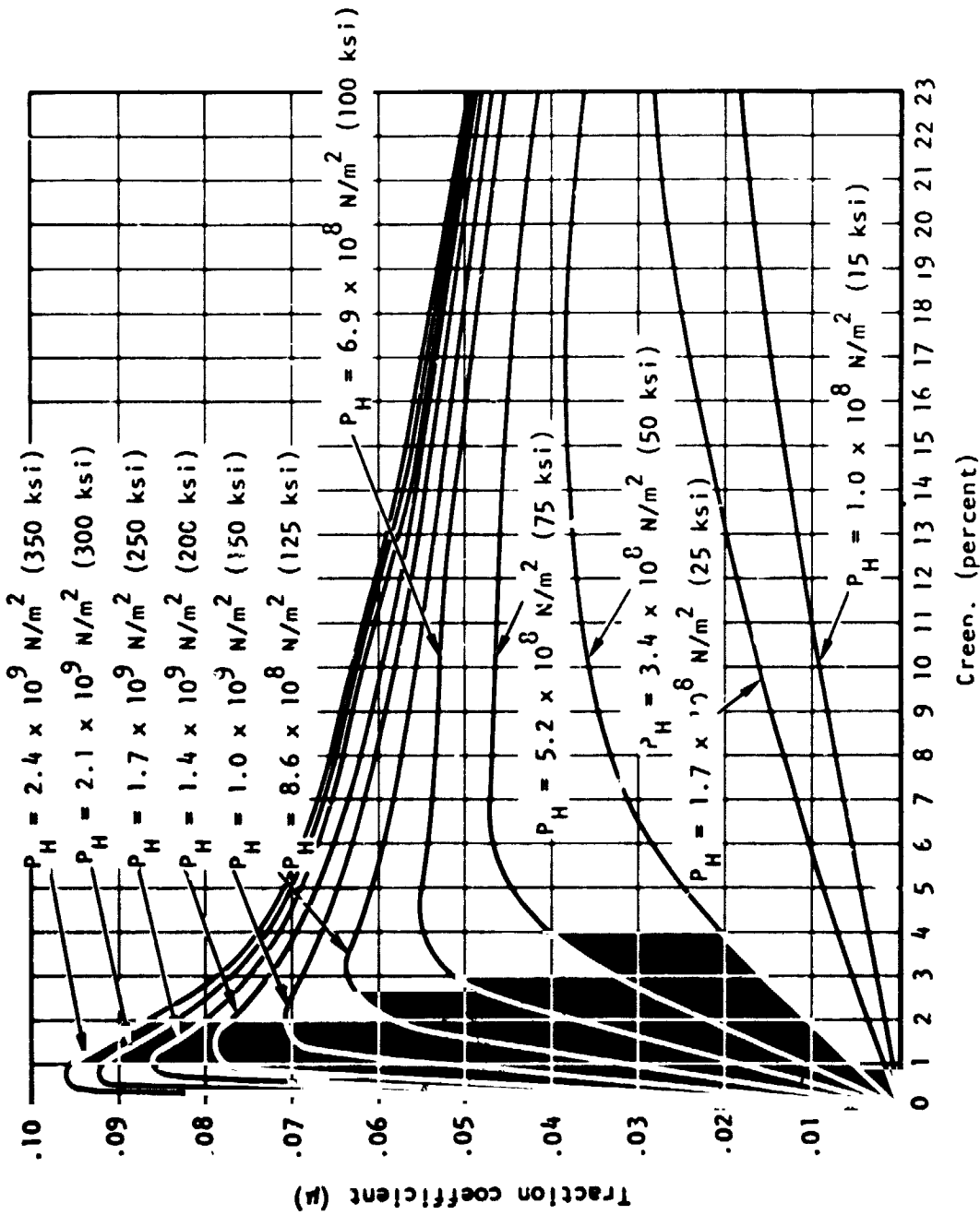
Research has been done establishing the interrelationship between the Hertz pressure, rolling speed, and spin. The results of this research are shown in figures 27, 28, and 29. Using the average Hertz pressure, the Hertz pressure factor is found by interpolating in figure 27. Similarly, the rolling speed and spin correction factors can be found by interpolating in figures 28 and 29, respectively. The traction coefficient versus percent creep curves are then modified for the actual operating conditions by multiplying them by these correction factors and a special factor for the specific fluid to be used.

To evaluate the contact loss, the contact area is subdivided into 450 subdivisions of equal size. The total creep, traction coefficient, and contact and tangential forces are calculated for each area and summed.

The actual Hertz pressure for the area being evaluated is calculated based upon the actual pressure distribution presented above and is assumed to be constant over the elemental area.

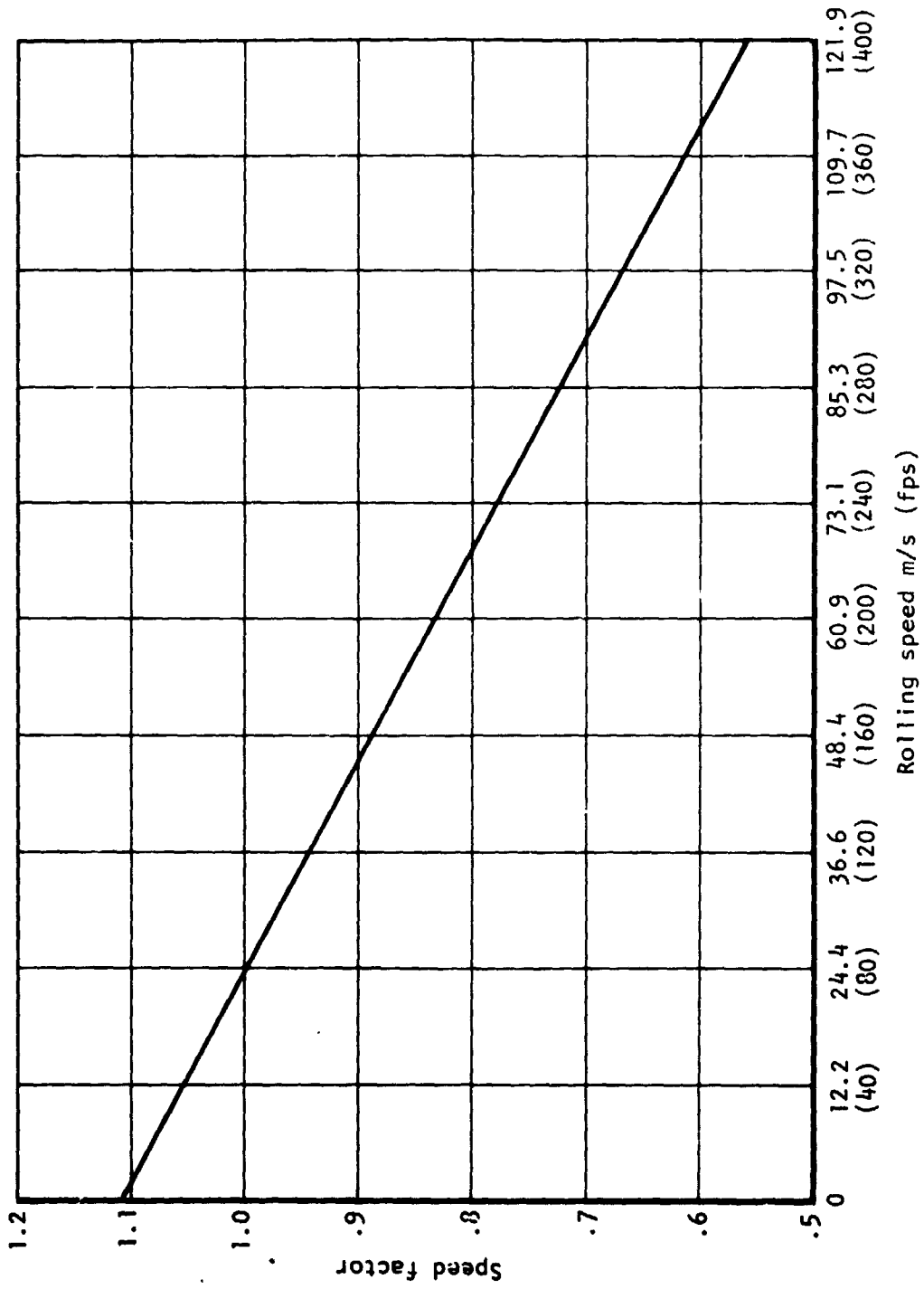
Given the Hertz pressure and the average traction coefficient needed to transmit the torque under the given operating conditions, the percent creep due to the tangential shearing can be found by interpolation (fig. 26). The creep due to spin is calculated directly, and the two are added vectorially. Having found the total percent creep, the program then returns to the parameters shown in figure 26, using the percent creep and Hertz pressure and finds, by interpolation, the actual traction coefficient. If this total value is less than that needed, the drive will not transmit the torque but will slip.

The elemental tangential and contact forces are calculated using the elemental traction coefficient. The tangential force, contact force, and percent creep are summed for all the elements. The elemental losses are calculated by multiplying the total shear rate by the elemental tangential force. The total contact loss is the sum of the elemental losses times the power through the toroid.



S-46723

Figure 26.—Traction coefficient vs creep (no spin present), P_H = mean Hertz pressure.



S-46728

Figure 28.--Rolling speed factor.

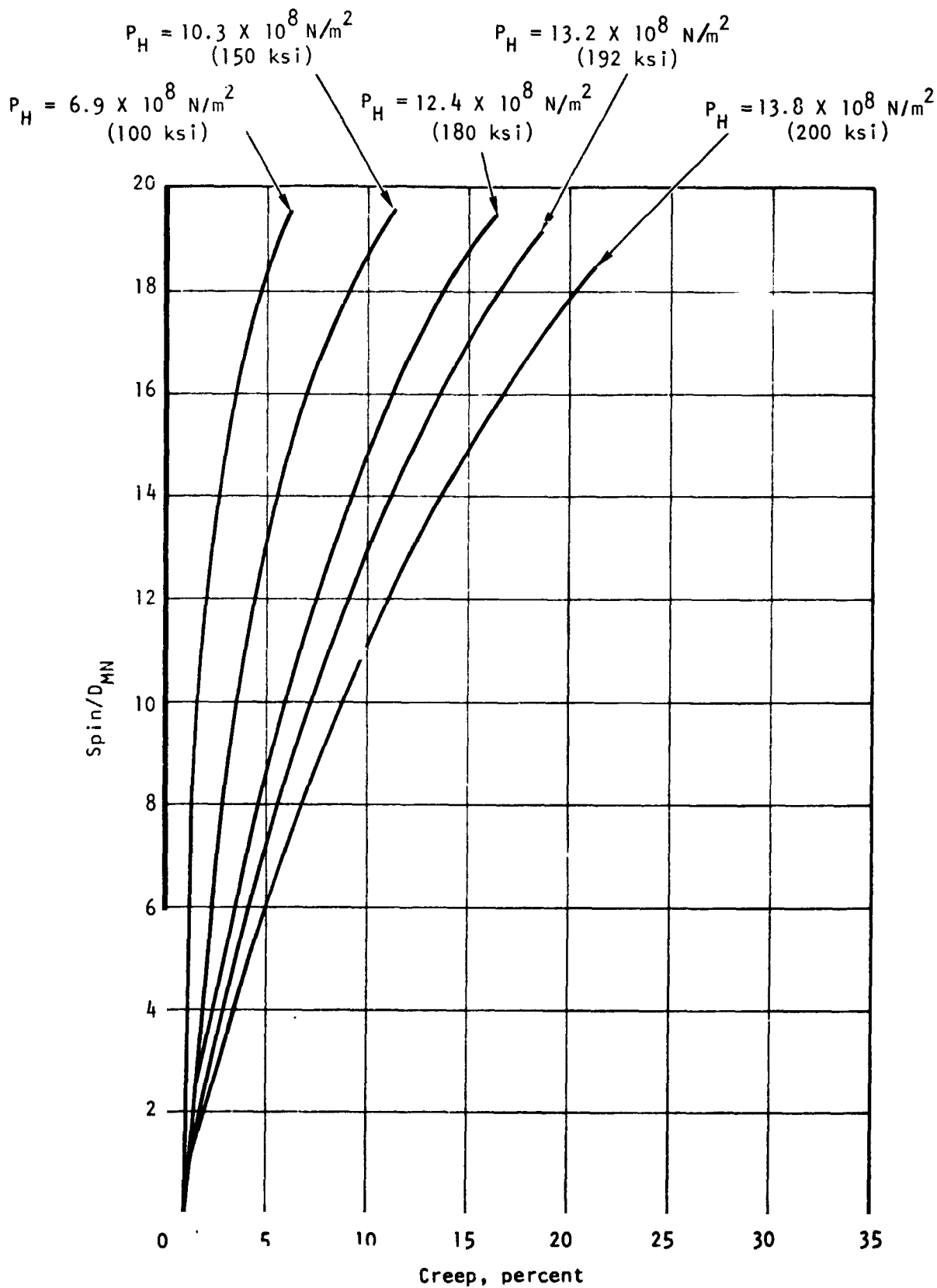


Figure 29.--Spin correction curves, P_H = mean Hertz pressure

127-A

Analysis Step 1, Parametric Study

The parametric study was the first step toward selecting a CVT configuration. The purpose of the study was to determine the effect perturbations in certain CVT parameters have on the overall toroidal cavity performance. The ratio of the cavity diameter to the toroid diameter (aspect ratio) (refer to fig. 16), the physical size, the ratio of the roller transverse diameter to the cavity diameter (conformity), the velocity of the contact, and the type of traction fluid were all varied independently according to predetermined ranges (table 1).

The CVT configuration used in the parametric study was a simple, single-toroid cavity design with a reduction gearset at the input and output ends of the toroid cavity, as shown in figure 30. The gearsets were included so that the contact velocity could be varied.

Only those parameters listed above were changed. All other operating parameters were held constant during each computer modeling run. The runs were made under the following operating conditions: input speed, 21 000 rpm; power, 16 kW (22 hp); and CVT ratio, 0.35:1. Each run consisted of "operating" the CVT at 6 discrete ratios that spanned the toroid cavity ratio range. The data from these runs were plotted and studied. The plots are presented in Appendix B, and the trends observed resulting from the study are presented in table 2.

The objective of this study was to select a CVT cavity configuration that would have high efficiency, low Hertz pressure, low to moderate energy dissipation through the traction contact, and be as small as possible. Based on the observed trends, to achieve the highest efficiency and the lowest Hertz pressure and energy dissipation, the CVT should be as large as possible and turn as fast as possible.

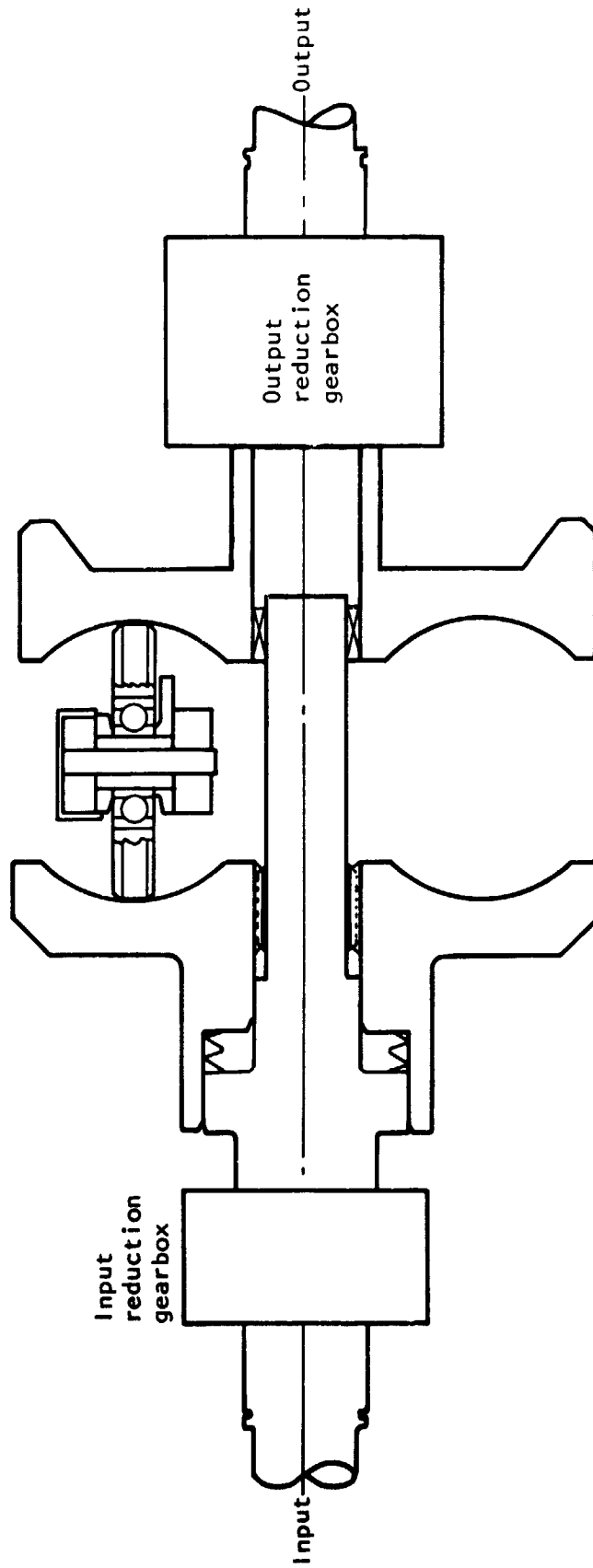
Therefore, size became an important selection criteria. With this in mind, the data were evaluated to establish the performance benefit that results from stepped increases in the toroid size. The nominal toroid diameter was selected as 112 mm (4.4 in.). This diameter selection was based on research conducted by Milton Scheiter at General Motors in 1957, where he chose a 112-mm (4.4-in.) toroid diameter for his research design of a toroidal traction drive of up to 75 kW (100 hp) and 244 N-m (180 lb-ft) of torque for automobile service. A 10-percent step in the toroid diameter was selected, yielding the 100-mm (3.96-in.), 112-mm (4.4-in.), and 123-mm (4.84-in.) diameters evaluated. The aspect ratio range and conformity range were determined in a similar fashion.

The first task, after the computer runs were made and the data were recorded, was to compare the performance for the three toroid sizes and select one for the design configuration comparison. The comparison was performed at one drive ratio. The drive ratio of 0.35:1 was selected after reviewing a tabulation of the percent change in performance at each of the different ratios when going between two toroid diameters (Appendix B). The largest changes in efficiency and energy dissipation occurred at this ratio; therefore, small changes in performance would be easily observed.

TABLE 1.--GEOMETRY SUMMARY

DTOR = 0.10 m (3.96 in.)	$\frac{DCAV}{DTOR} = 0.8$		CONF = 0.5	 Selected geometry
	$\frac{DCAV}{DTOR} = 0.9$		CONF = 0.6	
	$\frac{DCAV}{DTOR} = 1.0$		CONF = 0.7	
DTOR = 0.11 m (4.4 in.)	$\frac{DCAV}{DTOR} = 0.8$		CONF = 0.5	
	$\frac{DCAV}{DTOR} = 0.9$		CONF = 0.6	
	$\frac{DCAV}{DTOR} = 1.0$		CONF = 0.7	
DTOR = 0.12 m (4.84 in.)	$\frac{DCAV}{DTOR} = 0.8$		CONF = 0.5	
	$\frac{DCAV}{DTOR} = 0.9$		CONF = 0.6	
	$\frac{DCAV}{DTOR} = 1.0$		CONF = 0.7	

2-46744



S-46718

Figure 30.--Parametric study configuration.

TABLE 2.--PARAMETRIC STUDY TRENDS

Input conditions: Flywheel input speed, 21 000 rpm Flywheel input power, 16 kW (22 hp)			
Parameter	Efficiency	Input disc Hertz pressure	Output disc energy dissipation intensity, W/mm ²
Aspect ratio (0.8 to 1.0)	Decreases	Decreases	Decreases slowly
Physical size (toroid diam 100 mm to 123 mm)	Increases	Decreases	Decreases
Conformity (0.5 to 0.7)	Decreases	Decreases	Almost constant
Input disc speed (3000 to 6000)	Increases	Decreases	Increases at mid-speed ranges, same at extremes
Traction coefficient (Mobile 62, Santotrac 30, Santotrac 50)	Decreases at low speeds Increases at high speeds	N.A.	Increases at low speeds Decreases at high speeds

Having selected the drive ratio, the data were plotted for each aspect ratio, comparing the performance for each size. These plots, shown in figures 31, 32, and 33, were used in selecting a toroid diameter of 112 mm (4.4 in.).

A 100 mm (3.96-in.) toroid diameter was found to have high energy dissipation irrespective of the aspect ratio and high Hertz pressure. The energy dissipation ranged from 64.4 to 78.4 W/mm² for a moderate power level of 16 kW (22 hp).

A 122-mm (4.4-in.) toroid diameter was determined to be the optimum size and was selected over one of 123 mm (4.84 in.) because the increased size would result in only a 1-percent increase in efficiency, whereas the weight penalty would be significant. The disc weight is proportional to the toroid diameter to the cubic power. In addition, the weight of other ancillary parts would increase as they were made larger, including the housing, in both length and girth, and the rollers and roller mounting structure. This weight increase would result in a proportional cost increase.

The energy dissipation trends shown in figure 32 indicate a significant reduction as the toroid diameter is increased; however, the energy dissipation value of approximately 52 W/mm² for the 112-mm (4.4-in.) toroid diameter is

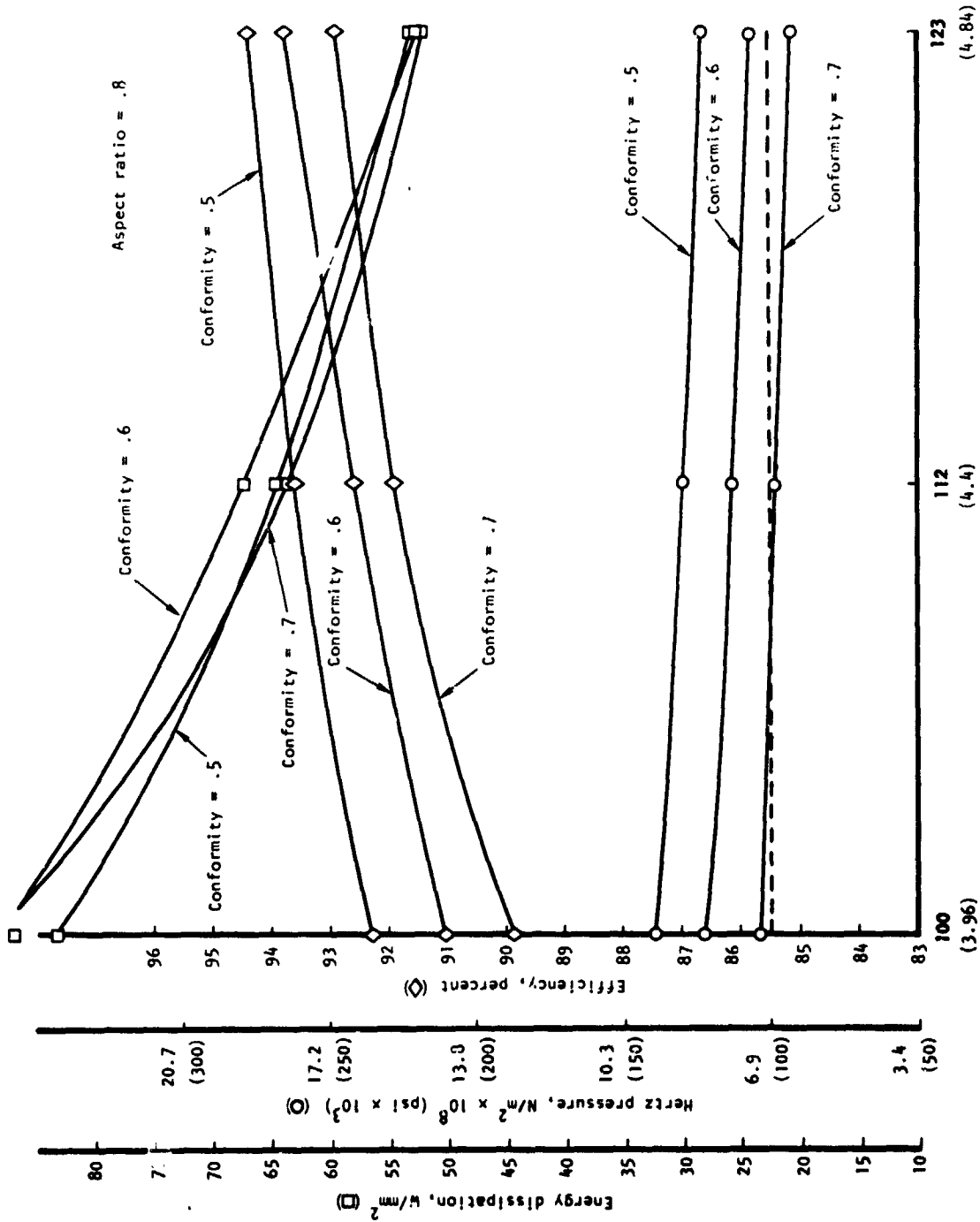


Figure 11.—Performance with aspect ratio of 0.8:1, 22 hp, input speed of 21 000 rpm, and CVT ratio of 0.35:1.

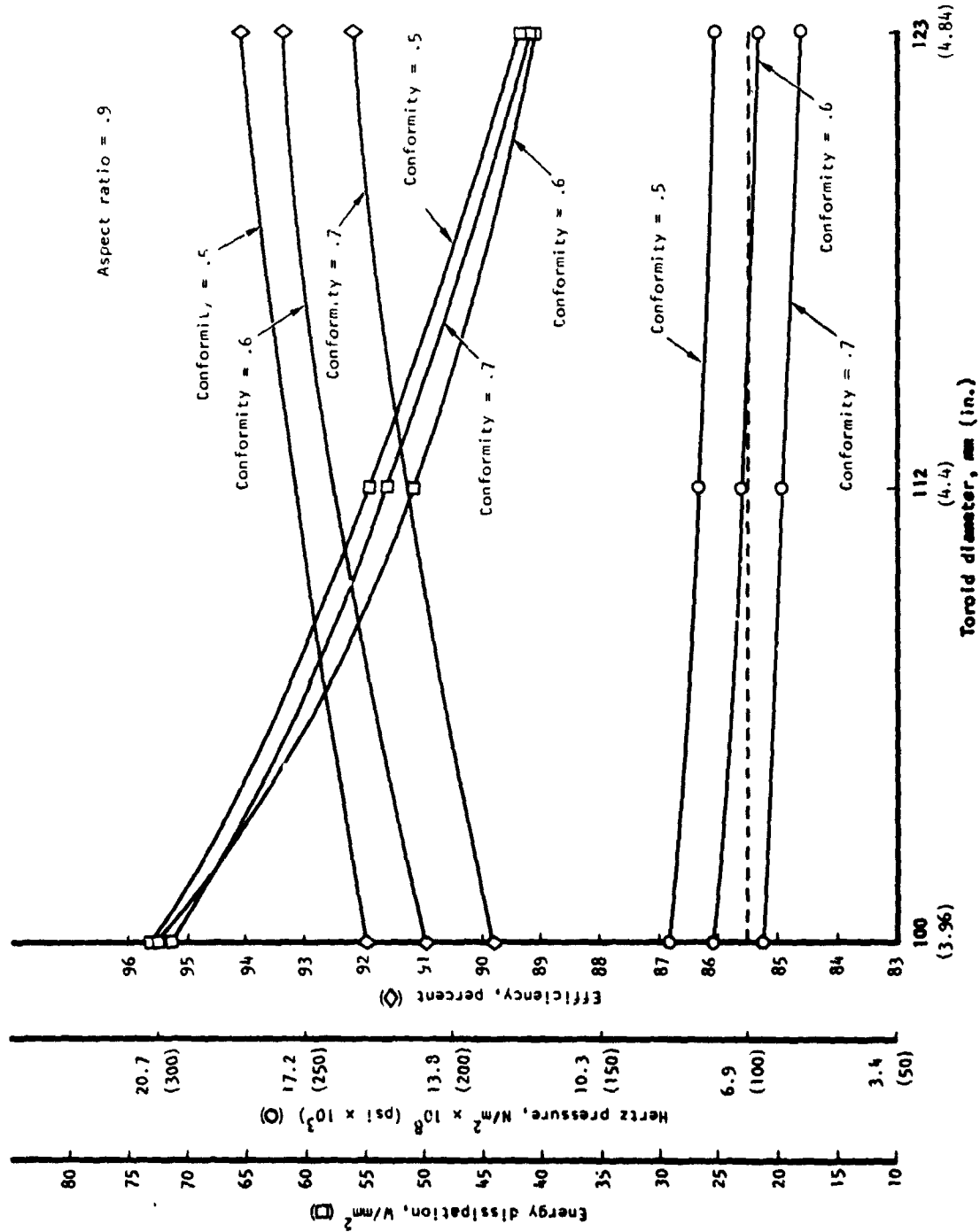


Figure 32.---Performance with aspect ratio of 0.9:1, 22 hp, input speed of 21 000 rpm, and CVT ratio of 0.35:1.

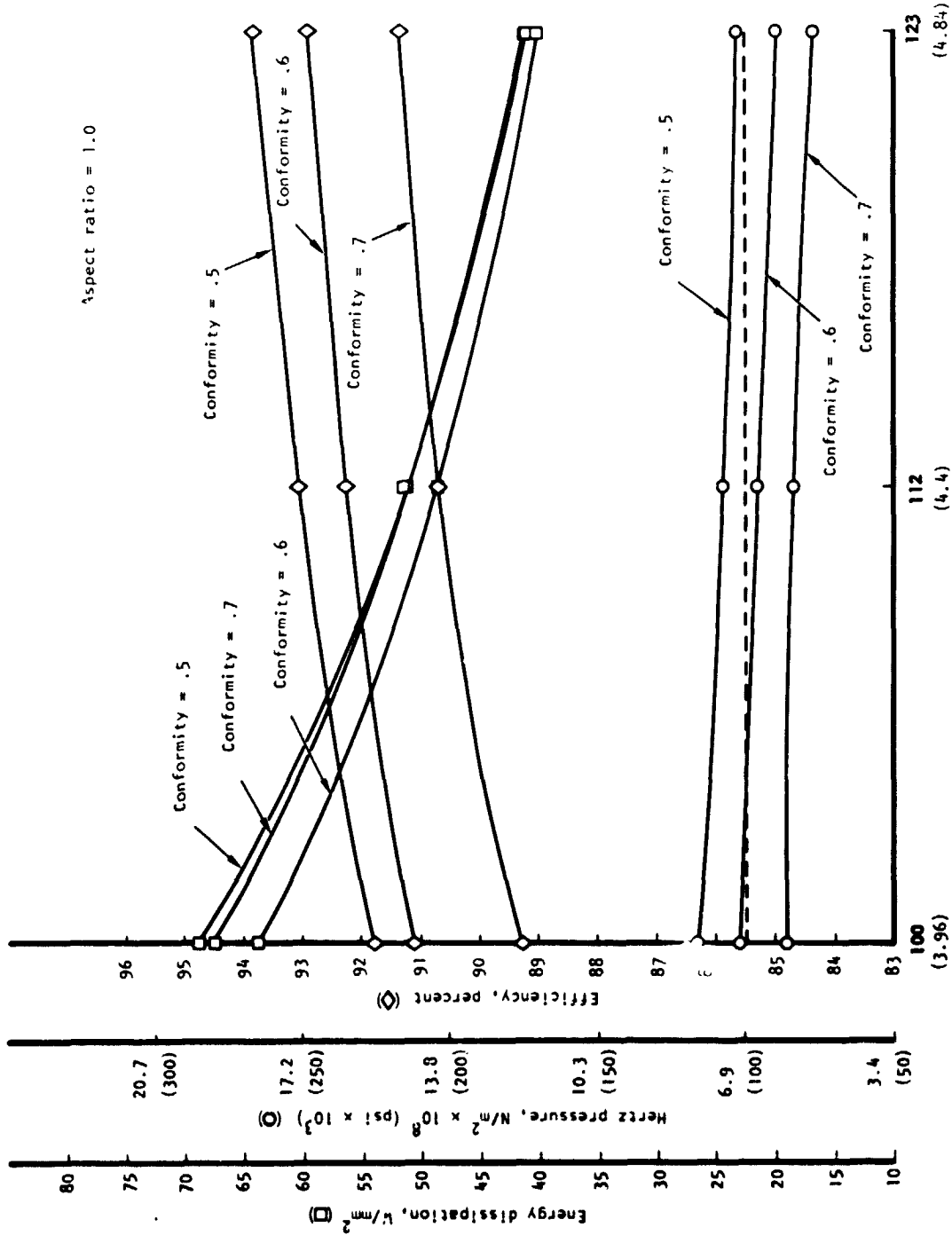


Figure 33.---Performance with aspect of 1.0:1, 22 hp, input speed of 21 000 rpm, and CVT ratio of 0.35:1.

believed to be satisfactory for the cavity design, and a further reduction associated with the 123-mm (4.84-in.) toroid diameter is not required.

Similarly, the mean Hertz pressures for the 112-mm (4.4-in.) toroid diameter are within the operating stress levels of the contact surfaces. An increase in toroid diameter does not result in a significant decrease in mean Hertz pressure and is therefore not required.

The aspect ratio and conformity were selected after evaluating plots of the performance data for the 122-mm (4.4-in.) toroid diameter at the various aspect ratios and conformities (fig. 34). An aspect ratio of 0.9:1 was selected.

The 0.9:1 aspect ratio was selected over an 0.8:1 ratio because it presented a 7.6-to 9.3-percent decrease in Hertz pressure and up to a 10-percent decrease in energy dissipation with less than a 1-percent drop in efficiency. The 0.9:1 ratio was also selected over a 1.0:1 ratio because the weight consideration became significant. Again, the Hertz pressure dropped to 5.6×10^8 N/m² (82 000 psi) with an aspect ratio of 1.0:1.

A conformity of 0.6 was selected. Its energy dissipation was the lowest of any of the conformities, and the Hertz pressure range was also the lowest while staying above 6.9×10^8 N/m² (100 000 psi). A comparison of the Hertz pressure range for each conformity is shown in table 3.

TABLE 3.-- HERTZ PRESSURE COMPARISON

Toroid diameter: 112 mm (4.4 in.) Aspect ratio: 0.9:1	
Conformity	Mean Hertz pressure range, N/m ² (psi)
0.5	1.96×10^9 to 8.15×10^8 (284 403 to 118 287)
0.6	1.74×10^9 to 7.14×10^8 (253 097 to 103 621)
0.7	1.54×10^9 to 6.14×10^8 (224 006 to 89 151)

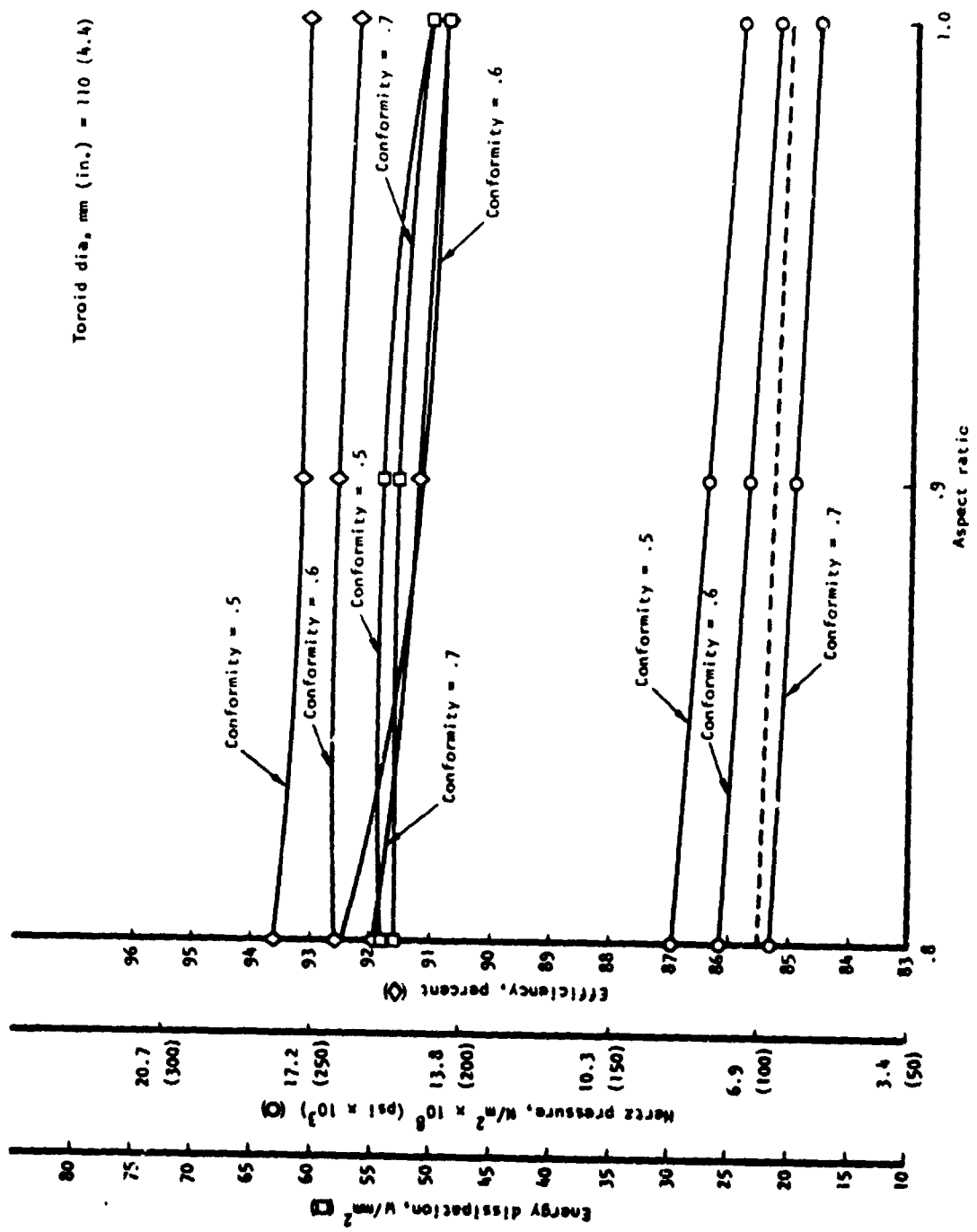


Figure 34.—Performance with toroid diameter of 110 mm (4.4 in.), 22 hp input speed of 21,000 rpm, and CVT ratio of 0.35:1.

A toroid diameter of 112 mm (4.4 in.), a cavity diameter of 100 mm (3.96 in.), an aspect ratio of 0.9:1, and a conformity of 0.6 were selected as the toroid geometry for the CVT design configuration comparison.

Analysis Step 2, Configuration Selection

The selection of the final CVT configuration was made after evaluating and comparing the five candidate configurations. In each case the toroid cavity geometry conformed to that selected in the parametric study: an aspect ratio of 0.9 and conformity of 0.6.

The first step in the selection process was to determine whether each design configuration could meet the design requirements. This consisted of evaluating each design configuration with regards to meeting the power, speed, and ratio requirements. A design configuration was eliminated from further consideration if it was too large, demonstrated low operational efficiency, or could not meet the design requirements without an advance in the state of the art.

The second step was to analyze the remaining design configurations by use of the computer simulation. The final design selection was made based on a review of the five CVT configurations and by an examination of the computer simulation performance data. The regenerated, dual cavity, full toroidal design was selected over the other four configurations. The selected design is capable of meeting the program goals and specifications without an advance in the state of the art. The selected design provides an infinitely variable transmission ratio range without the use of a slipping clutch. In addition, the balanced load, dual cavity toroid CVT has better performance than the alternate approaches provide.

Each of the design configurations is discussed below.

Baseline configuration.--A single cavity full toroidal traction CVT with traction differential planetary output section in load balance (Baseline drive, fig. 4) was the baseline design for the CVT study.

Detailed analysis of the baseline design revealed large differences in the axial load capabilities between the two traction sections. As a result, the Hertzian pressure forces on the variable ratio section and the regenerative section (planetary differential) were difficult to balance simultaneously. Because the planetary differential was used to force balance the toroidal section, it was subjected to identical axial loads. Also, because the ring-to-sun ratio was selected to meet the specified output speed requirement, there was little flexibility in selecting the contact angle of the planets or the number of planets. Analysis of the gyroscopic forces developed when running the differential planetary carrier with the planet axis nonparallel to the carrier rotational axis, showed that decreasing the planet contact angle to reduce the contact load increases the gyroscopic unbalance to an unacceptable value. For use with lower output speeds, a reasonable engineering compromise may be made and a servicable drive designed.

Regenerated, dual-cavity configuration.--A regenerated, dual-cavity, full toroidal CVT (fig. 8) was the second design approach that was examined. To

meet the specified output speed requirements, a geared planetary differential was used on the output of the CVT. Through the selection of an input speed reducer of 3:1, the flywheel speed was reduced to optimum CVT operating speeds.

Power is transferred from the center output section of the CVT, to the ring of the planetary gear differential through a jackshaft with a 1.85:1 reduction ratio. The ring-to-sun ratio of the differential is 4.5. This provides a transmission output speed range from zero to 5000 rpm with an input speed range from 28 000 to 14 000 rpm.

In practice, the output speed was actually designed to go slightly negative. This allows the load type control system the capability of unloading the CVT from excessive torques when operating in the fully regenerated condition (zero output speed). To provide further protection, a torque limiter clutch was incorporated in the regenerated power loop.

Because of the recycled power within the CVT when operating at reduced output speeds, the CVT losses are increased and the efficiency decreased over a straight nonregenerated CVT.

Shifted, dual-cavity configuration.--A nonregenerated configuration was also analyzed. The design included a dual-cavity, full toroidal CVT incorporating one or more shifts to provide maximum efficiency (fig. 6). Without regeneration, the CVT did not have internal recycled power. It could be somewhat smaller, and operate with less losses; however, the CVT output speed could not go to zero. A slipping clutch was judged capable of providing acceptably smooth startup and adequately low creep speed for stop and go traffic, if the minimum CVT output speed was kept below 200 rpm. Because the flywheel power source had a 2:1 speed reduction while the vehicle speed was increasing, the CVT had to have a ratio range of 50:1 to provide a 200 rpm minimum output speed.

The full cavity toroidal CVT has a maximum usable ratio range of about 8:1 (2.8:1 to 0.35:1). Thus, a single-shift step of 6.25:1 or double-shift steps of 2.5:1 each, are required. The double-shift design was judged to be overly complex and was not pursued. The single-shift configuration shift step was analyzed and is very promising for an advanced design CVT.

A detailed examination of the shifting process revealed that the reduction lock-out clutch must be modulated to smoothly hold driveline torque while the CVT ratio was adjusted for synchronization. A review of the available technology indicated that such a controlled shift with a modulated clutch was beyond the current state of the art. General Motors was successful with a maximum shift of 1.8:1 using electronic controls. The same shift using hydraulic controls was not acceptable. With the rapidly progressing state of the art in electronic controls, a shift step of 2:1 could probably be used and a development program could produce the technology for a 7:1 shift. Such an effort is viewed as a required technological advancement.

Series, dual-cavity configuration.--A series or tandem design configuration consisting of dual toroidal cavities in series (fig. 5) was analyzed. The preliminary analysis showed this design configuration to require a large secondary toroid disc and complex roller control system. The second toroidal drive would

have to be designed to handle all torque and speed multiplication from the front drive, resulting in an excessively large toroid size. In addition, the two toroid drives would require different loading forces as they moved to various ratios creating a force balancing problem similar to that described for the baseline drive. The roller control system would be much more complex than for the other design configurations because both rollers would need to be controlled independently. A logic system would have to be included in the controller to determine which drive was adjusted in response to a change in operating conditions. Based on these considerations the series or tandem design configuration was dropped from further consideration.

Inverse-regenerated dual cavity configuration.--An inverse-regenerated design configuration (fig. 7) was analyzed as a possible alternative to the straight regenerated configuration. In this configuration, the input shaft drives the ring gear of the epicyclic gearset while the output from the variable ratio toroidal drive drives the sun gear. The planet carrier is the transmission output.

Unlike the regenerated transmission, minimum output speed (zero) is obtained when the variable ratio toroidal drive is in a maximum speed-up ratio. The pitch line velocity of the sun gear is equal to the pitch line velocity of the ring gear.

Maximum recycled power occurs when the toroidal drive is running at maximum speed. This increases losses and reduces the life rating for both the traction drive components and support bearings.

The inverse-regenerated configuration was rejected, therefore, because it demonstrates poorer efficiency and reduced life rating at maximum operating speed.

Analysis Step 3, Design Optimization

The purpose of the CVT design optimization was to obtain the smallest, lightest, lowest in cost, and most reliable design within the selected design configuration constraints. The optimization procedure consisted of performing stress, weight, reliability, and maintainability analyses to select the size, materials, and design details that would achieve the optimal CVT design. The results of these analyses are presented below. The preliminary design layout of the optimized regenerative CVT design configuration is presented in Appendix D.

Stress analysis.--The stress analysis was directed toward three critical areas of the CVT: the Hertz stress on the disc and roller, the Hertz stress on the gears, and the critical speed of the main shaft.

The critical speed analysis was performed using a lumped parameter, transfer matrix, computer program that included the effects of shear deformation, rotary and polar inertia, and bearing support stiffness and dampening characteristics. The input and output bearing spring rates were assumed to be 2.4×10^9 N/m (350 000 lb/in.) and 3.1×10^9 N/m (450 000 lb/in.), respectively. The input planetary ring gear and both input disc masses were included in the analysis.

The program calculated the critical speeds and critical speed mode shape. The first critical speed (bending mode) of the CVT main shaft system occurred at 19 690 rpm. This critical speed was 211 percent of the maximum operating speed of 9333 rpm and provided a more than adequate critical speed margin. The first critical speed mode shape is shown in figure 35.

Because the transmission jack shaft was about the same diameter as, and shorter than, the main shaft, its critical speed was higher than that of the main shaft. The maximum operating speed was 7150 rpm; therefore, the critical speed margin of the transmission jack shaft was even higher than for the main shaft.

A summary of the mean Hertz stresses on the roller and disc over the entire operating range is shown in table 4. These stresses were calculated as described in the CVT simulation subsection.

The mean Hertz stress in the discs and roller range from $22.4 \times 10^8 \text{ N/m}^2$ (324 ksi) to $6.2 \times 10^8 \text{ N/m}^2$ (89 ksi) over the entire operating envelope that is from 7.5 to 75 kW (10 to 100 hp) and 14 000 to 28 000 rpm. The lower Hertz stress level is slightly below the $6.89 \times 10^8 \text{ N/m}^2$ (100 ksi) minimum design guideline selected during the preliminary design phase; however, because this low stress occurs only at the low power levels, the potential for skidding is small.

These preliminary stress analyses show that the CVT design is acceptable for the specified operating conditions.

The gear train was analyzed using the AiResearch general gear train analysis program. This program performs elastic analysis of the gear teeth due to the interaction between meshing gears of the system. The program uses Monte Carlo techniques for optimizing specific parameters, such as: diameter change, diametric pitch, and center distances. The gear types that can be analyzed by this program include parallel and crossed axis spur and helical gear sets. The program calculates tooth deflections, Hertz stresses, bending stresses, temperature rise, and efficiency for instantaneous loadings. The gear train configuration, gear mesh identification numbers, and input and output speeds used in the analysis are shown in figure 36. The loading conditions of the gear tooth and analysis results are presented in table 5.

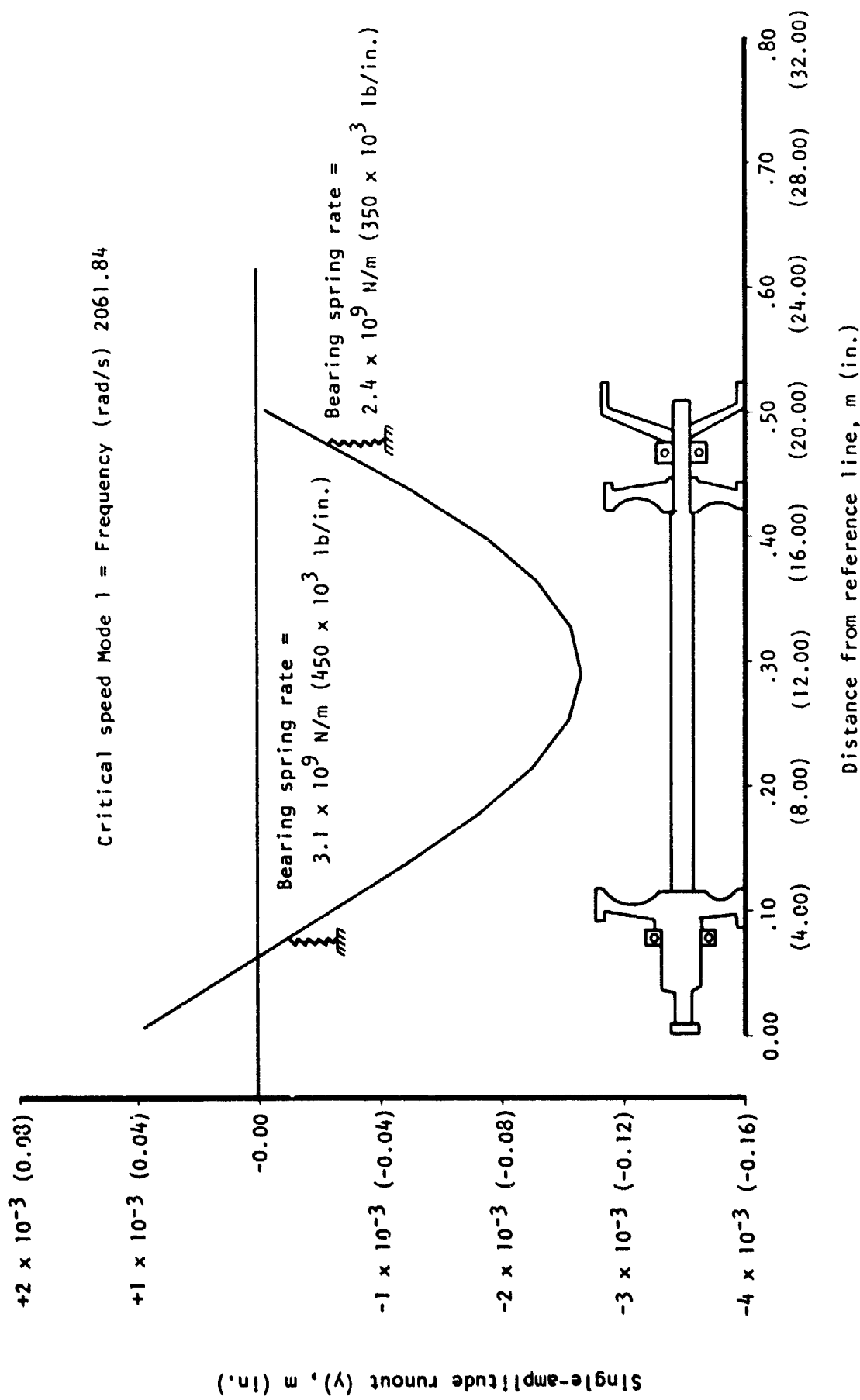
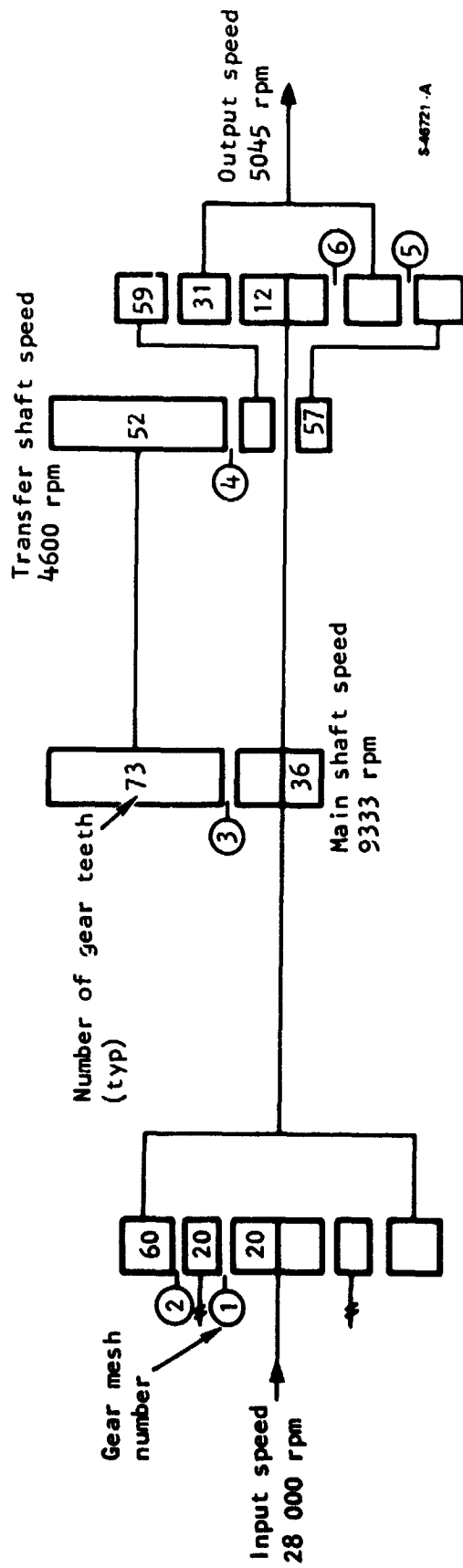


Figure 35.--First critical speed mode shape.

TABLE 4.--ROLLER AND DISC MEAN HERTZ STRESS RANGE SUMMARY,

$N/m^2 \times 10^8$ (ksi) INPUT SPEED (rpm)

Output power, kW (hp)		Input Speed		
		14 000 rpm	21 000 rpm	28 000 rpm
7.54 (10)	Input	11.4-6.2 (165-89)	22.4-6.2 (324-89)	22.4-6.5 (324-95)
	Output	10.3-8.9 (149-129)	16.1-7.9 (233-115)	16.1-7.4 (233-107)
14.9 (20)	Input	14.2-7.1 (206-103)	22.4-7.1 (324-103)	22.4-7.6 (324-110)
	Output	12.8-10.1 (186-147)	16.1-9.1 (233-133)	16.1-8.6 (233-124)
29.8 (40)	Input	17.4-8.5 (252-123)	22.4-8.5 (324-124)	22.4-9.1 (324-132)
	Output	15.6-12.2 (227-177)	16.1-10.9 (233-158)	16.1-10.3 (233-149)
52.2 (70)	Input	18.6-9.9 (269-144)	22.4-9.9 (324-145)	22.4-10.7 (324-155)
	Output	17.0-14.3 (247-208)	16.1-12.8 (233-186)	16.1-12.1 (233-175)
75.0 (100)	Input	18.6-11.0 (269-160)	22.4-11.1 (324-16.1)	22.4-11.9 (324-172)
	Output	17.5-15.9 (254-230)	16.9-14.2 (245-206)	16.7-13.4 (242-194)



S-46721-A

Figure 36.--Operating conditions for gear train analysis.

TABLE 5.--GEAR ANALYSIS RESULTS

Gear mesh	Ratio	Hertz stress N/m ² (ksi)	Average efficiency	Tangential force, N (lb)
1)	3.0:1 (Ring-to-sun)	1.1 x 10 ⁹ (161.8)	98.8	666 (149.8)
2)		1.1 x 10 ⁹ (161.8)	99.4	666 (149.8)
3)	1.85:1 (Overall)	8.1 x 10 ⁸ (117.5)	99.5	1934 (435.1)
4)		7.4 x 10 ⁸ (107.1)	98.6	2440 (549)
5)	4.5:1 (Ring-to-sun)	8.1 x 10 ⁸ (117.5)	98.8	772 (173.6)
6)		8.1 x 10 ⁸ (117.5)	99.4	772 (173.6)

As the gear analysis shows, the stress levels are well below the 1.38×10^9 N/m² (200 ksi) max. Hertz stress, which is the maximum level normally used in standard automotive industry practice (ref. 6). The preliminary gear train design is adequate for the operating conditions specified.

Cost, size, and weight.--The cost of the CVT is expected to be comparable to that of present day automatic transmissions. Both the part count and weight of the CVT are less than those for a present day transmission. In addition, no special gears, bearings, seals, or materials are needed, and though the surface condition, material conditions, and hardness of the rollers and discs must be controlled, no special processes are needed.

A detailed weight analysis was performed on the CVT. The total predicted weight for the CVT and all ancillary equipment (controller, plumbing, etc.) is 68 kg (150 lb). Details of the weight analysis are presented in Appendix C. A study was performed in 1976 to estimate the weights and manufacturing costs of automotive systems and parts (ref. 7). A list of weights for various automatic transmission configurations is presented in table 6.

TABLE 6.--TRANSMISSION WEIGHT CHART

Type transmission	Weight, kg (lb)	Automatic transmission weight to CVT weight ratio
3-speed, rear wheel drive	65 (144)	0.95:1
3-speed with lock-up, rear wheel drive	71 (157)	1.05:1
4-speed rear wheel drive	77 (170)	1.13:1
4-speed with lock-up, rear wheel drive	83 (183)	1.22:1
3-speed with lock-up, front wheel drive	70 (155)	1.03:1
4-speed with lock-up, front wheel drive	82 (181)	1.21:1

The three-speed automatic transmission is the only configuration weighing less than the CVT. The other configurations weigh 3 to 22 percent more.

A size comparison is presented in figure 37. The CVT size was compared to a standard Chrysler 904 model 3-speed automatic transmission. As figure 37 shows, the CVT is shorter by approximately 76 mm (3 in.) and slightly taller by approximately 38 mm (1.5 in.).

Reliability.--The preliminary reliability analysis of the CVT included the following components: bearings, discs and rollers, gears, and main shaft.

Survivability techniques were used to evaluate the loading and stresses in the component and then to determine the probability of the component surviving the specified operating life by comparing the operating stresses to the material strength. A normal distribution was assumed for each material strength value with 78 percent of the mean value to be at 3 standard deviations. The probability of survival was determined based on the number of standard deviations between operating stress and mean strength using tables of the standard normal distribution. The bearing survival was predicted using standard bearing life calculation methodology.

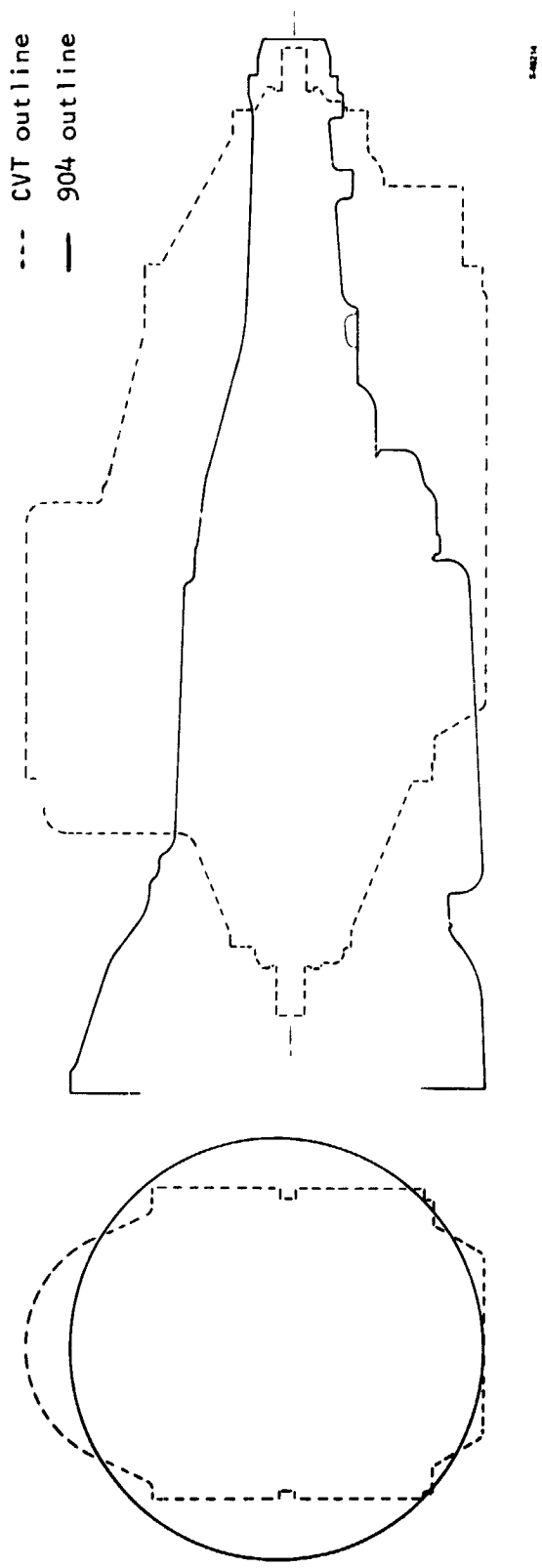


Figure 37.--CVT and Chrysler 904 size comparisons.

A summary of the preliminary reliability analysis is presented in table 7. As the table shows, there is a 98 percent probability that the aforementioned components will achieve the specified 2600 hr life when operating under the following conditions:

- (1) Average input speed = 21 000 rpm
- (2) Average output speed = 5000 rpm
- (3) Weighted average output power = 16 kW (22 hp)

TABLE 7.--PRELIMINARY RELIABILITY ANALYSIS SUMMARY

Component	Probability of survival
Bearings (10)	>0.983
Discs and rollers	>0.999999
Gears (14)	>0.999999
Main shaft	>0.99996
Total	>0.983

Noise.--The traction type configuration is inherently quiet because the traction elements are in constant contact, and there is no torsional pulsation or vibration since the elements roll on each other. When a traction element is coupled to a properly designed gear train, the CVT noise level will be quieter than that of an equivalent automotive transmission.

Maintainability.--The disc type traction drive CVT design selected from this study requires low maintenance. The CVT components are designed for greater than the specified 2600-hr operating life. No part replacement will be required during this time under normal operating conditions.

The CVT does contain a traction fluid that is used for cooling, lubrication, and torque transmission. The Santotrac 30 fluid selected for use in the CVT is a synthetic naphthenic base fluid. Because of the Hertz pressure levels present and the low energy dissipation through the traction contact, the fluid should give over 5000 hr of service life; however, leaks may develop, and overheating of the fluid can cause the fluid to break down. This fluid, however, is stable to a higher temperature than standard petroleum-based transmission fluids. The fluid level and fluid condition should be checked at each vehicle maintenance interval, and should be added or changed as necessary.

A fluid filter is located in the hydraulic system before the fluid pump. The purpose of this filter is to trap particulates entrained in the traction fluid. The filter will require minimal maintenance during the life of the CVT. This maintenance will consist of checking and cleaning the filter. The filter maintenance interval will correspond to the regular vehicle maintenance interval.

The CVT control system uses a hydraulic power supply. It is a simple force balance system that has been described earlier. This system will be adjusted at the time of manufacture of the transmission and should not need additional adjustment during the life of the transmission.

Analysis Step 4, Roller Control System Analysis

In order to study the transient load and motion characteristics of the CVT, an analog computer simulation was generated from a math model describing a vehicle containing a regenerative CVT. Only fundamental characteristics of the CVT/vehicle system are contained in this math model, which includes descriptions of the following subsystems:

- (1) Flywheel energy source with gearing
- (2) CVT torus
- (3) Torus roller control system
- (4) Torus output gearing
- (5) Vehicle with drive axle and clutch

The system math model, with detailed descriptions of these subsystems, is shown in the block diagram of figure 36. The system variables are shown in the system schematic of figure 39. A list of system variables is contained in table 8, and a list of system parameters in table 9. All mechanical elements, except the flywheel, are assumed to be massless, (no inertia) and rigid (no flexibility). The math model can be modified to add the inertias and spring rates of the development unit when this information is available.

Flywheel.--The flywheel section of the system math model consists mainly of an inertia (J_F) upon which the load torque (T_F) acts. Also included in this section is the gearing ratio (REDT) through which speed signals are reduced and the torque amplified. The load torque into the gearing (T_I) is the sum of the torques transmitted to the transmission input shaft from the CVT torus (T_{T1}) and from the transmission output gearing sun gear (T_S).

CVT torus.--The CVT torus consists of the input and output discs and the traction roller located in the center of the toroid cavity (fig. 39). Torque and speed are transmitted between the input and output discs with a continuously varying ratio. The ratio variation is achieved by varying the angle of inclination of the roller in the toroid cavity. Torque transmission between the input and output discs is assumed lossless, but the traction velocity loss, called creep, between the roller and the discs is included in the model. Creep is approximated from the digital computer model data as:

$$\text{Creep (ft/sec)} = 2.43 \times 10^{-4} (HP_F^{0.15})(N_F^{0.3})(N_{DO}^{0.8}) \quad (25)$$

where

HP_F = Power of the flywheel speed and load torque

N_F = Flywheel speed (rpm)

N_{DO} = Drive shaft speed (rpm)

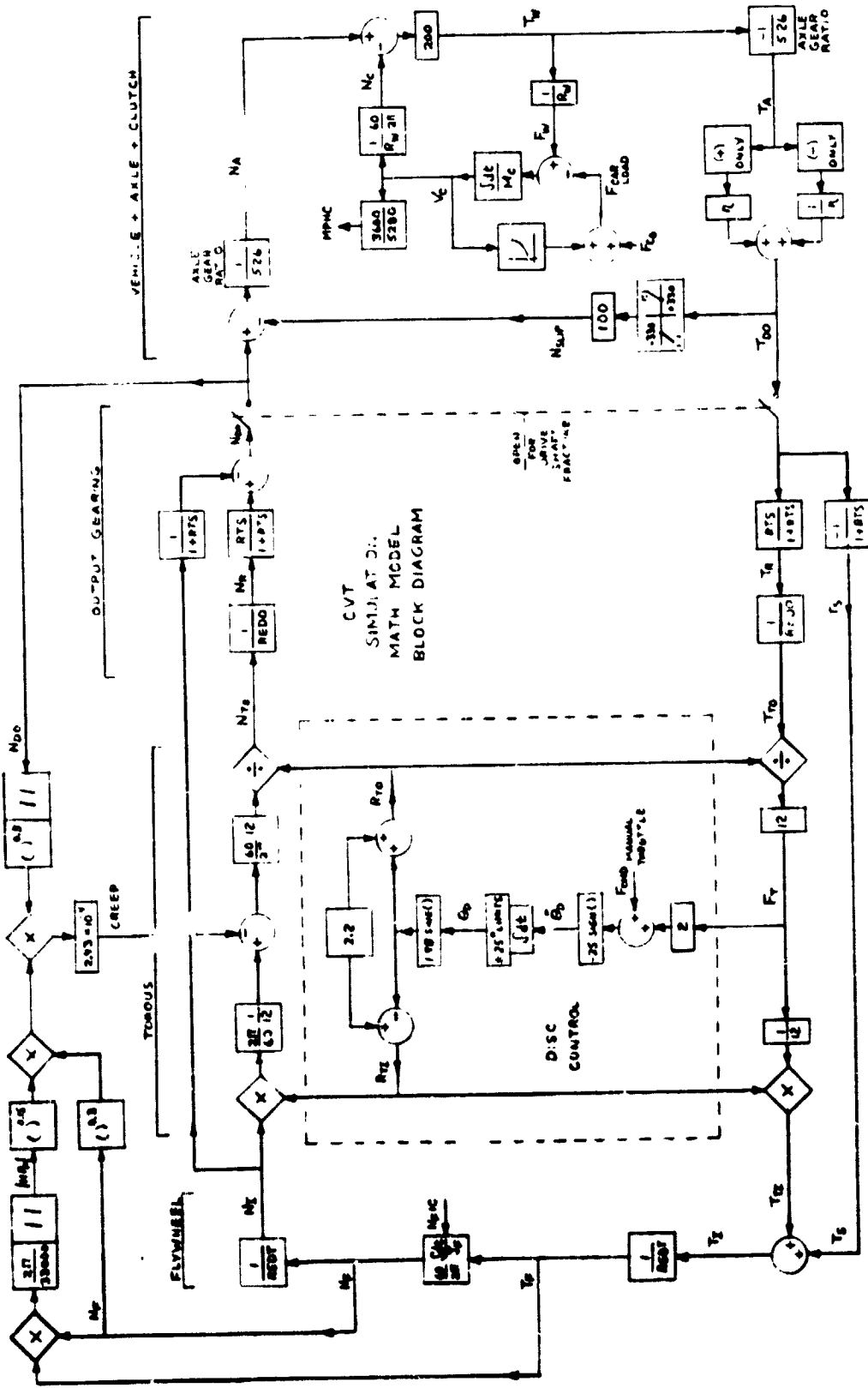


Figure 38.---Simulation math model block diagram.

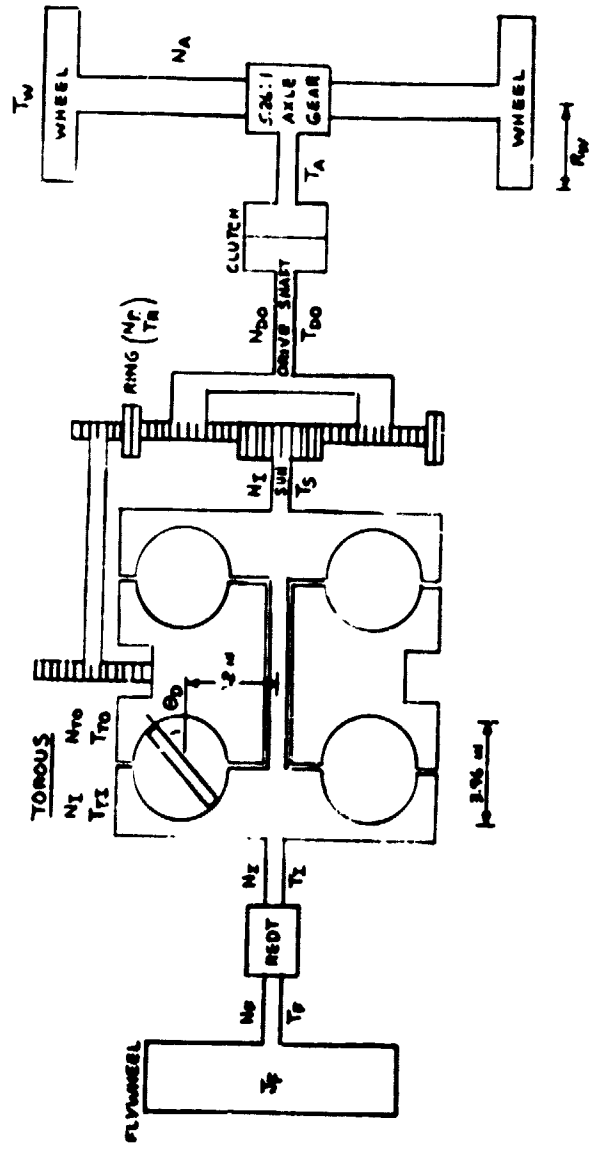


Figure 39.--Simulation math model schematic.

TABLE 8.--LIST OF SYSTEM VARIABLES

Variable	Definition	Units
CREEP	Velocity loss across torus	m/s (ft/s)
F _{CAR LOAD}	Total force load on vehicle	kg (lb)
F _{CO}	Constant part of vehicle load	kg (lb)
F _{CMD}	Disc servo force commanded	kg (lb)
F _T	Disc tangential force	kg (lb)
F _W	Vehicle wheel traction force	kg (lb)
H P _F	Flywheel power loss (gain)	kW (hp)
M P _{HC}	Vehicle speed	km/hr (mph)
N _A	Vehicle axle speed	rpm
N _C	Vehicle speed relaxed to axle	rpm
N _{CO}	Drive shaft speed	rpm
N _F	Flywheel speed	rpm
N _I	Input torus speed	rpm
N _R	Ring gear speed	rpm
N _{SLIP}	Drive shaft speed loss due to clutch slip	rpm
N _{TO}	Output torus speed	rpm
R _{TI}	Input torus radius from disc contact point to shaft \mathcal{C}	m (in.)
R _{TO}	Output torus radius from disc contact point to shaft \mathcal{C}	m (in.)
T _A	Drive shaft load torque without axle gearing efficiency losses	N-m (lb-ft)
T _{DO}	Drive shaft load torque with axle gearing efficiency losses	N-m (lb-ft)

TABLE 8.--LIST OF SYSTEM VARIABLES--Continued

Variable	Definition	Units
T_F	Flywheel load torque	N-m (lb-ft)
T_I	Total shaft load torque at torus	N-m (lb-ft)
T_R	Ring gear load torque	N-m (lb-ft)
T_S	Sun gear load torque	N-m (lb-ft)
T_{TI}	Input torus load torque	N-m (lb-ft)
T_{TO}	Output torus load torque	N-m (lb-ft)
T_W	Axle drive torque from wheel traction	N-m (lb-ft)
V_C	Vehicle speed	km/hr (mph)
θ_D	Disc inclination angle to shaft \mathcal{C}	deg
$\dot{\theta}_D$	Disc inclination rate	deg/s

The CVT torus model does not include axial loading provisions or its effect on torque and speed transmission characteristics, except through the creep equation.

Torus roller control.--Control of the roller inclination angle (θ_D) is achieved through a force balance between a commanded servo force level (F_{CMD}) and the sum of the disc tangential forces occurring between the disc edge and the two discs (F_T from each disc). Any force imbalance causes an inclination rate of 25 deg/s in a direction toward relieving the imbalance. The rate limit is obtained by limiting the force servo rate by controlling hydraulic fluid flow. With a torus radius of 56 mm (2.2 in.) and a disc radius of 50 mm (1.98 in.) the roller contact radii are:

$$\text{Flywheel side: } R_{T1} \text{ (in)} = 2.2 - 1.98 \sin \theta_D \quad (26)$$

$$\text{Axle side: } R_{T0} \text{ (in)} = 2.2 + 1.98 \sin \theta_D \quad (27)$$

The disc angle of inclination is limited to ± 27 deg, resulting in an achievable ratio range of 0.42:1 to 2.39:1. The indicated sign convention indicates that when R_{T0} is greater than R_{T1} , a speed reduction exists between the torus input and output discs with an appropriate torque amplification. The converse is true when R_{T0} is less than R_{T1} .

TABLE 9.--LIST OF SYSTEM PARAMETERS

Parameter	Definition	Value
J_F	Flywheel inertia	0.558 N-m/s ² (4.94 lb-in./s ²)
M_C	Vehicle mass	173.5 kg-mass (116.57 lb-s ² /ft)
REDO	Gear reduction ratio between output torus and ring gear	1.85:1
RED ⁻	Gear reduction ratio between flywheel and input torus	3.00:1
R_W	Vehicle wheel radius	0.581 m (1.916 ft)
RTS	Ring gear to sun gear radius ratio	4.5:1
	Total gear efficiency at axle	0.96
n	Disc diameter	100 mm (3.96 in.)
	Disc center to shaft \mathcal{C} radius	55.9 mm (2.2 in.)
	Axle gear reduction ratio	5.26:1
	Disc inclination angle limits	± 27 deg
	Disc inclination angle rate limits	± 25 deg/s

Torus output gearing.--Drive shaft motion and torque result from the summation of two power paths ending in a planetary gear arrangement. Power goes directly through the CVT to the planetary sun element and through the toroid cavity to the planetary ring element. The path to the ring element also contains a gear ratio reduction (REDO) between the toroid output disc and the ring gear. The planet carrier is directly coupled to the drive shaft. The drive shaft speed (N_{DO}) is defined by:

$$N_{DO} \text{ (rpm)} = \frac{N_{TO}}{1 + \frac{1}{RTS}} \times \frac{1}{REDO} - \left(\frac{N_1}{1 + RTS} \right) \quad (28)$$

where

RTS = Ring to sun gear ratio

N_{TO} = Torus output disc speed (rpm)

N_1 = Torus input disc speed (rpm)

With a load torque (T_{DO}) applied to the drive shaft, the torques in the two paths become:

$$T_{TO} = \frac{RTS}{1 + RTS} \frac{T_{DO}}{REDO} \quad (29)$$

$$T_S = \frac{-1}{1 + RTS} T_{DO} \quad (30)$$

where

T_{DO} = Load torque on the output disc, N-m (lb-ft)

Vehicle with axle and clutch.--A torque limiting device has been included in the simulation to limit the CVT output torque to 447 N-m (330 lb-ft). The torque limit is simulated by a slip clutch between the CVT output and vehicle axle. Axle speed (N_A) is modeled in the simulation and is equal to the drive shaft speed (N_{DO}), less any speed loss due to clutch slip, divided by the axle gear ratio. The inertial load of the car, plus windage and grade loads, is modeled by causing the two-wheel traction torques (T_F) to be generated as a function of the speed differential between the axle speed and the car speed related to the axle. The wheel traction torque for two wheels is defined by:

$$T_F \text{ N-m (lb-ft)} = 200 (N_A - N_C) \quad (31)$$

where

N_C = Vehicle speed related to axle (rpm)

The axle torque (T_A) equals the wheel torque with a sign reversal to indicate loading on the transmission in contrast to thrust on the vehicle. The drive shaft load (T_{DO}) differs from the axle torque by virtue of the axle gear ratio and the axle gear efficiency (η) of 96 percent. This efficiency is a lumped efficiency representing losses through the system gearing and changes magnitude from η to $1/\eta$ to account for load and drive torques of the car upon the transmission.

Road loading on the vehicle is an exponentially increasing function of vehicle speed and equals 1000 N (225 lb) at 128.7 km/hr (80 mph). A graph of the road loading is presented in figure 40.

Roller Control System Analytical Results

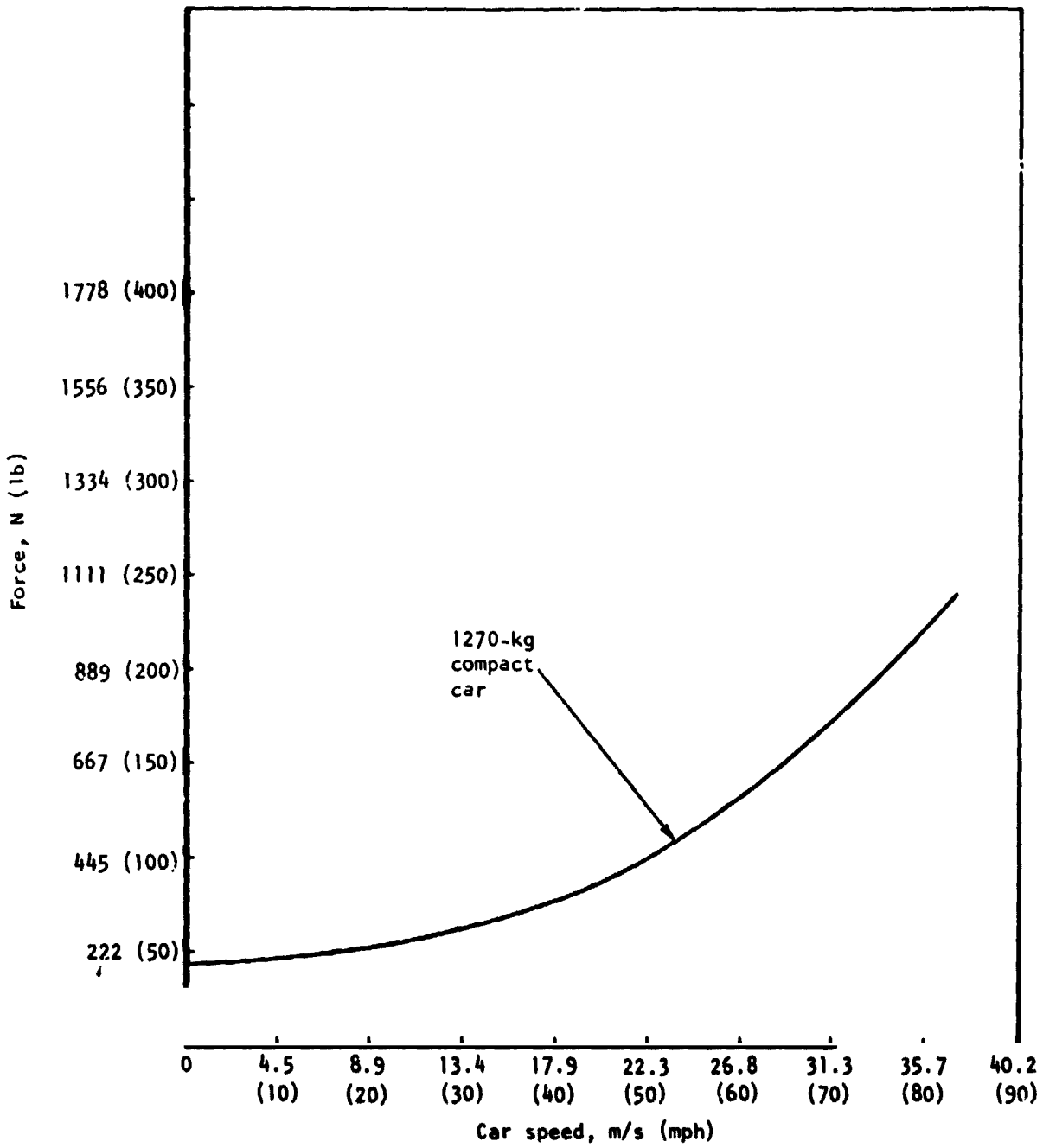
The purpose of the control system analysis is to evaluate the transient load and motion characteristics of the CVT disc and roller assembly. The analysis was performed utilizing the analog computer simulation described in the previous subsection and varying the command force in accordance with a predetermined schedule. This analysis included three parts: (1) evaluation of the slew rate of the roller as it moved from one ratio extreme to the other, (2) evaluation of the stability of the control system under maximum acceleration conditions, and (3) evaluation of the stability of the control system under a ramp increase and decrease in the command force. Each part is discussed below.

Slew rate.--The slew rate of the roller between ratio extremes was examined under two different operating conditions. First, slewing from maximum reduction to maximum overdrive, and second, slewing from maximum overdrive to maximum reduction.

Under normal operating conditions, the slew rate of the roller will track the change in velocity of the flywheel and vehicle because it is rigidly connected to both. This rate will be something less than the specified slew rate. Therefore, artificial operating conditions were imposed on the CVT to isolate it from the vehicle and flywheel after achieving an initial steady-state condition.

To slew from maximum reduction to maximum overdrive, the following procedures were used. A command force, 756 N (170 lb), was input to the CVT with 2668-N (600-lb) static drag load imposed on the vehicle. This caused the CVT to go to maximum reduction, driving the vehicle at a slow speed of approximately 0.38 m/s (2 mph). Then instantaneously, the vehicle load was removed while maintaining a constant flywheel speed and command force. This is analogous to fracturing the drive shaft in the actual vehicle and would yield the maximum slew rate.

Drive shaft fracture is simulated with switches that disconnect shaft speed from axle speed and load torques T_T and T_S from T_{DO} . Fracture thus causes T_T , T_S , and axle speed N_A to go to zero. The results are presented in figures 41 and 42 for flywheel input speeds of 14 000 and 20 000 rpm, respectively. Eight variables were plotted: command servo force, the sum of the toroid tangential forces ($2 F_T$), flywheel speed (N_F), roller angle of inclination (θ_p), ratio across the toroid cavity (R_{T0}/R_{T1}), vehicle speed (MPH_{CAR}), CVT output speed (N_{DO}), and torque (T_{DO}).



S-48713-A

Figure 40.--Road load.

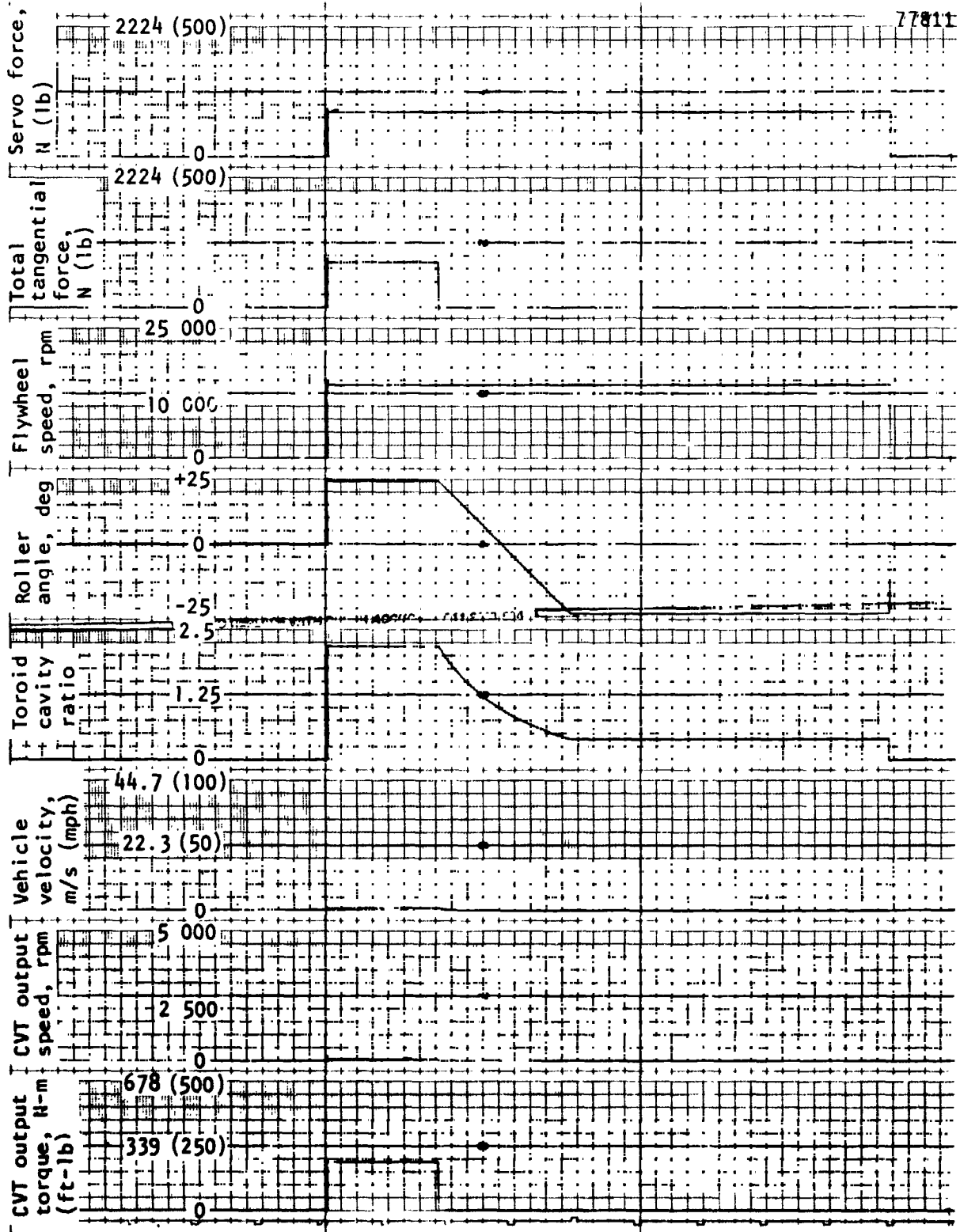
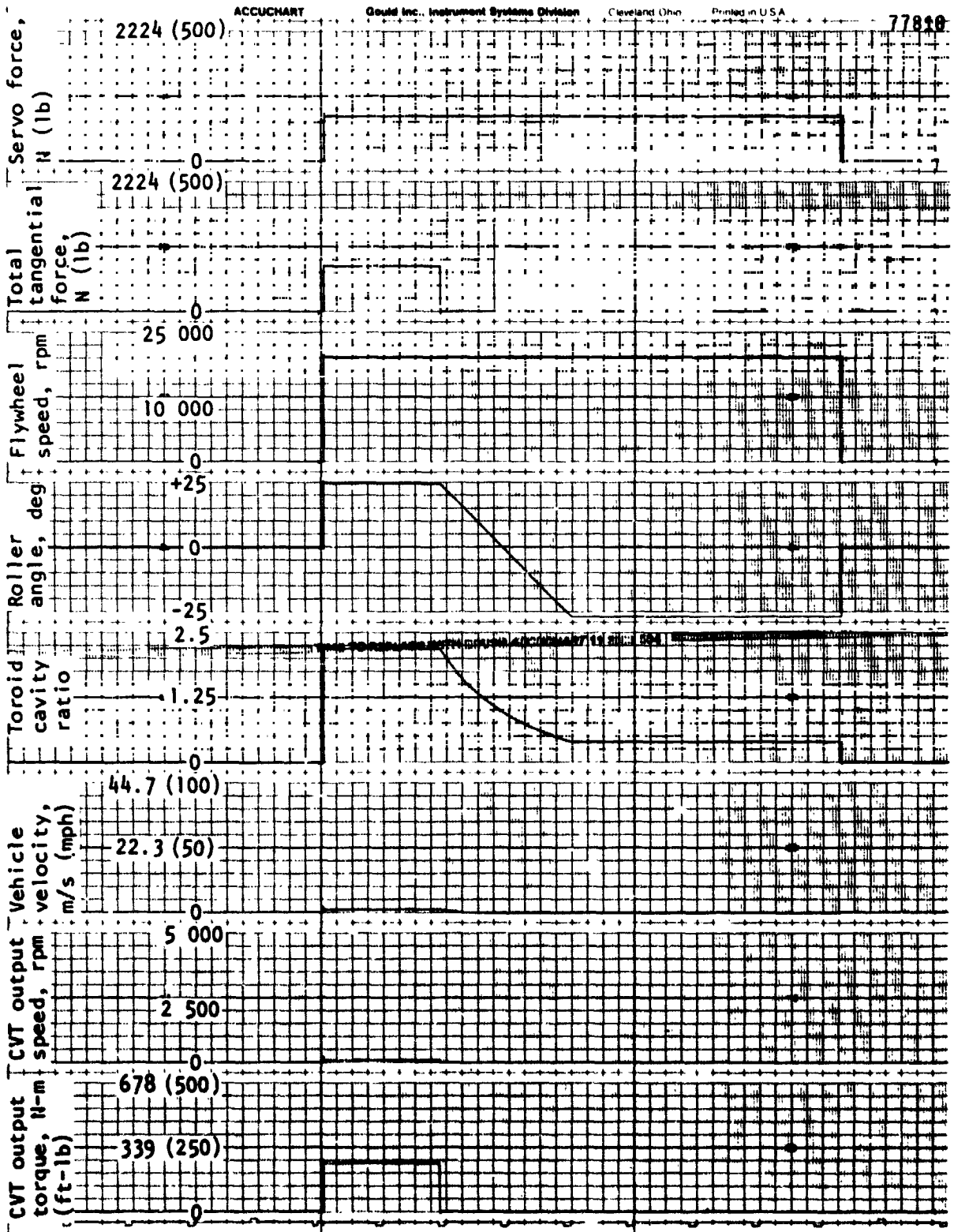


Figure 41.--Maximum reduction to maximum overdrive results for 14 000-rpm flywheel speed.



548711

Figure 42.--Maximum reduction to maximum overdrive results for 20 000-rpm flywheel speed.

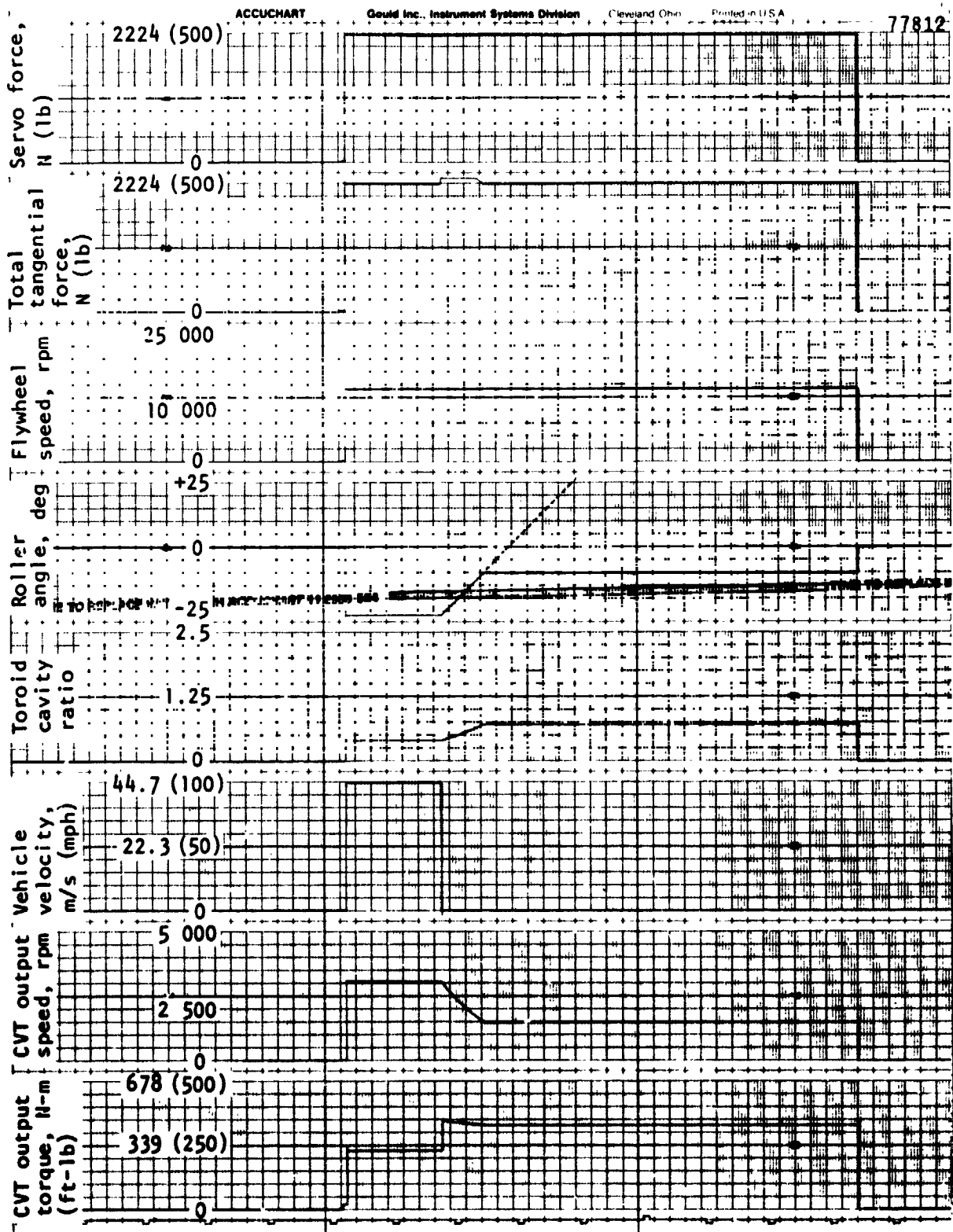
As figures 41 and 42 show, the toroid tangential forces went to zero when the load was removed, and the roller angle changed at a constant rate due to the constant command force from the initial position, +24 degrees, to the negative extreme, -27 degrees. The time ticks at the bottom of the plot show that the total elapsed time to traverse these ratio extremes was 2.08 s and 2.10 s, respectively. This is within 5 percent of the specification requirements.

It was not possible to slew from maximum overdrive to maximum reduction because of the high torques involved. For this condition, the maximum command force was input to the CVT, driving the CVT to maximum overdrive. Then, instantaneously, the vehicle was stopped while maintaining a constant flywheel speed and command force. The results are shown in figures 43 and 44 for flywheel input speeds of 14 000 rpm and 20 000 rpm, respectively.

Figures 43 and 44 show the step increase in the toroid tangential forces (the actual value of the force is unknown because it went off the scale), the decrease in CVT output speed, and the increase in CVT output torque up to the torque limit. This condition was analogous to driving a car into a wall. The transmission changed ratios to compensate for the sudden increase in the torque requirements. Once the torque limit was reached, the clutch began to slip and the CVT output speed, torque, and ratio reached a new steady state; however, the roller did exhibit a constant angular rate of change between the time the vehicle was stopped and the time the torque limit was reached. This line was extrapolated and the extrapolated portion appears as a dashed line in the figures. The extrapolated time to go between the ratio extremes is 2.18 s. It should be noted that the roller slew rate can be controlled to any level by modifying the hydraulic control system design. This analog computer analysis showed that the slew rate can meet the specification requirements.

Stability under maximum acceleration.--Two runs were made to evaluate the stability of the CVI control system under maximum acceleration conditions. In the first run, shown in figure 45, the command force was rapidly increased from zero to the maximum value. The CVT response was recorded while holding the flywheel speed constant at 20 000 rpm. Notice that at point A the toroid tangential force decreased from 2224 N (500 lb) to 1779 N (400 lb). This is due to the fact that the roller position was at an extreme, -27 deg, and the vehicle had reached steady state. The torque requirement had decreased because the vehicle was no longer accelerating, and the toroid tangential forces decreased to maintain equilibrium. The CVT was in equilibrium independent of the command force. Notice, that the command force can be decreased to 1779 N (400 lb) with no change in the steady-state condition. As the command force was decreased below 1779 N (400 lb), the roller began to change position, and the CVT output speed, torque, and vehicle speed began to decrease.

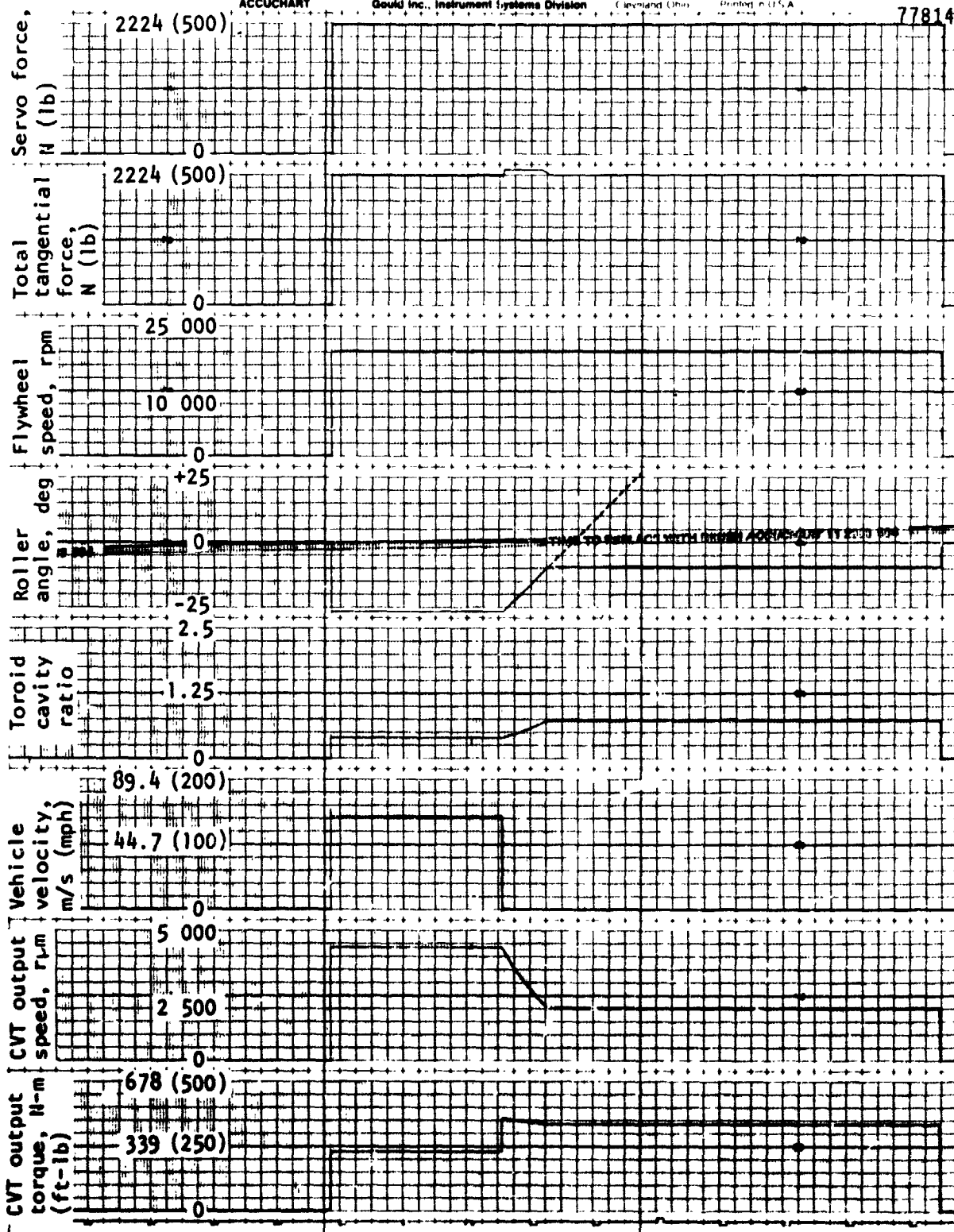
A second run was made allowing the energy to accelerate the vehicle to be extracted from the flywheel. The results of this run are presented in figure 46. The command force was increased from zero to 2224 N (500 lb). The plots show the flywheel speed decreasing as the vehicle accelerated. Again, the toroid tangential force dropped after the CVT reached maximum overdrive ratio. After approximately 45 s in the maximum overdrive condition, the



8-48768

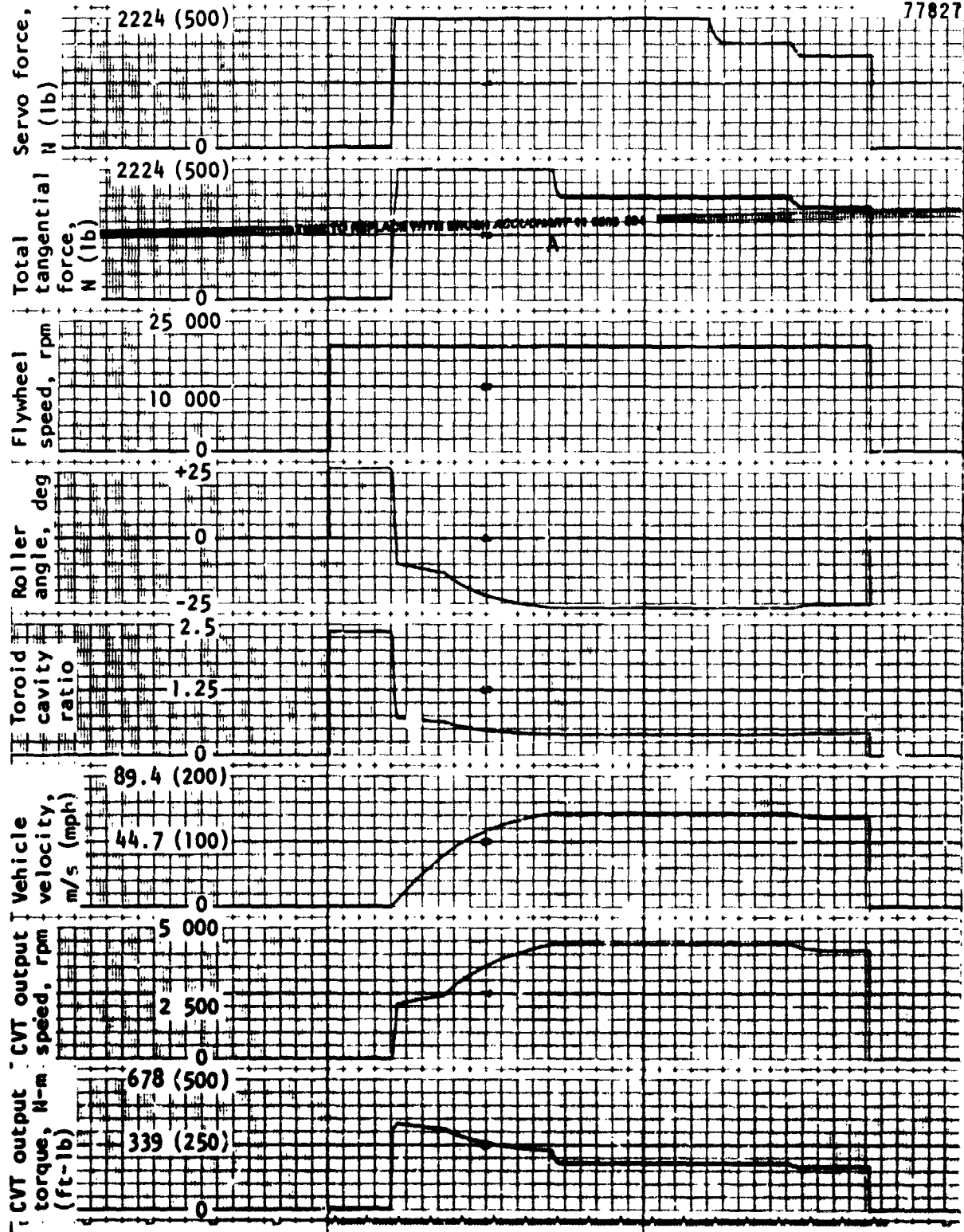
Figure 43.--Maximum overdrive to maximum reduction results for 14 000-rpm flywheel speed.

**ORIGINAL PAGE IS
OF POOR QUALITY**



8-48788

Figure 44.--Maximum overdrive to maximum reduction for 20 000-rpm flywheel speed.



6-48387

Figure 45.--Control system stability under maximum acceleration, first run.

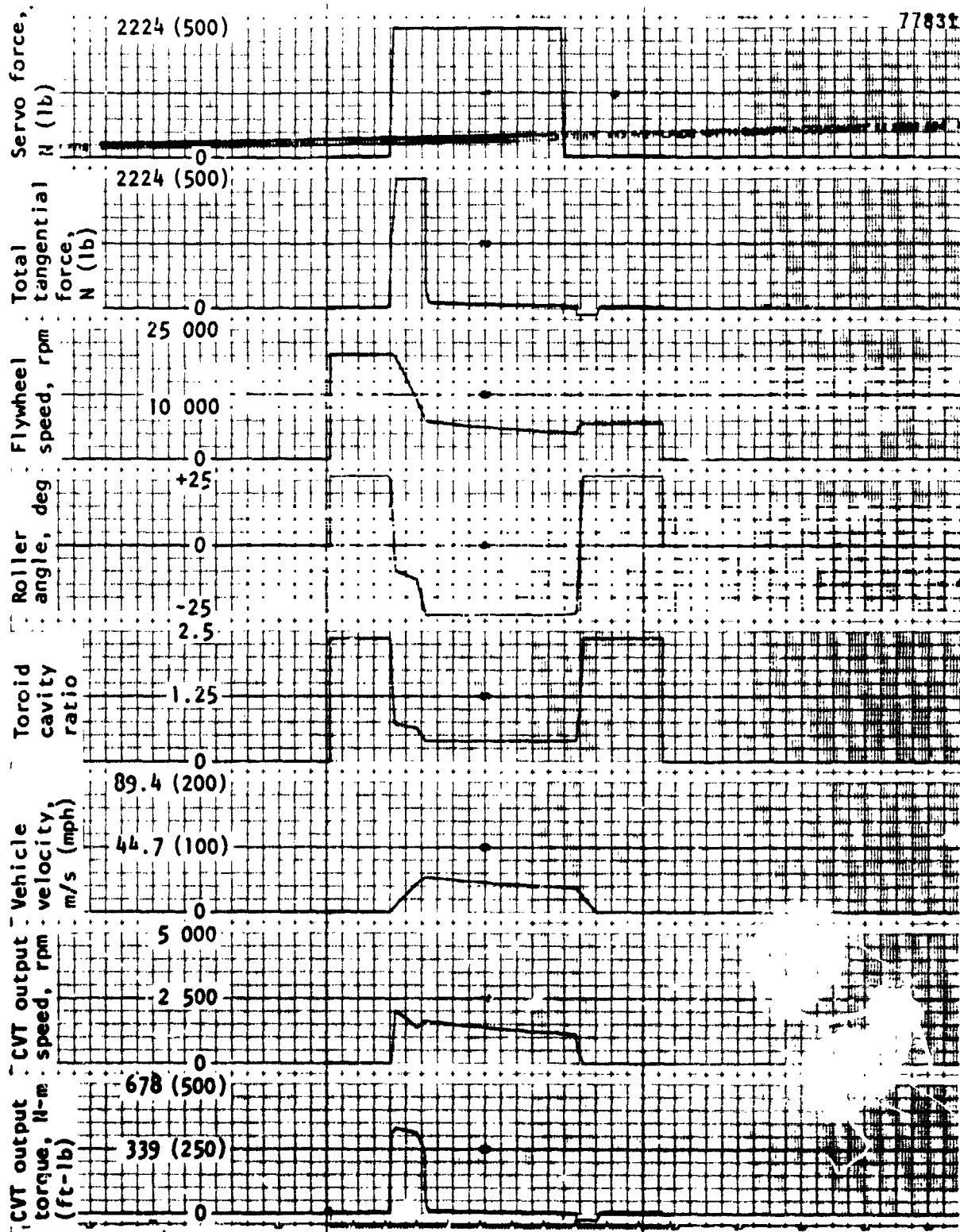


Figure 46.--Control system stability under maximum acceleration, second run.

command force was removed. This condition simulated regeneration of the flywheel. In this case, the inertia of the vehicle powered the flywheel through the CVT. When the command force was removed, a 5-s time delay was experienced because of the manual operating procedure of the analog computer. The control system response was to drive the roller to reduction. In this case, the transfer of energy from the vehicle to the flywheel occurred over a short period of time, approximately 2 s. The roller went to maximum reduction as the vehicle energy was transferred to the flywheel. This is shown by the slight increase in flywheel speed as the roller changed position and the vehicle speed dropped. Note that both the toroid tangential force and CVT output torque went negative, indicating power being transferred from the axle to the flywheel.

These two runs show that the control system is responsive to the command force supplied from the accelerator pedal. It responds quickly and smoothly, and is stable when the force equilibrium is achieved between the toroid tangential forces and torque on the output shaft. The second run also shows that the control system will control the roller position no matter which way power is transferred.

Stability under ramp command change.--The final run, shown in fig. 47, shows the control system response to a rapid increase and decrease in the command force with the vehicle initially at a steady-state velocity. The initial steady-state velocity that was selected was 43.3 km/hr (30 mph). The command force was then increased to 1112 N (250 lb) until the vehicle speed reached 96.5 km/hr (60 mph) and then was returned to its original level, 89 N (20 lb). The energy to accelerate the vehicle was extracted from the flywheel where the initial speed was 20 000 rpm. The system responded as expected. The roller was driven to maximum reduction, the flywheel speed increased, and the tangential force and output torque went negative when the command force was reduced.

Selected Design Description

The selection of the final CVT design configuration was made by comparing the five candidate configurations and by performing design optimization analyses. The selected design configuration is shown in fig. 1. A complete parts list appears in Appendix D. It is of regenerative design with two toroidal cavities in parallel using two rollers per cavity. Three gear sets are incorporated within the CVT housing to control the speeds through the toroid cavity.

The input shaft of the CVT is connected to a 3.0:1 planetary reduction gearset. A clutch mechanism is incorporated in this gearset to hold or release the planet carrier; therefore, when the planet carrier is released, the CVT is decoupled from the input power source.

The ring gear hub of the input reduction gearset drives the main shaft of the transmission. The main shaft is supported by two bearings: a ball bearing at the input end and a roller bearing at the output end to allow for thermal and mechanical expansion.

Two input discs, one at each end of the main shaft, are driven through splines by the main shaft.

The output discs are connected by a sleeve. One disc is brazed to the sleeve; the other is attached via splines to allow for axial displacements as the system is loaded and unloaded by the load cam mechanism.

The load cam mechanism is used to control the contact force between the discs and drive rollers as a function of the torque on the output discs. The load cam mechanism is located between the two output discs. It consists of a load cam, bearing rollers, and retainer. The rollers are held between the load cam and a surface of one output disc by the retainer. The load cam is pinned to the output gear.

As the output discs are driven, the cam rollers roll against the output disc and load cam creating an axial force on the output discs. This force is proportional to the torque on the output discs; and its magnitude is controlled by the shape of the load cam.

The axial force loads the output discs against the input discs through the rollers. It is reacted by the main shaft, isolating this force from the housing.

The contact force on the traction contact is proportional to the axial force and orientation of the drive rollers in the toroidal cavity.

The drive rollers are held in position between the input and output discs by a trunnion arrangement. The trunnion allows the roller to rotate in the toroid cavity. A force balance roller control system is employed to position the rollers within the toroidal cavities. The roller position sets the ratio across the toroidal cavity, thereby controlling the output speed. This control system is described in the Transmission Ratio Control subsection, and a preliminary analog computer analysis is presented in the Roller Control System Analysis subsection.

The output gear drives the transfer shaft that transfers the output power to the ring gear of the output reduction planetary gearset. The overall transfer shaft gear ratio is 1.85:1, and the output gearset has a 4.5:1 ring-to-sun ratio. The sun of the output planetary gearset is driven directly by the main shaft, and the CVT output shaft is driven by the planet carrier of the output planetary gearset.

A torque limiting device is integrated into the transfer shaft. This mechanism is designed to slip at a predetermined torque level, limiting overloads through the drive.

The power flow through the CVT is in through the input planetary gearset, across the toroidal cavities, through the 1.85:1 transfer shaft reduction, and out through the output planetary gearset. The regenerated power flow is through the sun gear of the output planetary gearset and return to the input toroidal cavities.

The transmission includes a self-contained, closed-loop hydraulic and lubrication system utilizing Monsanto Santotrac 30 traction fluid. A gear-driven lube pump is driven directly by the input end of the main shaft through a drive and idler gear arrangement. The pump supplies the lubrication for the hydraulic roller control and the transmission. Lubrication is supplied to all rolling elements by a series of oil jets connected by an oil galley system. The gears are lubricated by splash lubrication, with the oil flowing to the transmission sump by gravity return.

The CVT performance was determined under various operating conditions. The results of this analysis are presented in figures 48 through 62.

These figures present five CVT performance parameters plotted against transmission output speed at the five power levels specified: 7.5, 15, 30, 52, and 75 kW (10, 20, 40, 70 and 100 hp). The performance parameters evaluated are: efficiency, both overall and toroid cavity; life of the toroidal cavity elements; energy dissipation through the roller contacts; mean Hertz pressure; and contact aspect ratio.

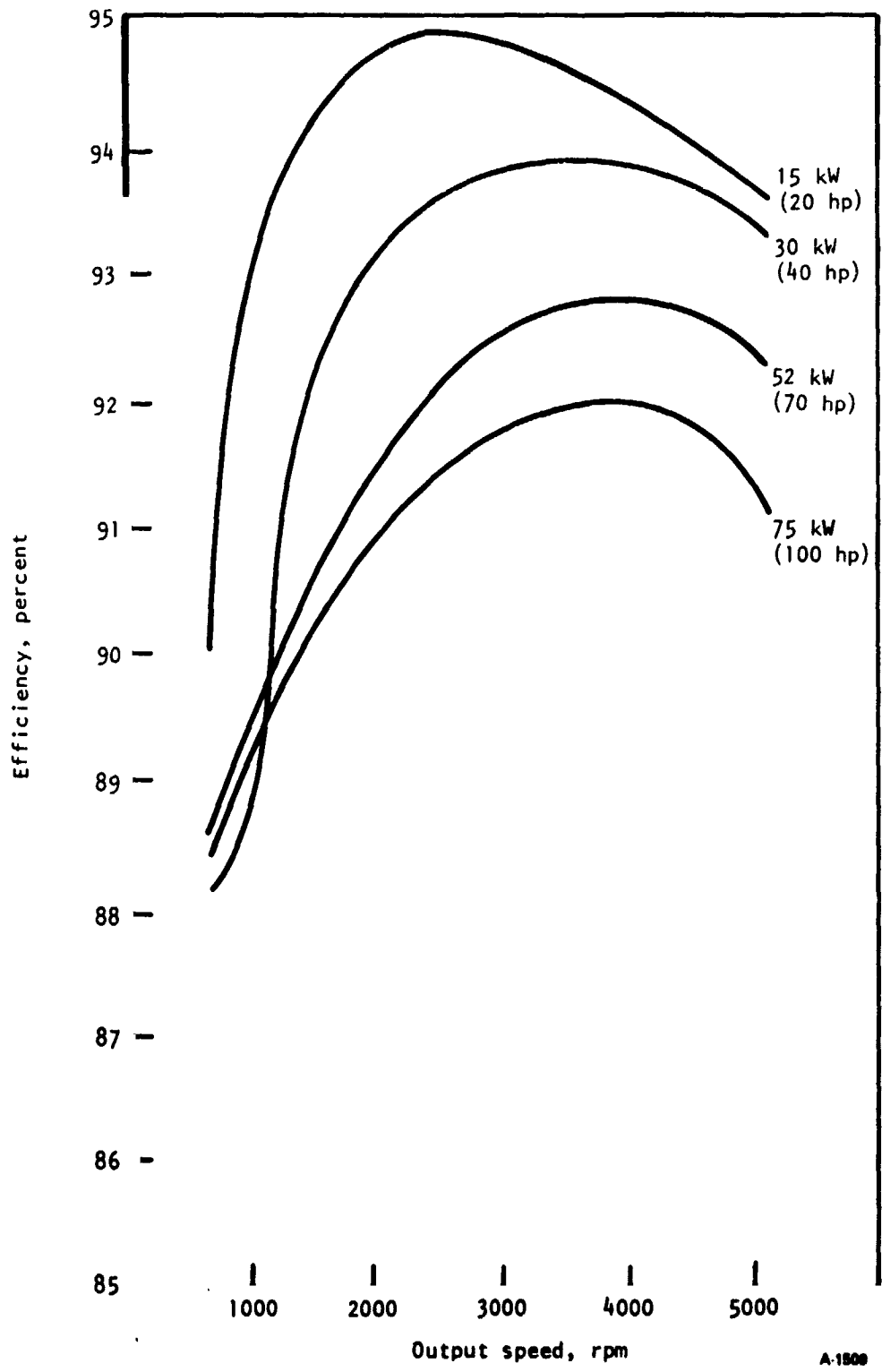


Figure 48.--Traction drive efficiency vs output speed, 14 000 rpm input speed.

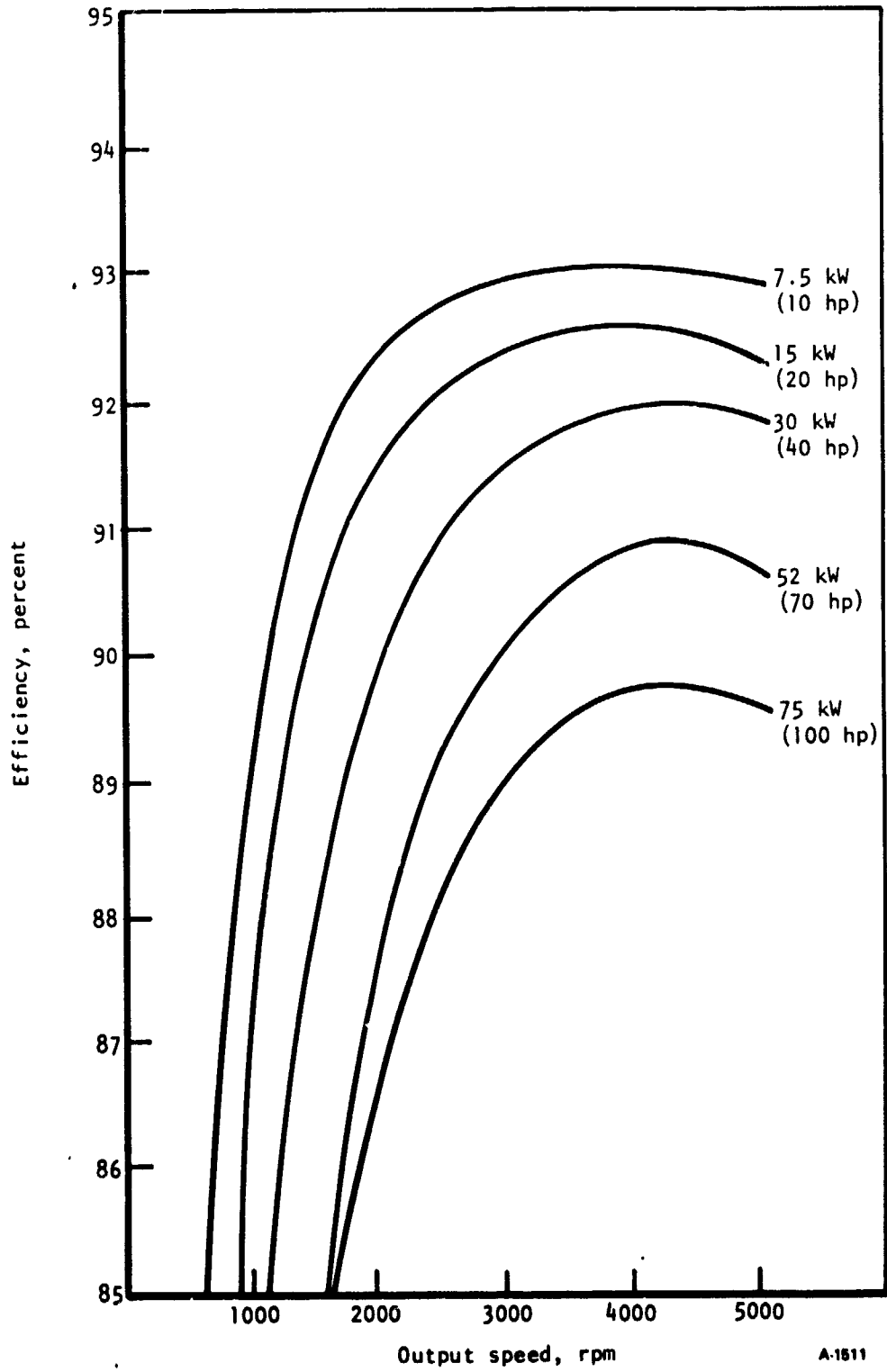


Figure 49.--Overall CVT efficiency vs output speed, 14 000 rpm input speed.

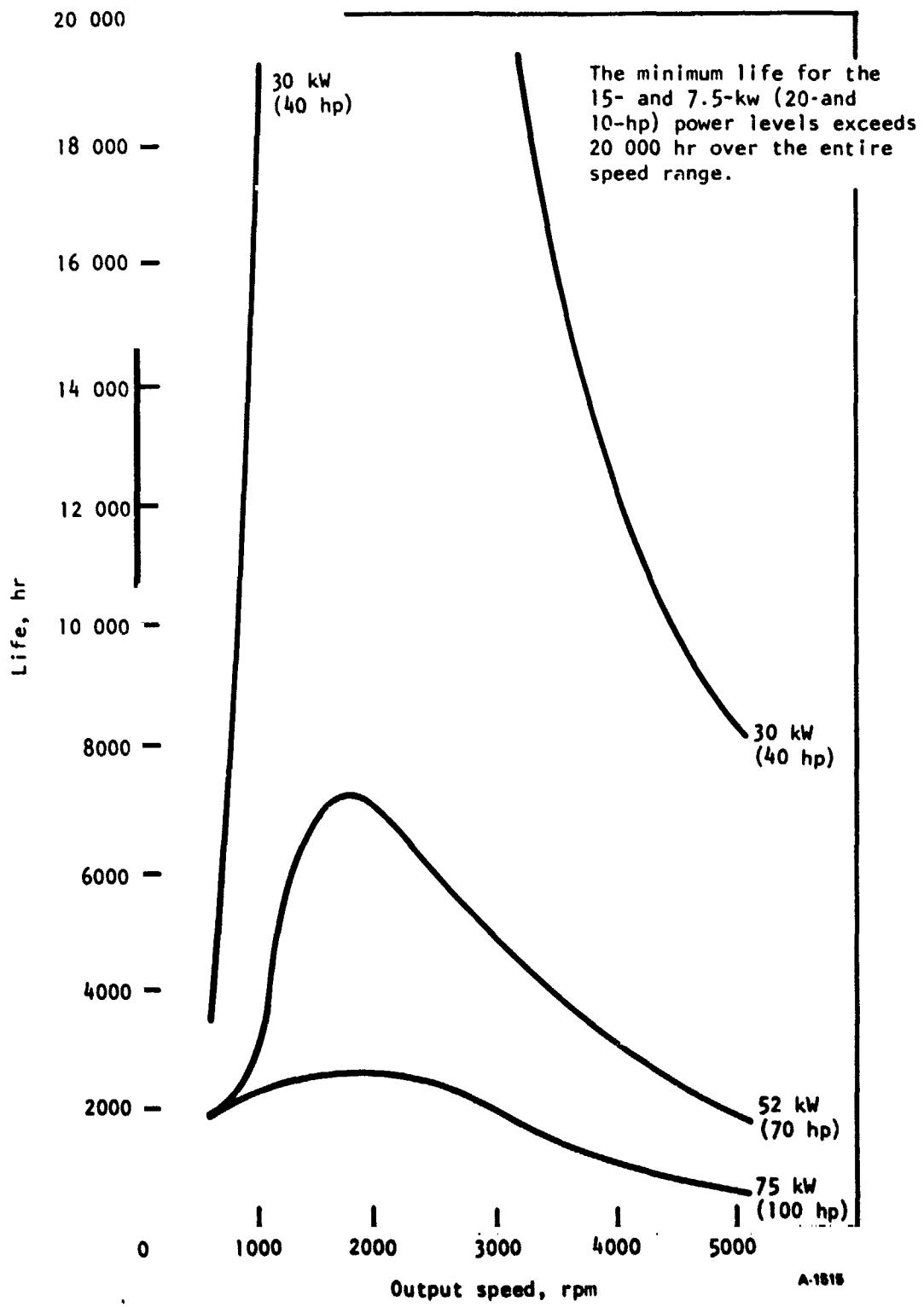


Figure 50.--Life vs output speed, 14 000 rpm input speed (toroid cavity components only).

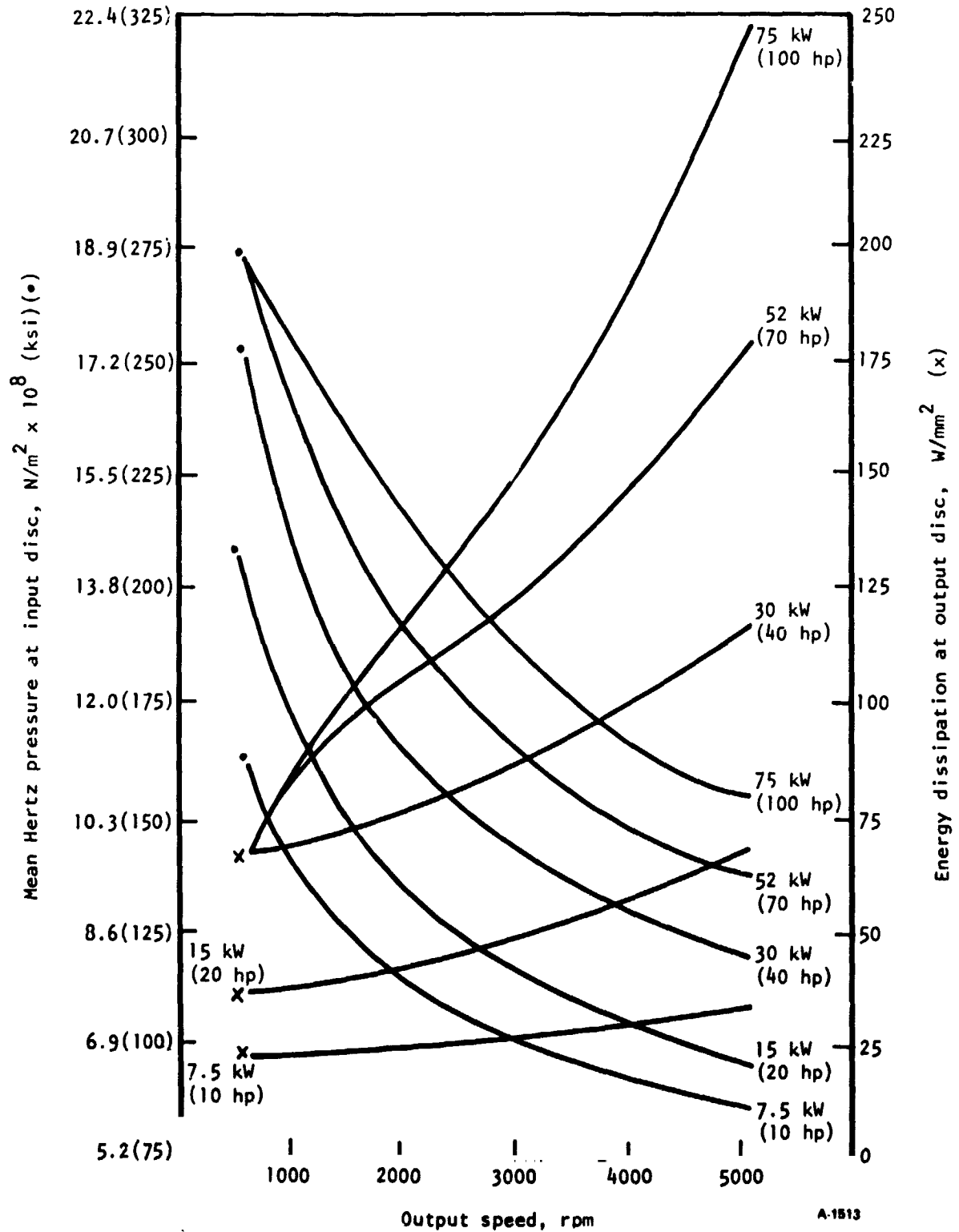


Figure 51.--Mean Hertz pressure and energy dissipation vs output speed, 14 000 rpm input speed.

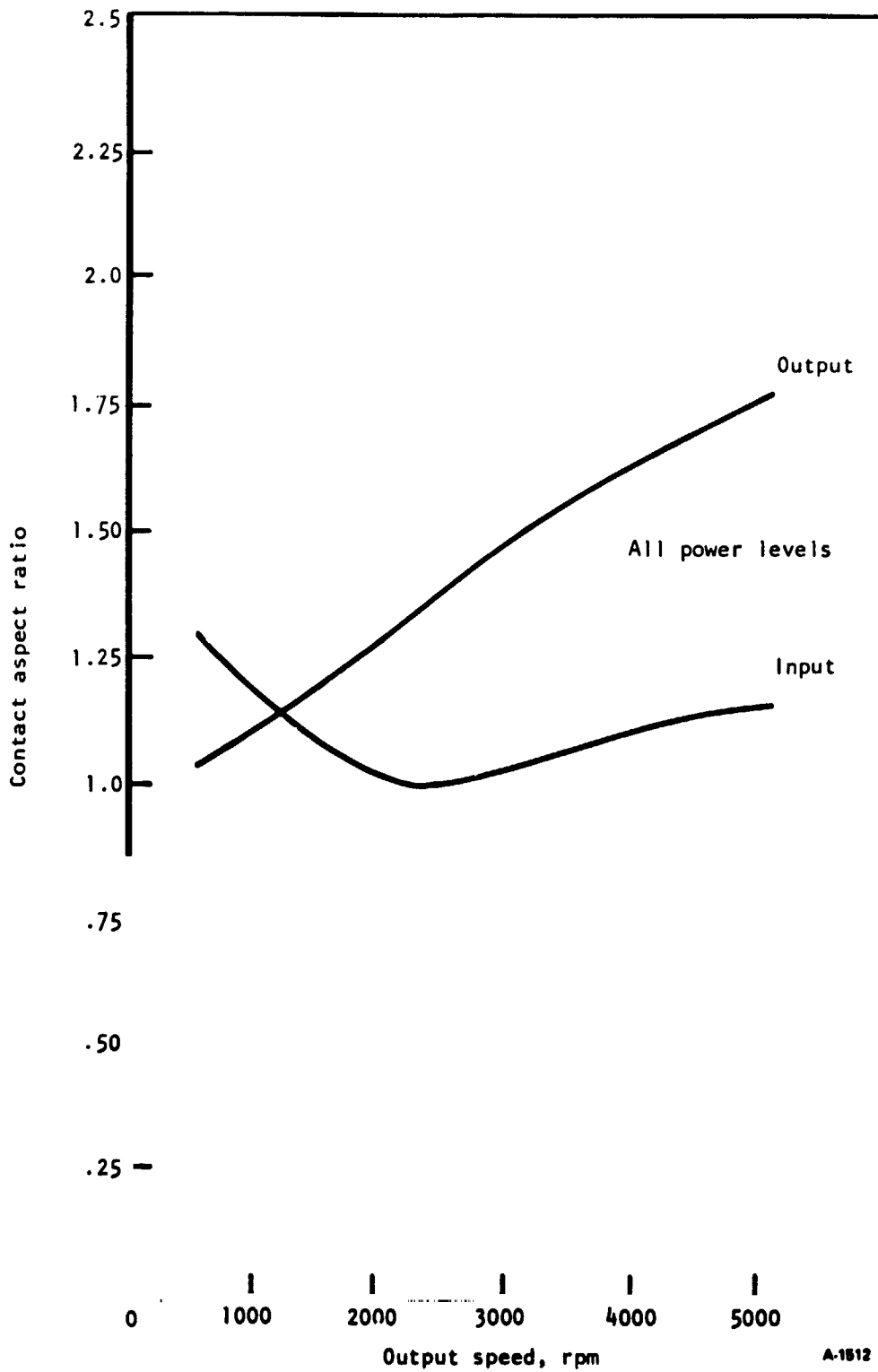


Figure 52.--Contact aspect ratio vs output speed, 14 000 rpm
 input speed (contact major axis/contact minor axis).

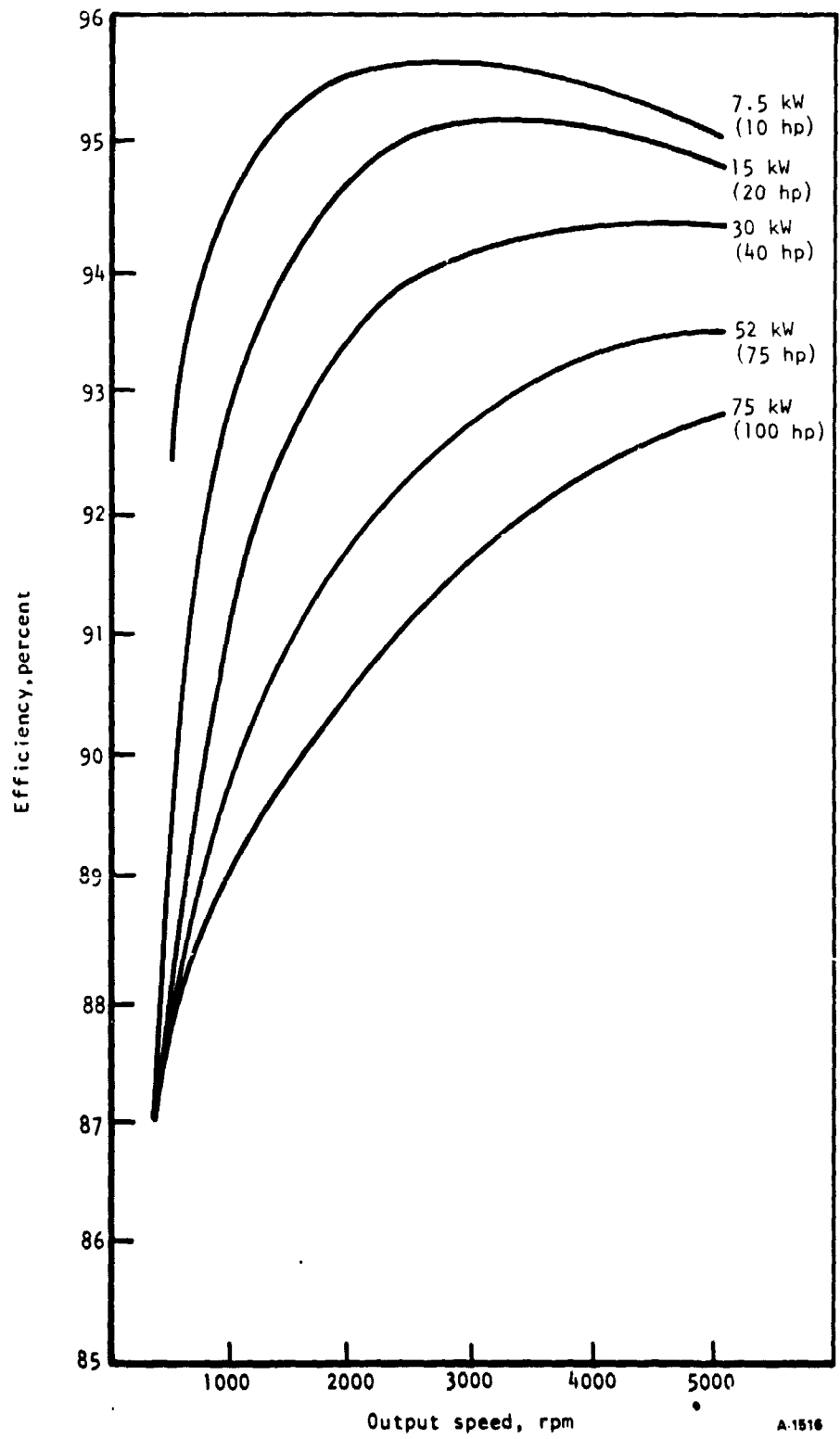


Figure 53.--Traction drive efficiency vs output speed, 21 000 rpm input speed.

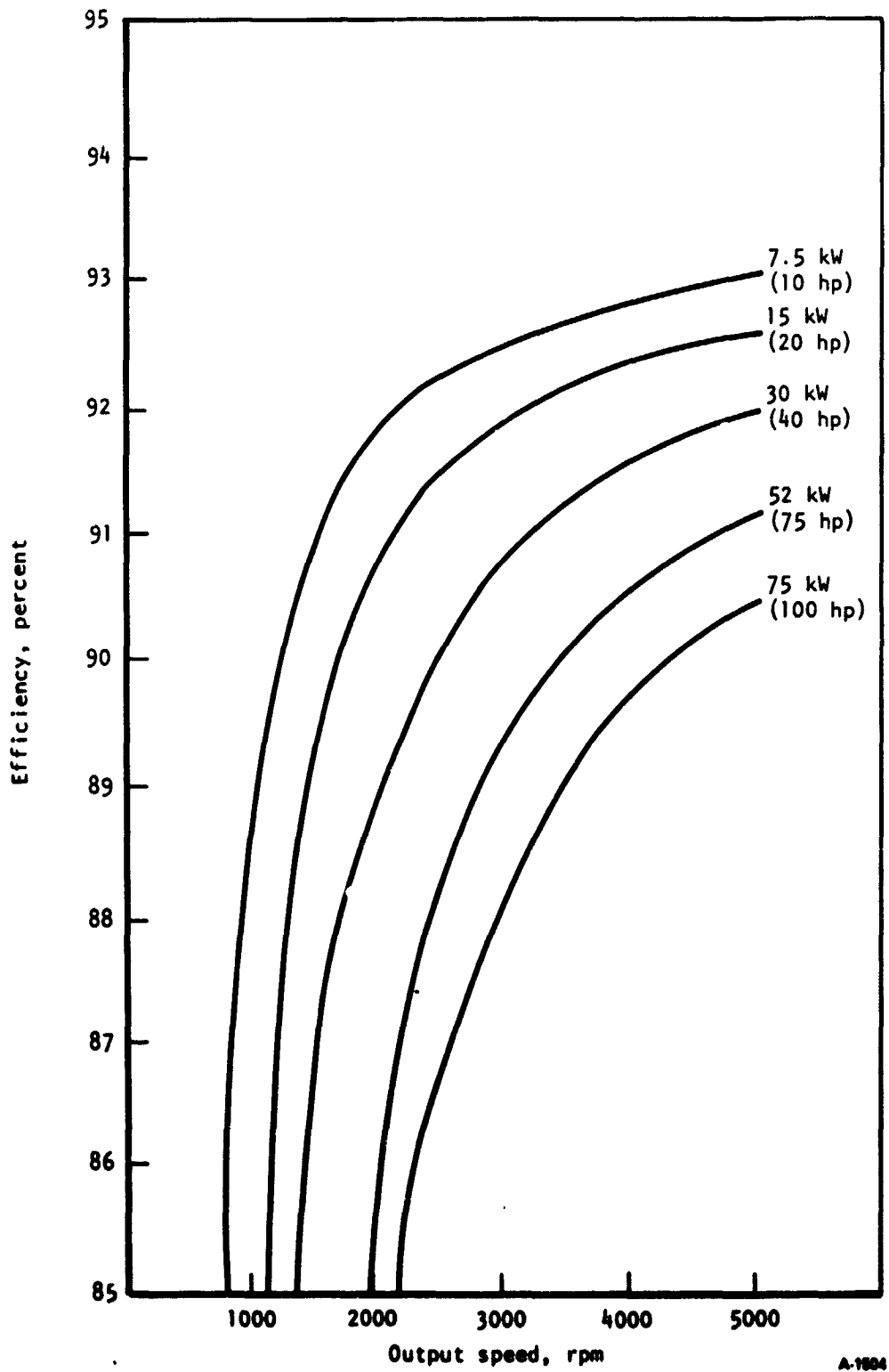


Figure 54.—Overall CVT efficiency vs output speed, 21 000 rpm input speed.

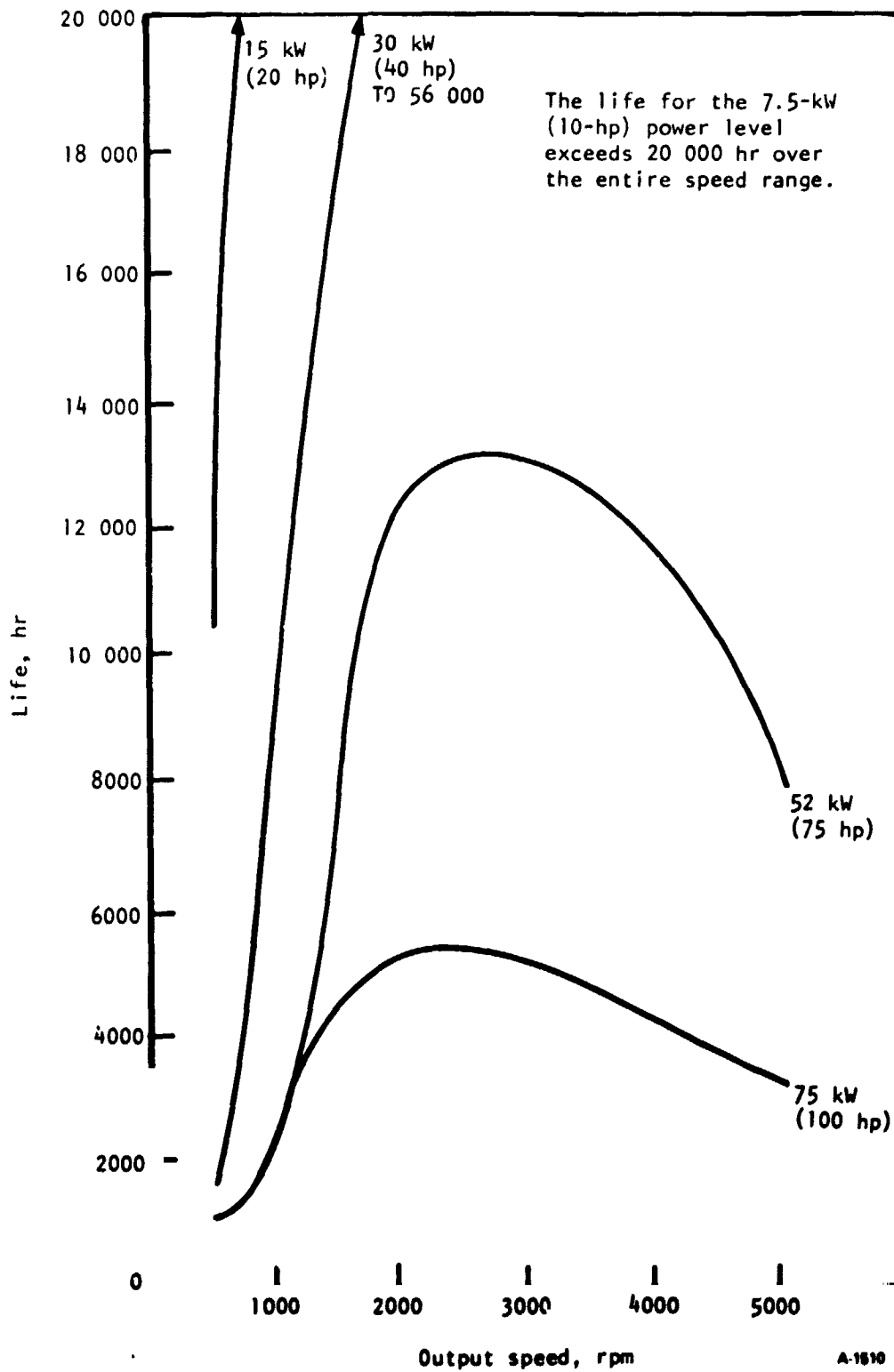


Figure 55.--Life vs output speed, 21 000 rpm input speed (toroidal cavity components only).

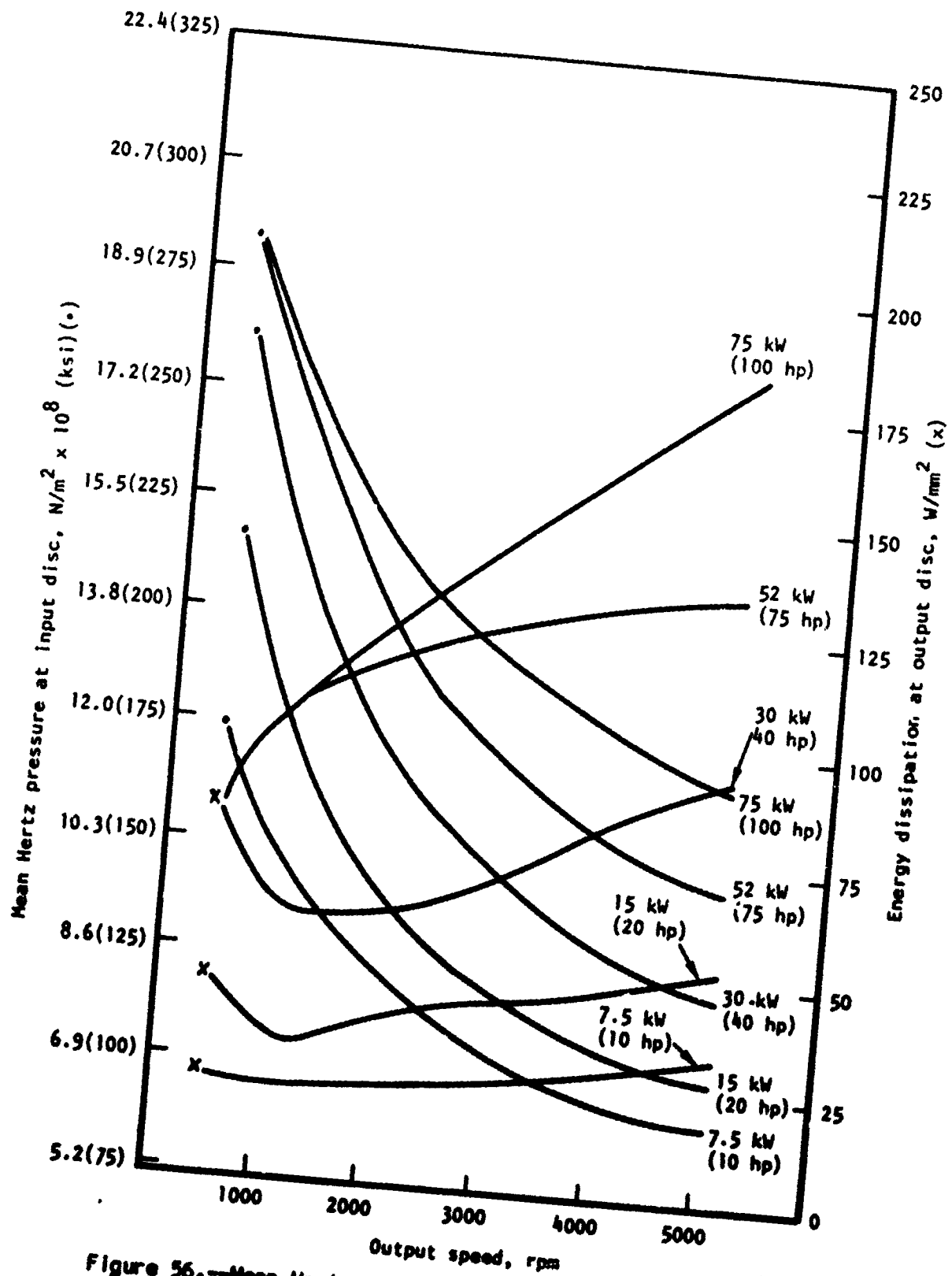


Figure 56.—Mean Hertz pressure and energy dissipation vs output speed, 21 000 rpm input speed.

A-1007

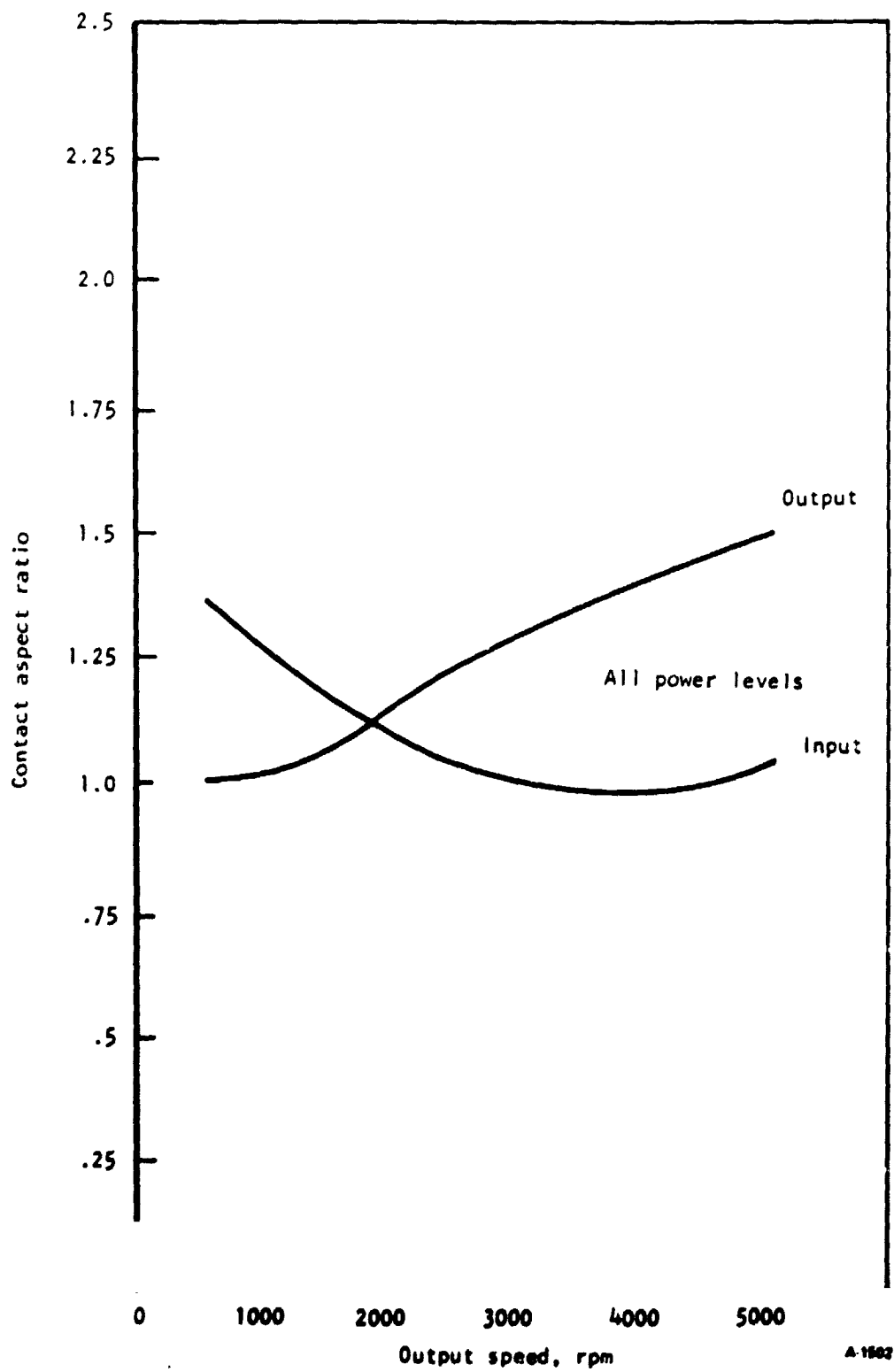


Figure 57.--Contact aspect ratio vs output speed, 21 000 rpm input speed (contact major axis/contact minor axis).

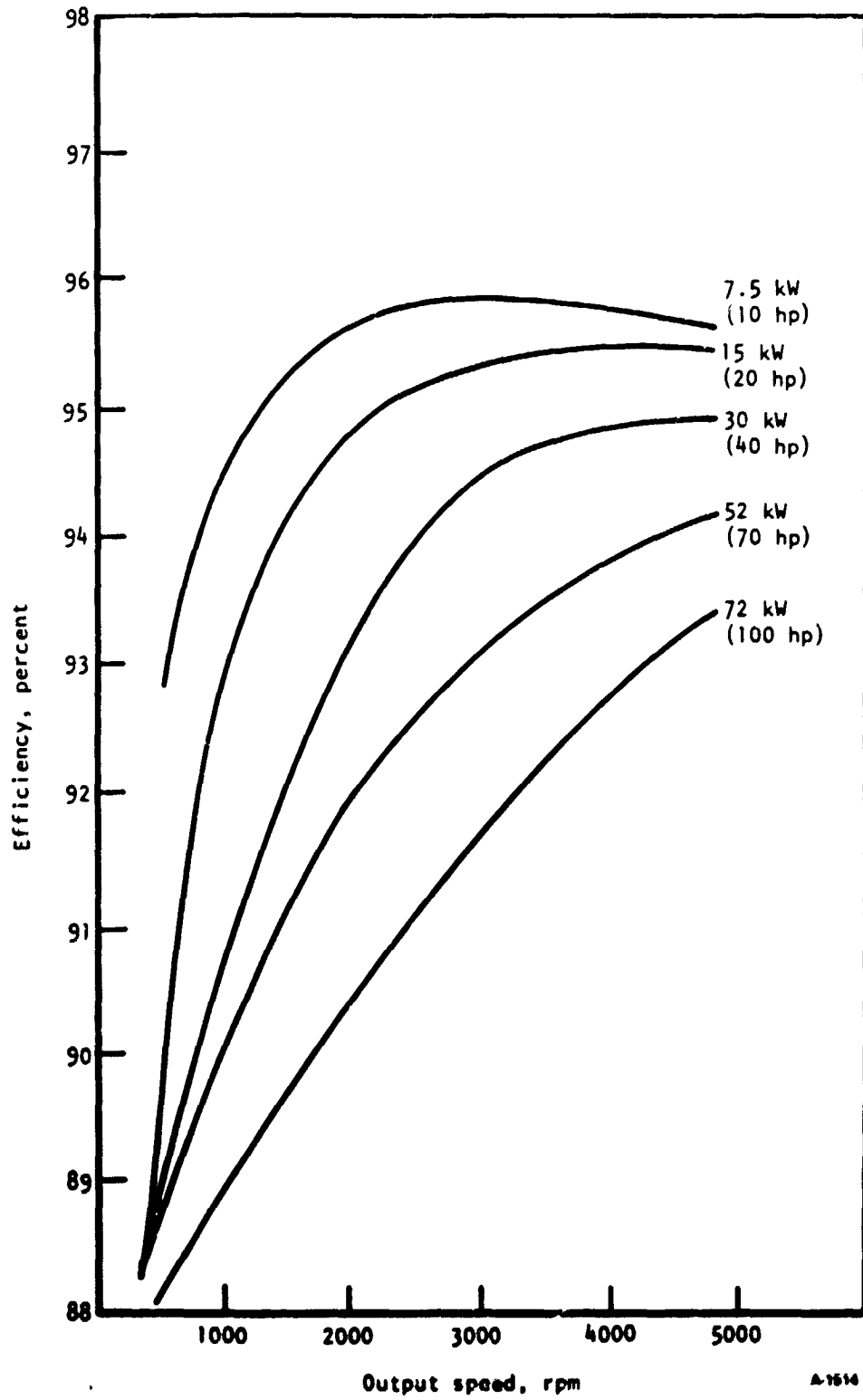


Figure 58.--Traction drive efficiency vs output speed, 28 000 rpm input speed.

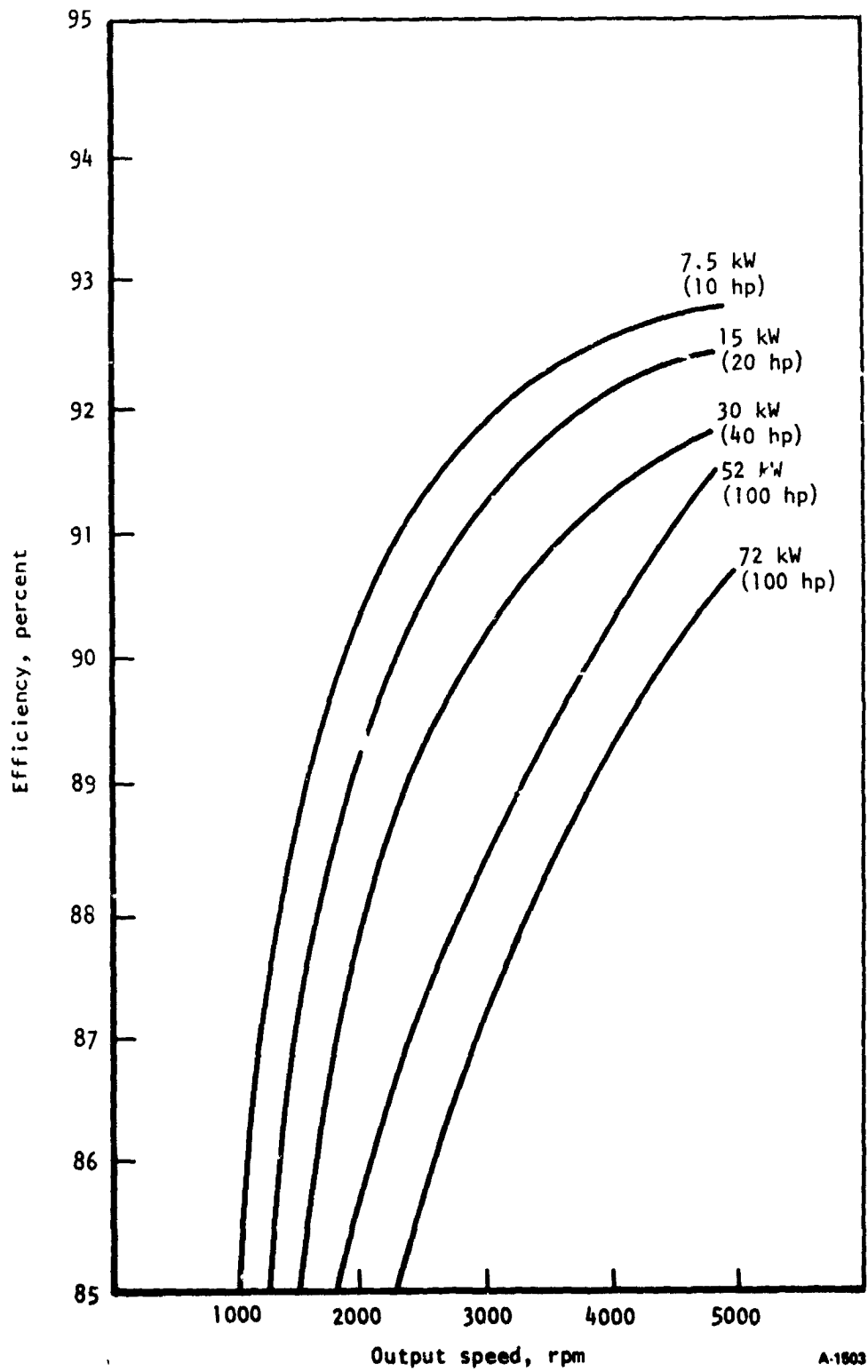
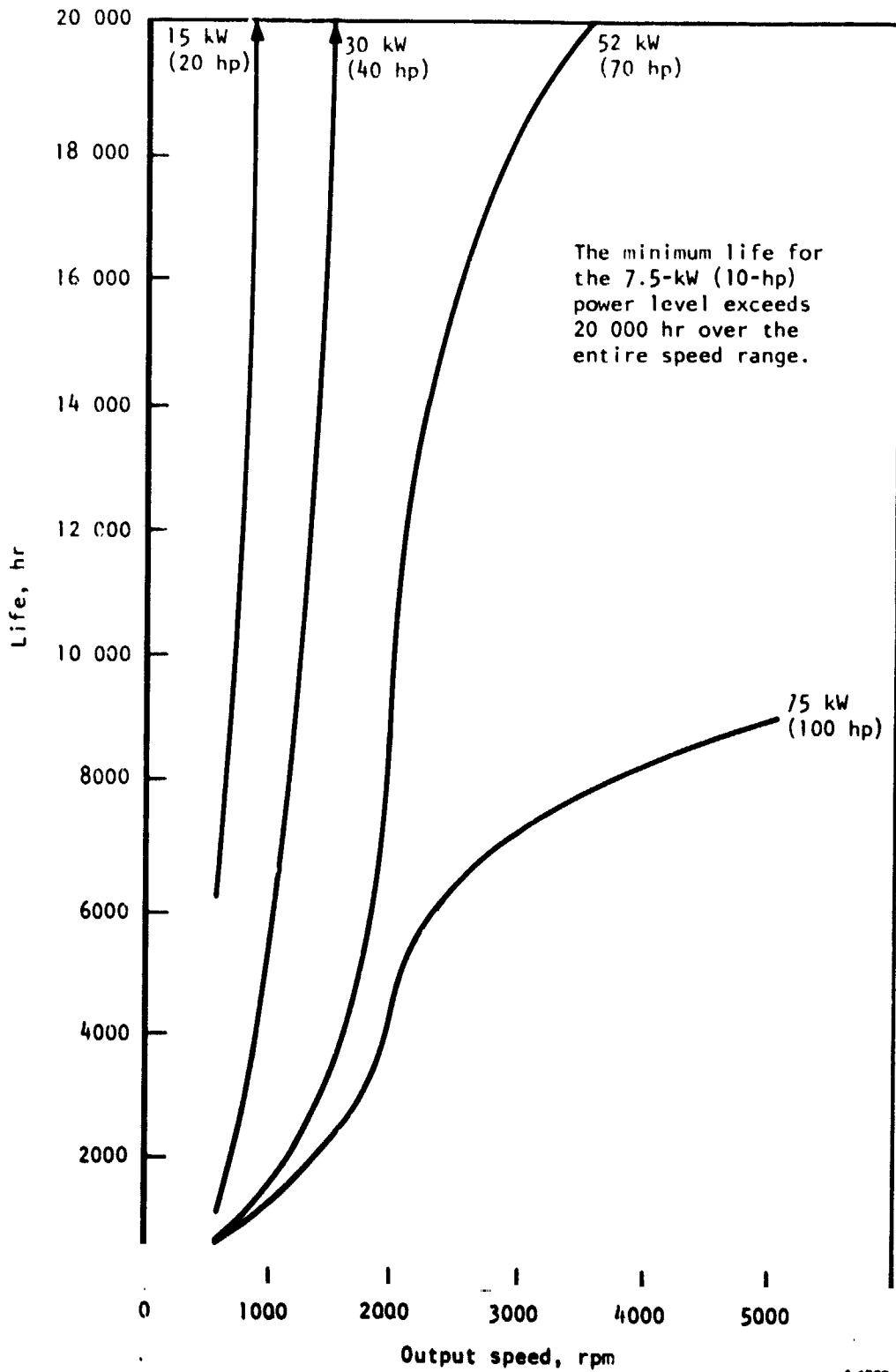


Figure 59.--Overall CVT efficiency vs output speed, 28 000 rpm input speed.



A-1905

Figure 60.—Life vs output speed, 28 000 rpm input speed (toroid cavity components only).

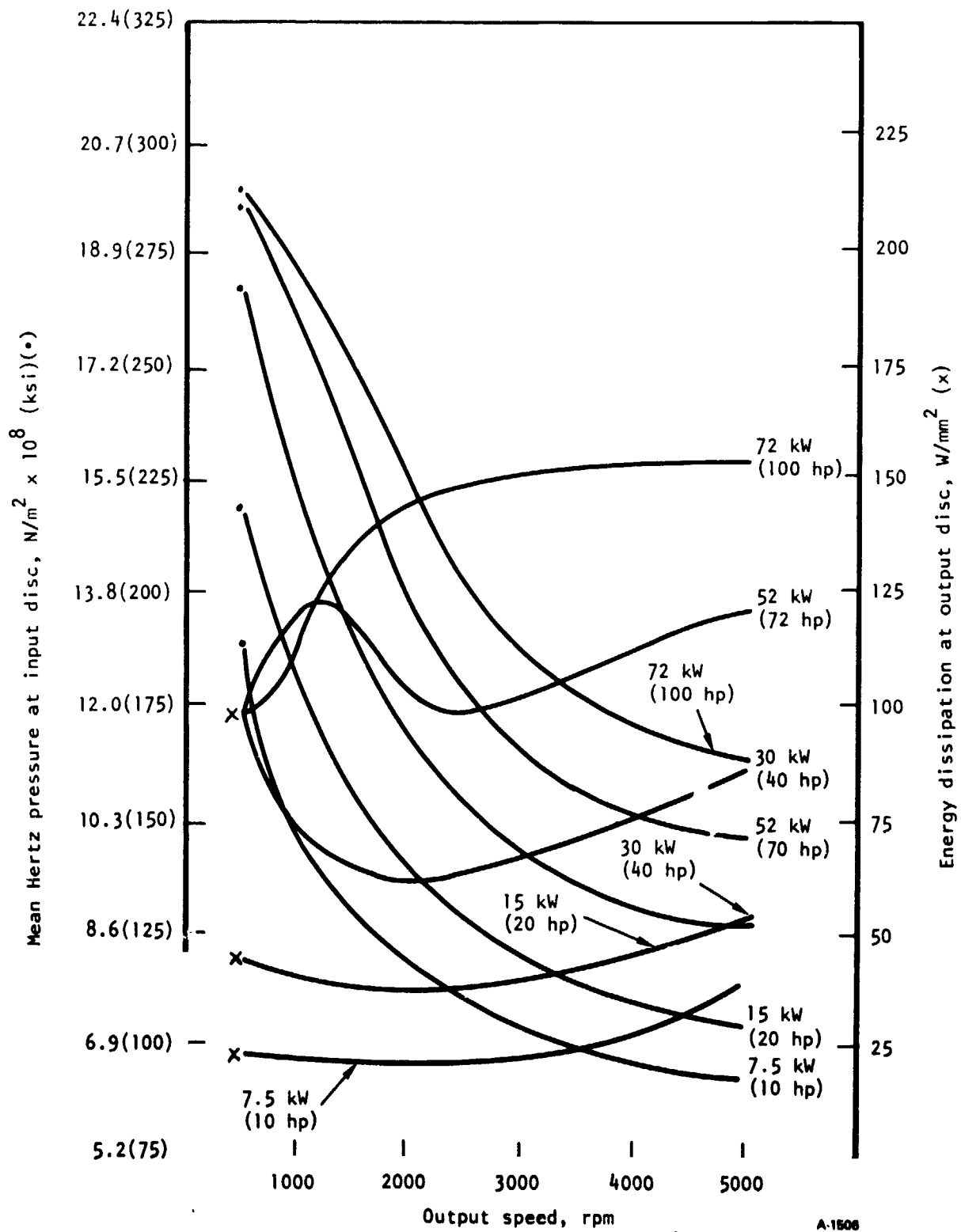


Figure 61.—Mean Hertz pressure and energy dissipation vs output speed, 28 000 rpm input speed.

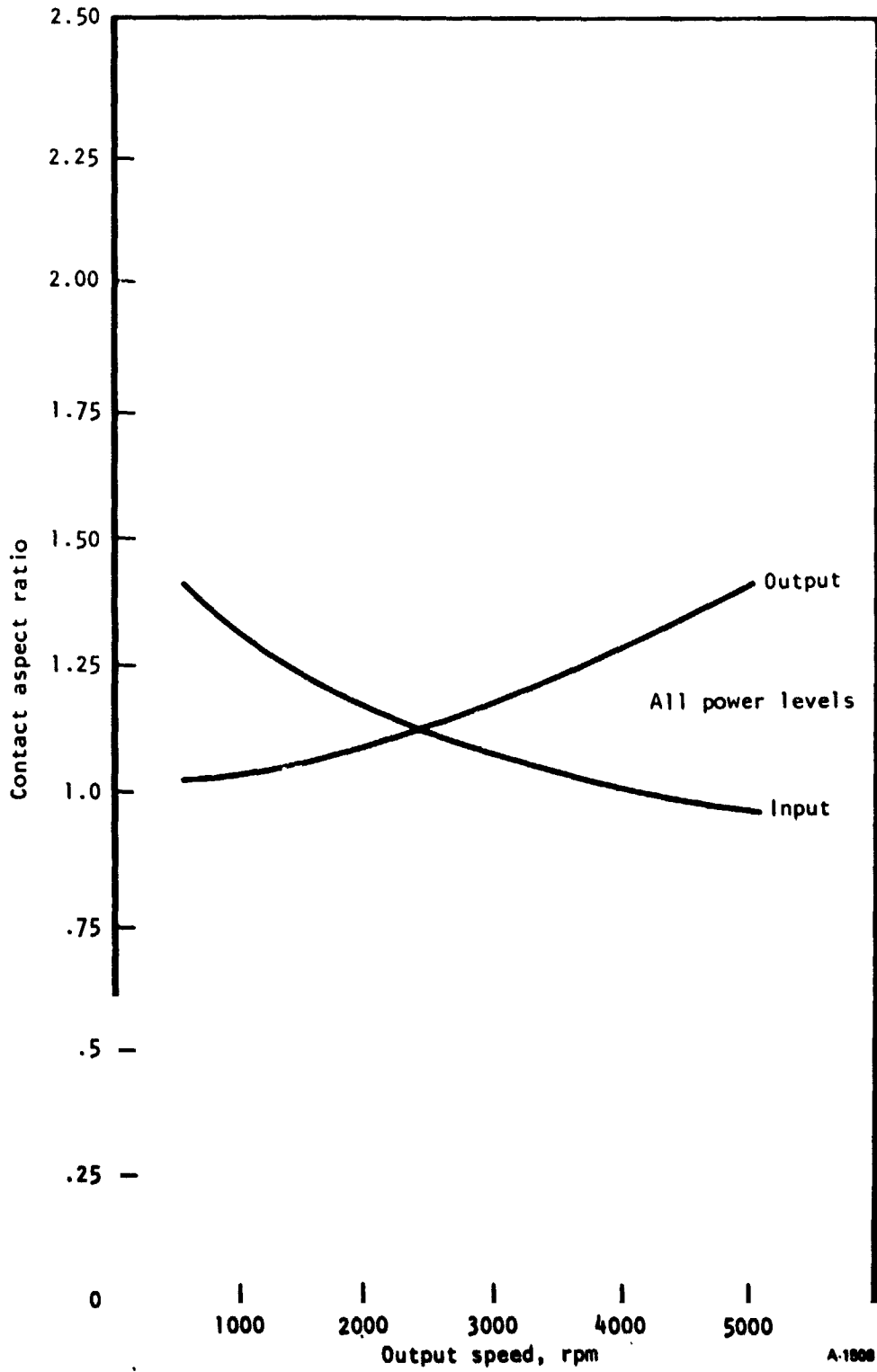


Figure 62.--Contact aspect ratio vs output speed,
28 000 rpm input speed.

TASK II, IDENTIFICATION OF REQUIRED TECHNOLOGY ADVANCEMENTS

Control System Development

While no technical problems are expected with the basic CVT design, or with the use of the epicyclic gearing required to expand the overall transmission speed ratio range through regeneration, it is expected that some development will be required in the control system for the CVT, in the traction fluid performance, and in the evaluation of the traction contact.

The control system is, therefore, identified as an area where technological advancement is required. This will involve the system dynamics of smoothly transferring power both ways between two very high inertia elements, the flywheel and the vehicle. Unlike a conventional heat engine, the flywheel has an operational speed profile that varies in the opposite direction to the vehicle speed. The control system must, by response to driver command, operate the transmission with a greatly increased ratio range, and control the amount and direction of the power flow to drive the vehicle.

This new type of control system has been modeled on the AiResearch analog computer. Using this initial simplified program, actual hardware mechanical characteristics can be added to evaluate alternate means of mechanizing the control function until an optimized control system is defined. A test bed CVT could then be built for dynamometer testing of the control model in actual hardware. By using two flywheels on a dynamometer, one on either side of the CVT, the complete vehicle can be simulated. During the testing of the CVT hardware on the dynamometer, any errors in the analog model will be identified and corrected. Through the combined use of the analog computer model and the dynamometer testing of real CVT hardware, a practical, qualified control system for a flywheel hybrid electric vehicle will be developed.

All aspects of this transmission/vehicle control system will be analyzed, tested, and developed to provide a smooth, producible system capable of providing the feel of current standard cars for the driver and passengers.

Traction Fluid Development

A second area of technical concern that warrants additional development is the traction lubrication fluid. In a traction drive, power is transmitted from one rolling element to another through shear in an elastohydrodynamic fluid film between the traction contacts. The better the oil in this film is able to resist the shearing action, the more power can be transmitted. This resistance to shear is primarily a function of the molecular structure of the oil, although various additives also have an influence.

The resulting developed tangential force transmitted by this shear action, when divided by the contact force holding the rolling elements together, is called the coefficient of traction (μ):

$$\mu = \frac{\text{Tangential force}}{\text{Contact force}} \quad (32)$$

Thus, a fluid that develops a high tractive coefficient is generally preferred for use in a traction drive.

In recent years, several chemical companies have developed special fluids that exhibit a high coefficient of traction. Unfortunately, all of these special traction fluids have other properties that can present problems for the design of an automotive CVT.

The primary problem is the temperature viscosity index. This is the rate at which the fluid viscosity increases (the fluid becomes stiffer) as the temperature decreases, and decreases as the temperature increases. A traction contact requires a fluid viscosity within a narrow range. If the fluid is too viscous, the contacts cannot roll out a thin elastohydrodynamic film, but instead roll up onto the oil and hydroplane. If the fluid becomes too thin, the fluid film will not be adequate for separating the rolling contacts, and contact wear and damage occur.

For many applications, traction drives can be operated under controlled temperature conditions, and a fluid with an appropriate viscosity at that temperature is chosen. For an automobile, however, operating temperatures are not controlled, and the fluid must not be too viscous for startup and operation below zero, or too thin for service when driving with high ambient temperatures.

The currently available traction fluids all have a rather high viscosity index and become too viscous for traction drive use at temperatures above the minimum required for automotive service. Santotrac 30, for instance, the least viscous of the standard Monsanto traction fluid family, cannot be used below about -25°C (-10°F). It also becomes marginally thin at the upper normal automotive operating temperatures. Some development work is currently being done. Monsanto now has experimental fluids reportedly serviceable to -55°C (-65°F), and at least one other company is working on a silicone fluid with a much lower viscosity index. These new fluids are at present too expensive to be used for automotive service and are not yet available with a complete additive pack.

The second difficulty with some high traction coefficient fluids is the tendency to entrain air. This is not the same as foam, where the air is encased in an oil film on top of the fluid, but rather is the retention of the air bubbles within the body of fluid. This causes a reduction of the bulk modulus when operating a hydraulic control system and some difficulty in scavenging. Normal deaeration techniques, such as centrifuging the oil or allowing a settling time in a reservoir, have only limited success at clearing air from the fluid until a sufficiently high temperature is reached. Within a few degrees of some specific temperature, the fluids will quickly release the air bubbles and behave like normal lubricants. For Santotrac 50, this temperature is about

80°C (180°F). Above this temperature the fluid remains clear like a normal lubricant, but below it, it rapidly turns milky white as soon as it is agitated and will remain that way for many minutes.

Traction Coefficient Verification

Test verification of the actual coefficient of traction developed by new fluids under conditions of contact size, rolling speed, contact spin, surface finish, and temperatures found in an automotive CVT is warranted. In conjunction with these tests, the limits of tolerable contact losses from the results of both the tractive shear and spin caused shear should also be found for the conditions that are encountered in real drives.

Most traction drive designers have traditionally established their own data based on extensive testing of their design with a preferred fluid. Until recently, this fluid was generally a silicone base fluid or a naphthenic base petroleum oil like Mobil 62. Historically, a number of problems were discovered with early silicone fluids and they lost favor, and production of Mobil 62 has been discontinued. Recently, there has been testing done with Sternal in England and other parts of Europe and with Santotrac fluids both here and abroad. Unfortunately, virtually all this data is held as proprietary. It is also generally not in sufficient depth to cover all the operating conditions found in an automotive CVT.

Published data for the new types of traction fluids is generally taken at only a single rolling speed and temperature and with a twin disc-type test machine operating with no contact spin. The designer is required to interpolate from a similar test point for a fluid that has more data. Such interpolations are often not completely valid. The designer must be conservative to account for this uncertainty with a traction drive; that is, he must assume that the fluid has a lower coefficient of traction than indicated by interpolation and must therefore use a higher contact force than necessary to carry the required tangential load.

This design practice can cause development problems. The excessive contact pressure will produce a larger contact area and greater hertzian pressure than required. The spin components of shear, inherent in a CVT traction contact, are therefore greater than anticipated. Excessive losses will be generated within the contact, and the drive can be damaged. With more definitive traction data, a much lower contact force can be used. The drive will still carry the required tangential load, but the spin losses will be greatly reduced and drive damage avoided.

It is interesting to note that in this case, the greater coefficient of traction produced by the fluid also produced contact losses greater than anticipated. This same phenomenon has also been observed when using these special high coefficient fluids in angle contact ball bearings and roller thrust bearings; both operating with high contact spin.

Contact Loss Verification

The limit on contact losses is an additional area where greater amounts of test data are required. Current techniques of computer-assisted analysis provide fairly reliable information on the actual losses occurring within the traction contact under a variety of conditions. The maximum loss limit that can be tolerated under operating conditions, prior to damaging the traction contacts, is not known. Some work has indicated that this limit may be as low as 40 W/mm^2 . Other work with gears indicates a limit as high as 200 W/mm^2 (a gear has more surface available for cooling for the same size pitch diameter). It is probable that the actual traction contact loss limit is between these two values.

Test data taken under actual drive conditions of spin, temperature, load, and the same number of rolling contacts per revolution is recommended.

TASK III, SUITABILITY FOR ALTERNATE APPLICATIONS

Electric Motor Powered Vehicle

To determine the suitability of a traction toroidal CVT for use in an electric vehicle with an electric motor only, the following vehicle specifications were used:

Vehicle: passenger car

Weight: 1700 kg (3750 lb)

Drive train: See figure 63

Motor: electric

Operating speed: 0 to 6000 rpm

Delivered power: 0 to 75 kW (0 to 100 hp)

Motor efficiency: See figure 64

CVT: mechanical traction - toroidal configuration

Output speed: 0 to 3000 rpm

Maximum delivered torque: 450 N-m (330 lb-ft)

Weighted average power out: 16 kW (22 hp)

System life: 2600 hr B-10

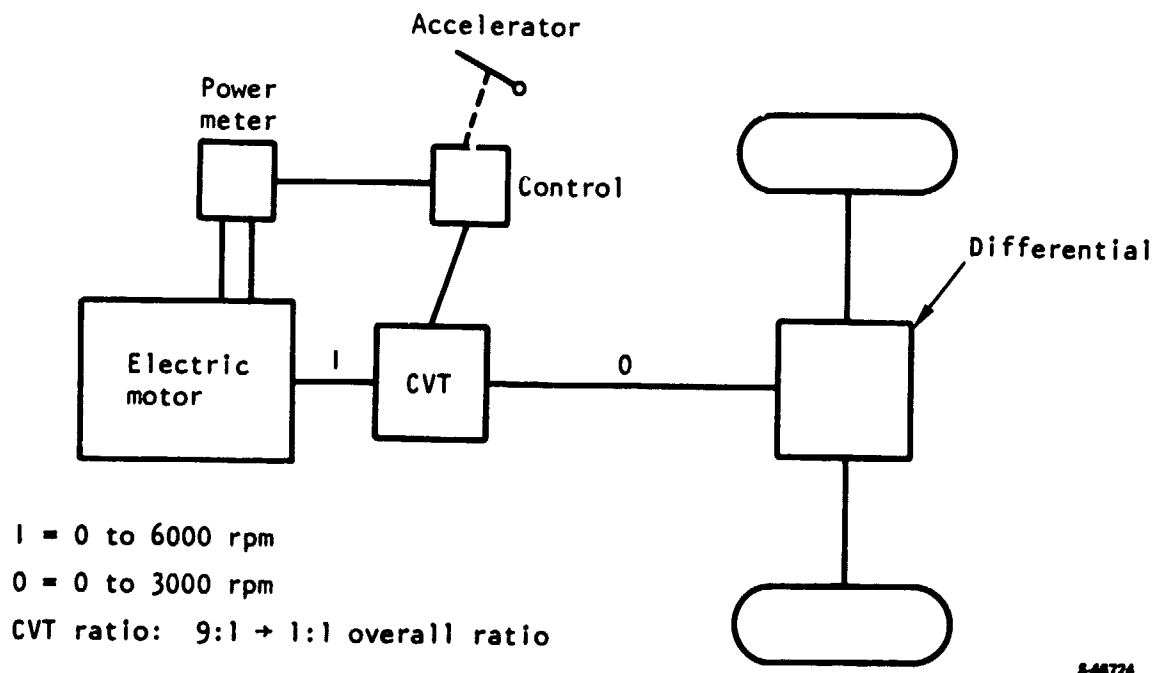
Ratio range: 9:1 to 1:1 (speed in/speed out)

Assumed:

Average output speed: 1500 rpm

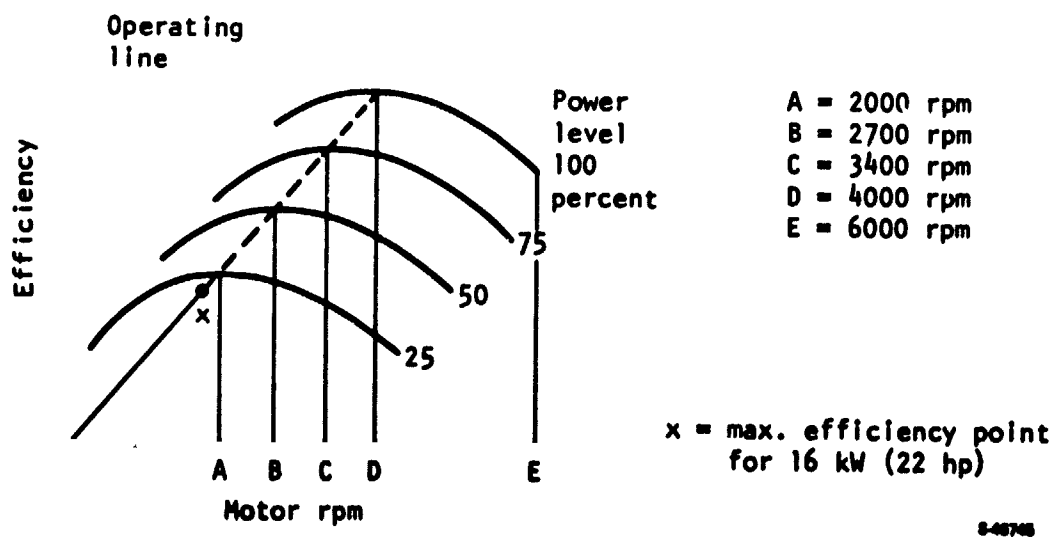
Average input speed: 1900 rpm (maximum efficient speed for
22 hp, fig. 64)

The CVT required for this application does not require the expanded speed ratio range necessary for the flywheel hybrid vehicle; therefore, the regeneration gearing will not be used. A straight 9:1 ratio range, dual cavity, full toroidal, variable ratio drive will provide ample speed range. To reduce the output speed of the variable ratio section to match the required speed of the differential, a 3:1 reduction unit will also be incorporated within the CVT. This combination will provide a CVT ratio range of from 9:1 reduction to direct drive; therefore, the output speed from the CVT can vary from 444 rpm to over



8-48724

Figure 63.--Drive line schematic for electric powered vehicle.



8-48748

Figure 64.--Electric motor efficiency, 75 kW (100 hp) motor.

3000 rpm with the motor at 4000 rpm the (maximum efficiency point for 100 percent power). At a motor speed of 2000 rpm (the maximum efficiency point for 25 percent power), the output speed can vary from 222 rpm to 2000 rpm.

The maximum torque load carried by the variable ratio drive for this application is 150 N-m (110 lb-ft):

$$\text{Maximum CVT torque} = \frac{450 \text{ N-m}}{3} = 150 \text{ N-m (110 lb-ft)}$$

This is compared to a maximum variable ratio drive torque of about 200 N-m (150 lb-ft) for the drive configuration selected under Task 1. The load capacity of the basic toroidal CVT varies to about the 2.8th power of the basic pitch diameter; therefore, the drive size for this electric vehicle application can be reduced to about 90 percent of the 112 mm (4.4 in.) toroidal cavity pitch diameter selected under Task 1.

The CVT configuration selected under Task 1 of this program would therefore be well suited for use in a pure electric vehicle to the above specifications, with the following modifications:

- (1) The input 3:1 reduction (with associated band clutch) required to reduce flywheel speed to acceptable CVT input speed would be eliminated.
- (2) The epicyclic gear set required to regenerate the flywheel powered CVT to zero output speed would be replaced by a straight 3:1 reduction gear set.
- (3) The basic pitch diameter of the variable ratio toroidal section would be reduced from 112 mm (4.4 in.) to 100 mm (3.97 in.).
- (4) The torque limiting clutch in the recycled loop of the flywheel powered, regenerated CVT would be eliminated or modified.
- (5) The control system for the pure electric powered vehicle would not be required to regulate the input shaft speed in the same manner as with the flywheel powered vehicle. It would have speed control characteristics set to optimize motor efficiency. The force control power roller steering system would be retained.

The CVT control system used with an electric motor having an efficiency curve shown in figure 64 will need to sense and/or control the motor speed (CVT input speed) as a function of the electric motor output power. One possible configuration would be to generate an electric or hydraulic signal proportionate to the motor power and to apply that signal to counterbalance the force from a flyball governor driven by the CVT input shaft. Such a system would proportion the CVT input rpm as a function of motor power. The CVT ratio would then assume a value within the overall ratio range necessary for transmitting power from the motor to the differential.

The load control, power roller steering system will lend itself very well to such a control system by using a simple 4-way spool valve connected to the

flyball system with the hydraulic output signals directly fed to the control cylinders.

There would be no new technological advancements necessary for the design modifications of the optimized CVT configuration for the pure electric powered vehicle application described under Task I.

The areas of engineering concern described under Task II of this report would also apply to this CVT application in order to advance the design from an engineering development to an actual production electric vehicle transmission.

Hybrid Electric Vehicle with an Internal Combustion Engine

To determine the suitability of the CVT design configuration selected under Task I of this program for an internal combustion (IC) engine/electric hybrid vehicle (shown in fig. 65), the following vehicle specifications were used:

Vehicle: passenger car

Weight: 1700 kg (3750 lb)
Drive train: See figure 65

IC Engine:

Maximum power: 75 kw (100 hp)
Minimum fuel consumption curve: See figure 66

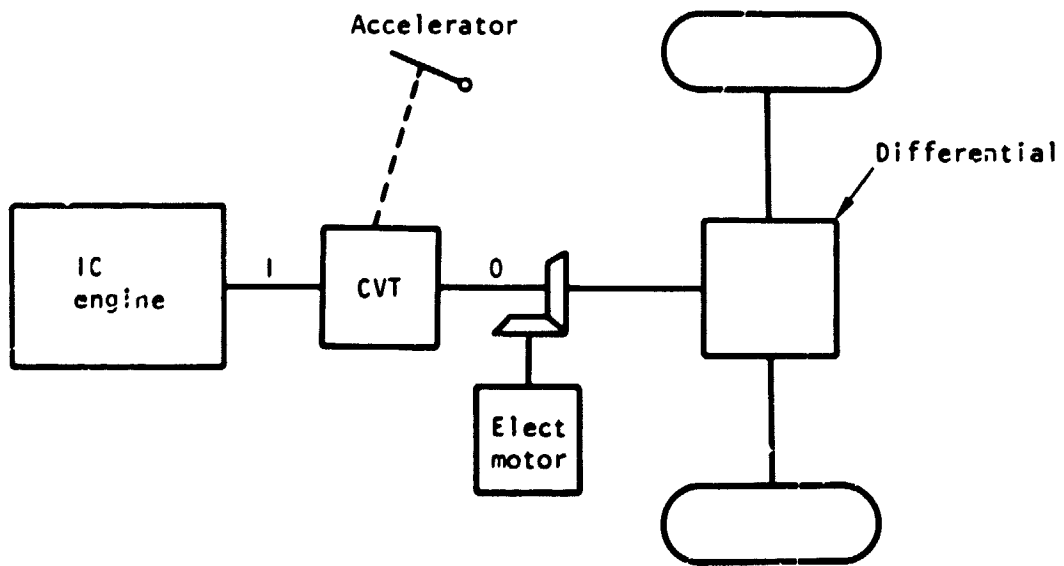
Assumed:

Maximum engine speed: 4000 rpm
Idle speed: 650 rpm

CVT: mechanical traction - toroidal configuration

Output speed: 0 to 3000 rpm
Maximum delivered torque: 450 N-m (330 lb-ft)
Weighted average power: 16 kW (22 hp)
System life: 2600 hr B10
Ratio range: Reverse to 0.55:1 in overdrive

In order to establish an optimized overall CVT ratio range, an engine performance map (shown in fig. 67) and a road load curve for the vehicle (shown in fig. 40) were assumed to calculate the extent of required transmission overdrive. Maximum overdrive is required to keep the engine on the



1: Assume 500 to 7000 rpm

0: 0 to 3000 rpm

CVT: Regenerated through zero output speed into reverse

5-46725

Figure 65.--Drive line schematic for electric/internal combustion engine hybrid vehicle.

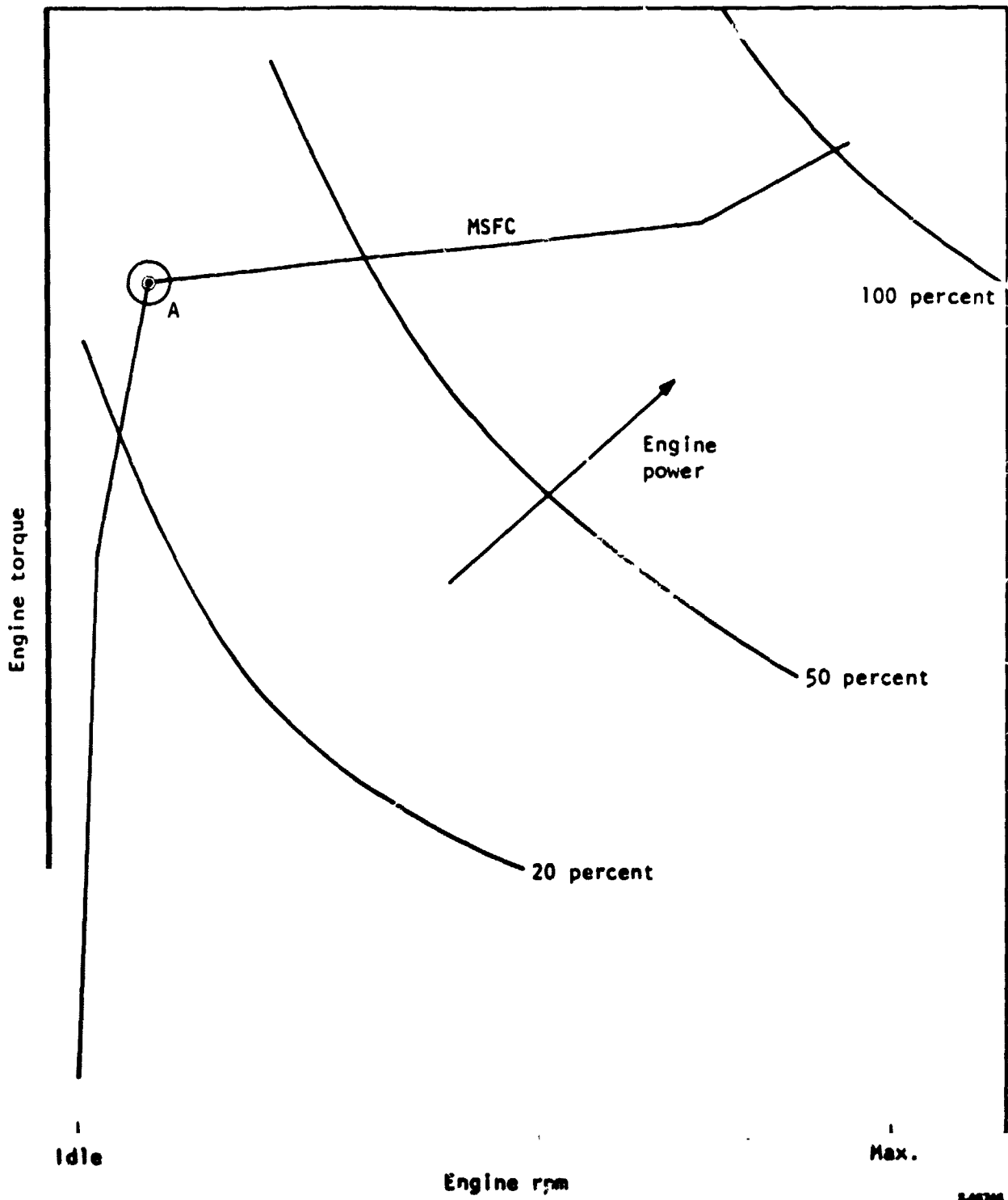


Figure 66.--Internal combustion engine minimum fuel consumption curve.

8-48748

minimum specific fuel consumption (MSFC) curve at the "knee" point just above idle speed, represented by Point A in figure 66. Typically, a 75 kW (100 hp) spark ignition engine will develop 15 kW (20 hp) at 1000 rpm when operating on the MSFC curve (fig. 67). Also typically, a vehicle of this inertia weight class will operate at 64.4 km/hr (40 mph) with only 11 kW (15 hp) for zero grade and zero wind conditions. If the maximum drive shaft speed of 3000 rpm represents a vehicle speed of 105 km/hr (65 mph), the transmission must be capable of delivering 1050 rpm output with a 1000-rpm engine speed, representing 64.4 km/hr (40 mph speed). This requires a 0.54:1 overdrive ratio on the CVT.

The CVT configuration selected in Task 1 can be used for the hybrid electric vehicle with an internal combustion engine with some modification to the gearing and a change in CVT toroid cavity size. By selecting a planetary ring-to-sun ratio of 2.32:1 with a variable ratio unit that goes from 3:1 to 0.33:1, the output of the CVT will go from reverse to a ratio of 0.55:1 in speedup. The torque load on this IC engine CVT will be somewhat greater than for the flywheel powered CVT because of the different ring-to-sun ratio necessitated by the shifted speed ratio range. The Task 1 transmission had a speed ratio from reverse to approximately direct drive, neglecting the 3:1 input reduction from the flywheel. For a 450 N-m (330 lb-ft) maximum delivered torque, the maximum toroidal drive torque will increase from the 200 N-m (146 lb-ft) of Task 1, to about 314 N-m (230 lb-ft). Because the toroidal drive has a load capability that varies to about the 2.8th power of the basic pitch diameter, the size of the toroidal drive will need to increase by about 18 percent from the Task 1 size.

The optimized CVT design configuration selected under Task 1 of this program is, therefore, also suitable for use with an IC engine, as specified above, with the following modifications:

- (1) Delete the 3:1 input reduction unit required for reducing flywheel speed to acceptable CVT speed.
- (2) Change the jack shaft transmitting power from the output of the toroidal drive to the ring of the epicyclic gear set from a 1.85:1 reduction to a 1:1 ratio.
- (3) Change the ring-to-sun ratio (RTS) of the epicyclic gears from 4.5:1 to 2.32:1.
- (4) Increase the basic pitch diameter of the toroidal elements from 112 mm (4.4 in.) to 132 mm (5.19 in.).

The reverse function requirement is provided automatically with this regenerated design, so no special reverse gear is required. The single F-N-R lever will only need to command that the toroidal drive ratio be changed to the maximum reduction stop when reverse is selected by reversing the hydraulic pressures in the load type, roller steering system. In both reverse and normal driving mode, zero output speed is commanded by reducing the hydraulic pressures in the roller steering system to zero as with the flywheel powered drive. With zero control pressure, the power rollers must go to the ratio position where they are not transmitting torque (i.e., zero output speed ratio).

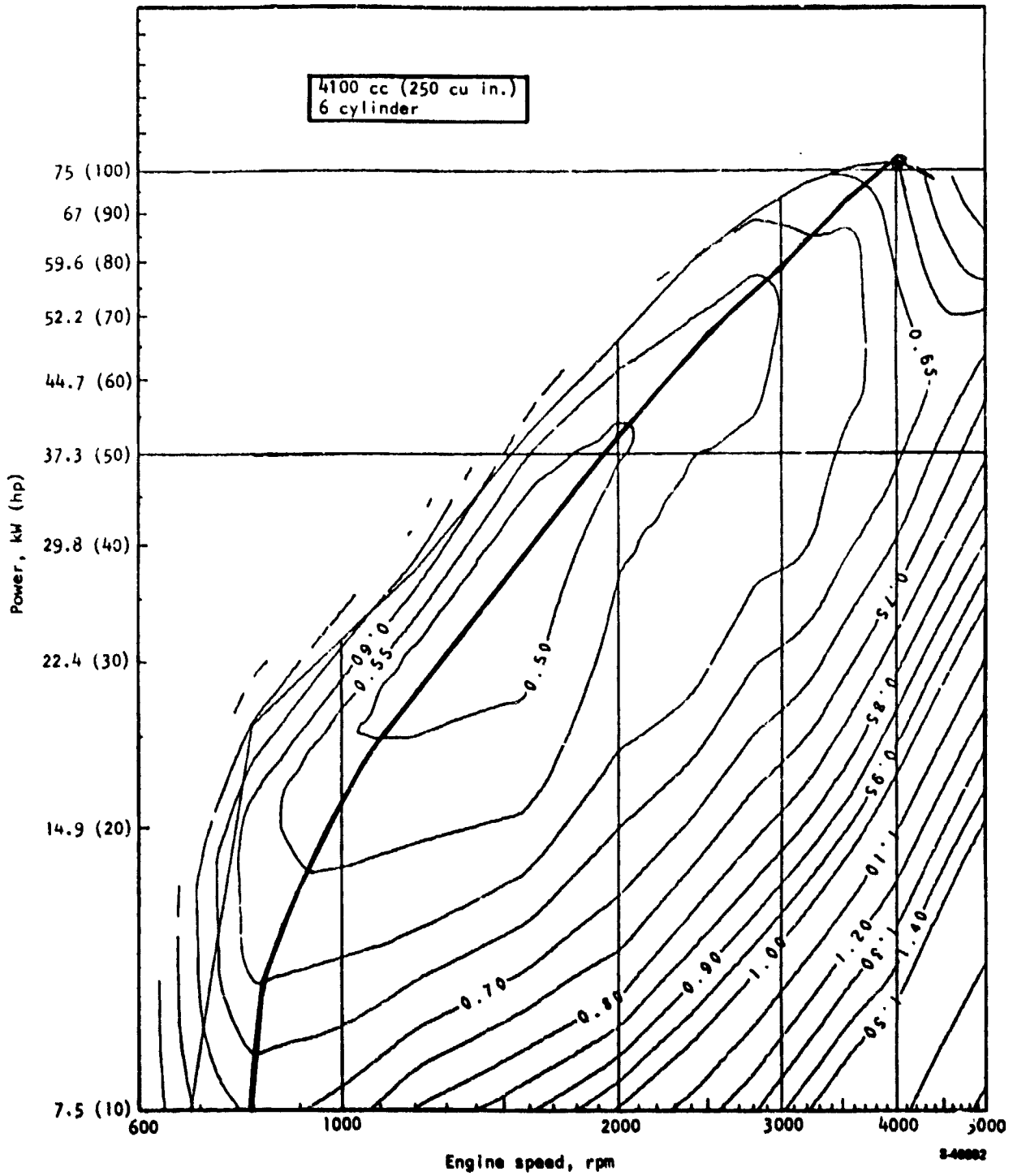


Figure 67.--MSFC curve map for 250-cu-in. six-cylinder engine.

The transmission control system that is required to keep the IC engine operating along the MSFC curve will need to sense engine vacuum and engine speed so that it controls the engine speed required for matching the power commanded by the driver. This IC engine/CVT control system is judged to be more complex than the electric motor powered system because of the power mixing of the motor and the IC engine. The control system for this application is therefore selected as the area where new technology is required. The accuracy with which the MSFC curve is to be followed will affect the complexity of the technological advancement.

No other technological advancements are considered necessary for adapting the Task I CVT to this application.

Scalability to Alternate Weight Vehicles and Torque Levels

The following examples show how CVT design parameters are determined for vehicles of differing weight and torque levels by scaling from the Task I CVT data.

Case 1.— Vehicle weight is reduced to 790 kg (1750 lb), and the maximum CVT output torque is reduced to 210 N-m (155 lb-ft). All other specifications from Task I apply.

The CVT for this application would be virtually identical to the optimized design configuration from Task I. The basic pitch diameter of the toroidal drive would be slightly reduced to save weight and cost. The amount of this reduction is computed through the following steps.

- (1) Determine the torque split from epicyclic gearing into toroidal drive:

$$\text{Torque split} = \frac{\text{RTS}}{1 + \text{RTS}} = \frac{4.5}{5.5} = 0.8182 \quad (33)$$

- (2) Determine the maximum torque on the traction drive by multiplying the maximum output torque by the torque split determined in (1) above divided by the torque reduction from the jackshaft ratio (1.85:1):

$$\begin{aligned} \text{Max. traction torque} &= \text{Max. output torque} \times \frac{0.8182}{1.85} \\ &= \text{Max. output torque} \times 0.442 \end{aligned} \quad (34)$$

- (3) Using the Task I max. output torque of 450 N-m (330 lb-ft):

$$\begin{aligned} \text{Max. traction torque} &= 450 \times 0.442 \\ &= 199 \text{ N-m (146 lb-ft)} \end{aligned} \quad (34a)$$

- (4) Using the Case 1 max. output torque of 210 N-m (155 lb-ft):

$$\begin{aligned} \text{Max. traction torque} &= 210 \times 0.442 \\ &= 93 \text{ N-m (69 lb-ft)} \end{aligned} \quad (34b)$$

(5) Determine the load ratio for Case 1 and Task 1:

$$\text{Load ratio} = \frac{\text{Max. traction torque Case 1}}{\text{Max. traction torque Task 1}} = \frac{93}{199} = 0.467 \quad (35)$$

(6) Since the toroidal variable ratio drive has a load capability that varies to about the 2.8th power of the basic pitch diameter for similar life with all other factors equal, the effective change in the toroidal pitch diameter is:

$$(\text{Load ratio})^{1/2.8} = (0.467)^{1/2.8} = 0.762 \quad (36)$$

(7) The Case 1 toroidal drive pitch diameter would therefore be:

$$\begin{aligned} \text{Case 1 pitch dia} &= \text{Task 1 pitch dia} \times 0.762 \\ &= 112 \times 0.762 \\ &= 86 \text{ mm (3.4 in.)} \end{aligned}$$

With this smaller size toroidal unit, the rolling speed would also be reduced. Some additional reduction in drive size could be derived by decreasing the input reduction ratio to increase the drive running speed. For this preliminary analysis, it is not necessary to delve in depth into this speed effect, as maximum rotational speeds, gear pitch line speeds, permissible gear sizes, bearing speeds, and the cost effects of using bearing speeds above Grade 3 bearings would all need to be considered. The drive size reduction because of speed effects is minimal compared to the above size change, and the slightly reduced rolling speeds will not adversely affect the sizing.

Case 2.--Vehicle weight is increased to 10 000 kg (22 000lb), and the maximum CVT output torque is increased to 2600 N-m (1900lb-ft). All other vehicle specifications from Task 1 apply.

By using the same logic of scalability as in Case 1 above, this 2600 N-m (1900lb-ft) CVT would require a 201 mm (8.25 in.) pitch diameter. With the same gear set combination as used in the optimized design configuration of Task 1, the maximum rolling speed will be over 126 m/s (415 ft/s), which is considerably above the tested limits. This design is, therefore, not acceptable without additional test data.

By selecting new gear ratios, an optimized configuration was evolved to reduce the rolling speeds. Reducing the rolling speeds increased the torque load that the traction drive must handle. A tradeoff between speed and torque was performed with the following results:

Input reduction:	4.667:1
Traction drive input speed:	3000 to 6000 rpm
Traction drive ratio range:	2.75:1 to 0.35:1

Traction drive output speed:

14 000 rpm flywheel: 1090 to 8571 rpm

21 000 rpm flywheel: 1636 to 9089 rpm

28 000 rpm flywheel: 2182 to 9640 rpm

Jackshaft reduction: 1.12:1

Epicyclic gearset: Ring/sun = 3.05

CVT output speed: 0 to 5000 rpm

The maximum torque load on the traction drive with this gear combination is:

$$\text{Max. CVT torque} \times \frac{\text{RTS}}{\text{RTS} + 1} \times \frac{1}{1.12} \quad (37)$$

$$2600 \text{ N-m} \times .753 \times \frac{1}{1.12} = 1748 \text{ N-m (1289 lb-ft)}$$

The largest known successful toroidal traction drive of this type was built by General Motors. The transmission was designed and tested for 1085 N-m (800 lb-ft) of torque in a turbine-powered bus. It had a 203 mm (8.0 in.) pitch diameter, dual-cavity toroidal drive.

The Case 2 drive would be 240 mm (9.45 in.) in pitch diameter.

$$\begin{aligned} \text{Diameter} &= 200 \text{ mm} \times \left[\frac{1748 \text{ N-m}}{1085 \text{ N-m}} \right]^{1/2.8} \quad (38) \\ &= 25.4 \text{ mm (9.45 in.)} \end{aligned}$$

Maximum rolling speed will occur at a flywheel speed of 28 000 rpm and a CVT output speed of 5000 rpm. Under this condition, the toroidal drive will be at a 0.622:1 ratio.

$$\text{Ratio} = \frac{6000 \text{ rpm in}}{9640 \text{ rpm out}} = 0.622:1 \quad (39)$$

The input disc contact radius for this ratio is:

$$\begin{aligned} R_c &= \frac{\text{Toroidal dia}}{1 + \text{Ratio}} = \frac{240}{1.622} \quad (40) \\ &= 148 \text{ mm (5.82 in.)} \end{aligned}$$

With a 28 000 rpm flywheel and a 5000 rpm output speed, this drive will have a rolling speed of 93 m/s (305 ft/s), which is slightly beyond the maximum

known tested traction rolling speed of 81 m/s (268 ft/s). There is no reason to expect that this rolling speed will present a problem, but test data should be obtained before the design is finalized.

Case 2--alternate.--For this heavy vehicle there are several alternate means for accomplishing a solution besides direct scaling up of the optimized CVT from the lighter vehicle.

One approach would be to reduce the maximum CVT output speed and use a different rear axle ratio to make up the difference. A reduced output speed would allow a broader choice in reduction ratios and in recycled power from the epicyclic gearset.

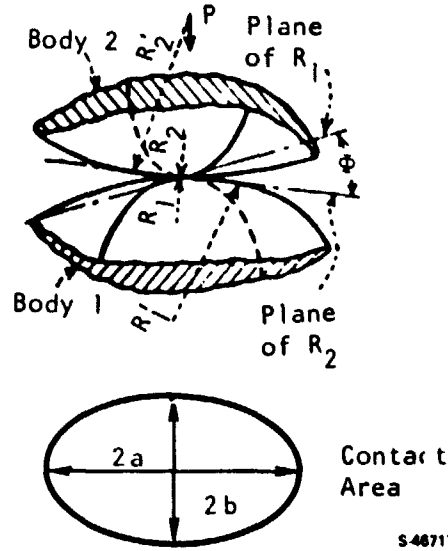
Another approach would be to use two smaller CVT's in parallel. The load type, power roller steering allows multiple drives to be operated in parallel from a single control system with all units equally sharing the load. This configuration would also allow the elimination of the differential, since each CVT would drive one rear wheel.

Finally, a multispeed, or shifted, CVT configuration could be considered for this heavy vehicle. The added complexity of synchronizing the shift points would require substantiation of the technology involved prior to a design finalization. The heavy vehicle could benefit substantially from the reduction in transmission losses associated with the shifted CVT configuration.

APPENDIX A

DETERMINATION OF CONTACT AREA DIMENSIONS

A general case of two bodies in contact is the following:



At the point of contact minimum and maximum radii of curvature are R_1 and R_1' for Body 1, R_2 and R_2' for Body 2. Then $1/R_1$ and $1/R_1'$ are principal curvatures of Body 1, and $1/R_2$ and $1/R_2'$ of Body 2, and in each body the principal curvatures are mutually perpendicular. Then:

$$\text{Max. } s_c = \frac{1.5 P}{\pi ab} \quad (41)$$

$$2a = \alpha \sqrt[3]{\frac{P\delta}{K}} \quad (42)$$

$$2b = \beta \sqrt[3]{\frac{P\delta}{K}} \quad (43)$$

$$y = \lambda \sqrt[3]{\frac{P^2}{K^2\delta}} \quad (44)$$

where

$$\delta = \frac{4}{\frac{1}{R_1} + \frac{1}{R_2} + \frac{1}{R_1'} + \frac{1}{R_2'}} \quad (45)$$

and

$$K = \frac{8}{3} \frac{E_1 E_2}{E_2 (1 - \nu_1^2) + E_1 (1 - \nu_2^2)}$$

α and β are given by the following table, where

$$\theta = \arccos \frac{1}{4} \delta \sqrt{\left(\frac{1}{R_1} - \frac{1}{R_{1'}}\right)^2 + \left(\frac{1}{R_2} - \frac{1}{R_{2'}}\right)^2 + 2\left(\frac{1}{R_1} - \frac{1}{R_{1'}}\right)\left(\frac{1}{R_2} - \frac{1}{R_{2'}}\right)} \quad (46)$$

		$\theta, \text{ deg}$															
		0	10	20	30	35	40	45	50	55	60	65	70	75	80	85	90
α	-	6.612	3.778	2.731	2.397	2.136	1.926	1.754	1.611	1.486	1.378	1.284	1.202	1.128	1.061	1.00	
β	0	0.319	0.408	0.493	0.530	0.567	0.604	0.641	0.678	0.717	0.759	0.802	0.846	0.893	0.944	1.00	
λ	-	0.851	1.220	1.453	1.550	1.637	1.709	1.772	1.828	1.875	1.912	1.944	1.967	1.985	1.996	2.00	

where

$R_1, R_{1'}, R_2,$ and $R_{2'}$ = mutually perpendicular radii of the curvatures of the two bodies

s_c = surface contact stress

P = total pressure

$2a$ = major axis

$2b$ = minor axis

y = deflection perpendicular to the contact area plane

E = modulus of elasticity

ν = Poisson's ratio

APPENDIX B

PARAMETRIC STUDY DATA

Data obtained during the parametric study are illustrated in figures 68 through 73 and summarized in tables 10 to 12. Typical plots of parametric study data were made to establish optimum geometric relationships.

These data were used in the selection of the toroid cavity geometry.

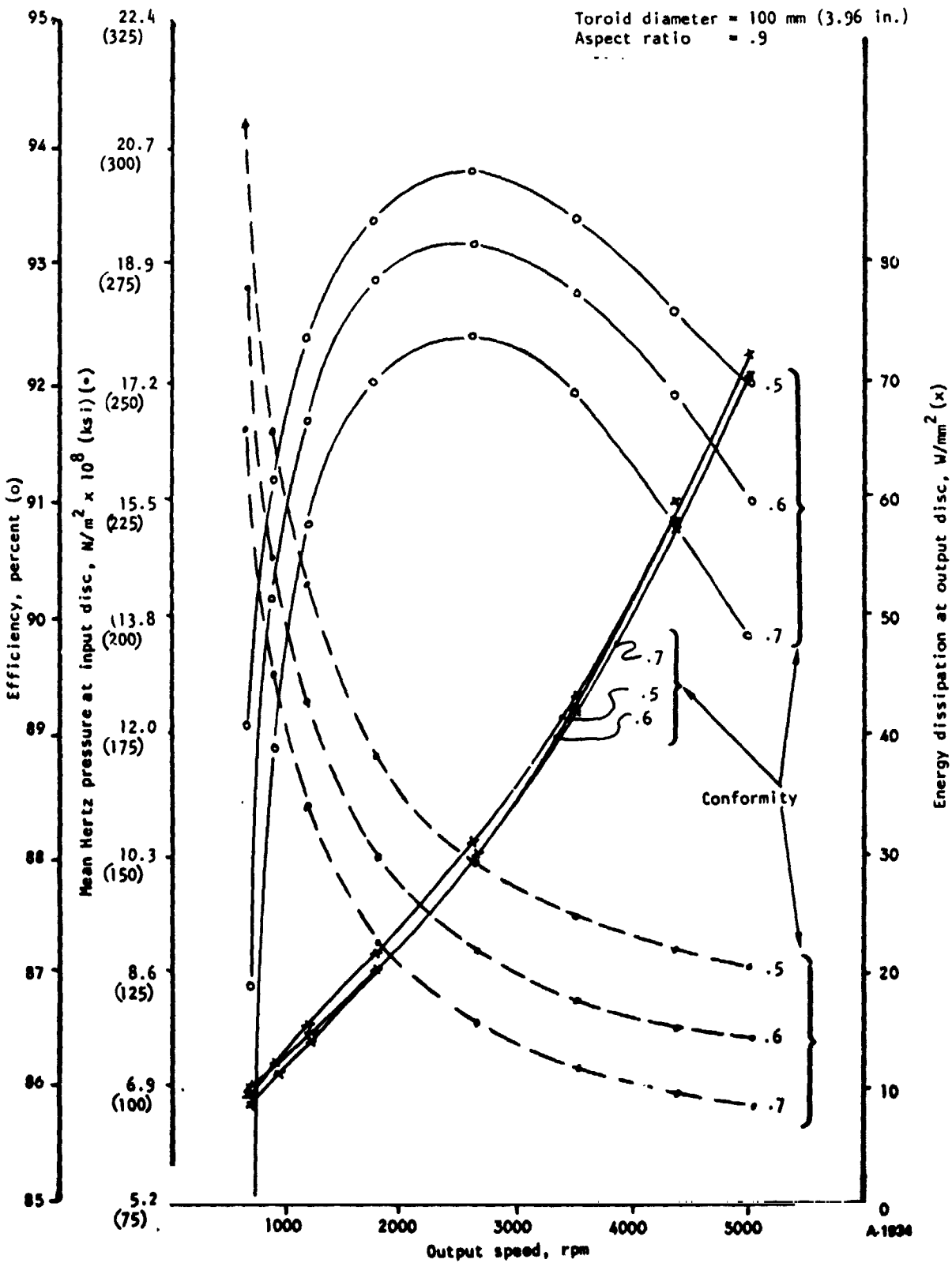


Figure 68.--Overall CVT efficiency, mean Hertz pressure, and energy dissipation vs output speed.

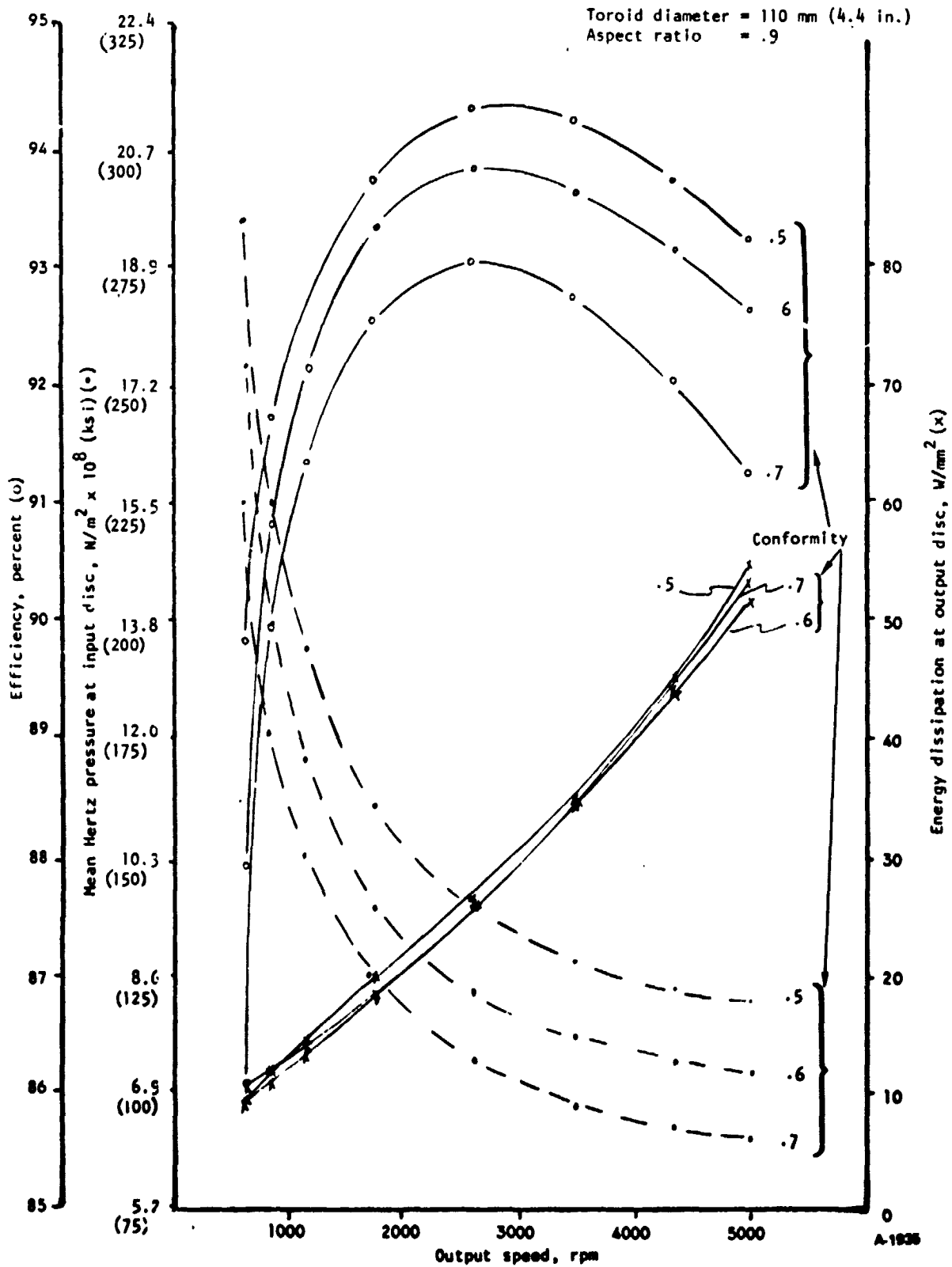


Figure 69.--Overall CVT efficiency, mean Hertz pressure, and energy dissipation vs output speed.

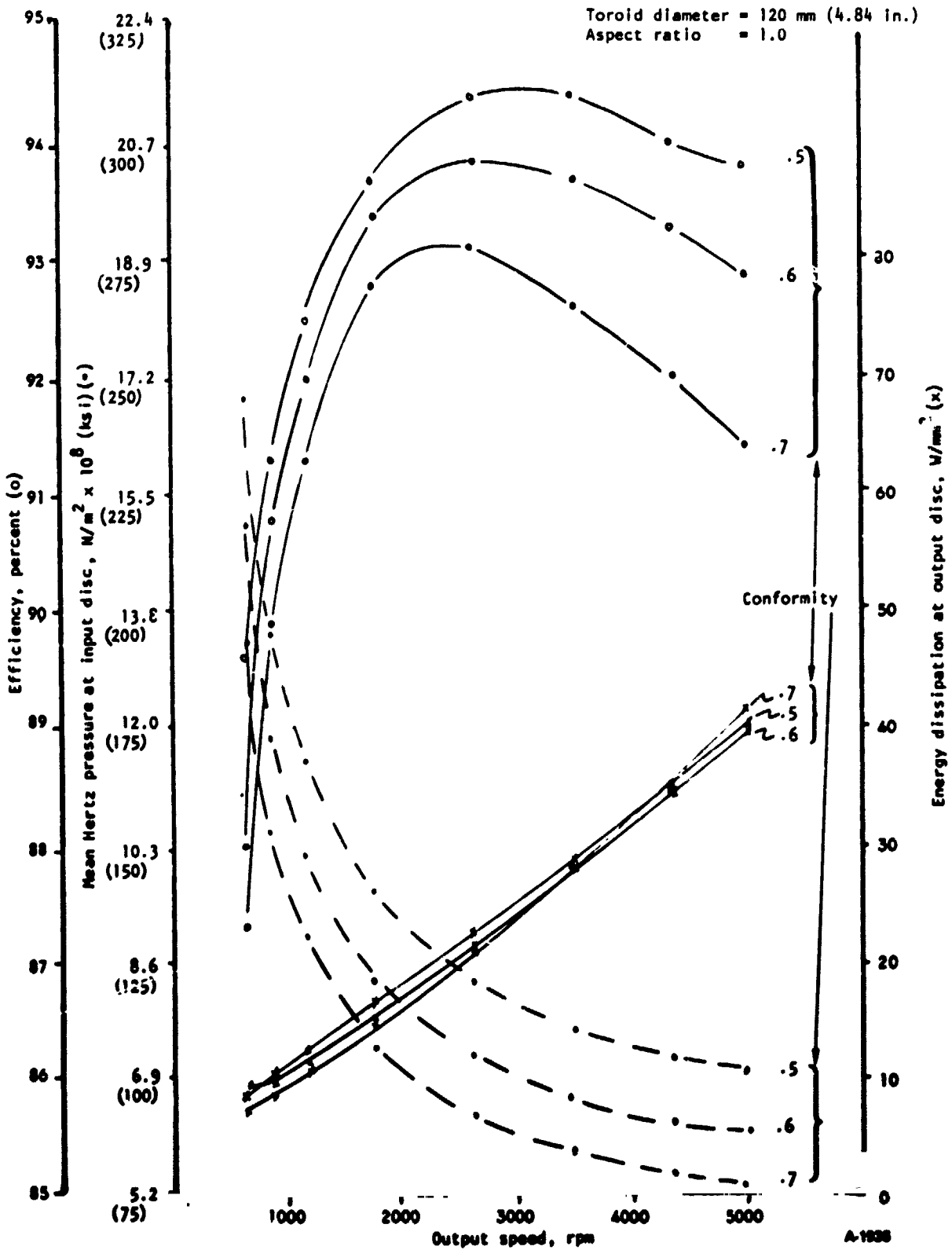


Figure 70.--Overall CVT efficiency, mean Hertz pressure, and energy dissipation vs output speed.

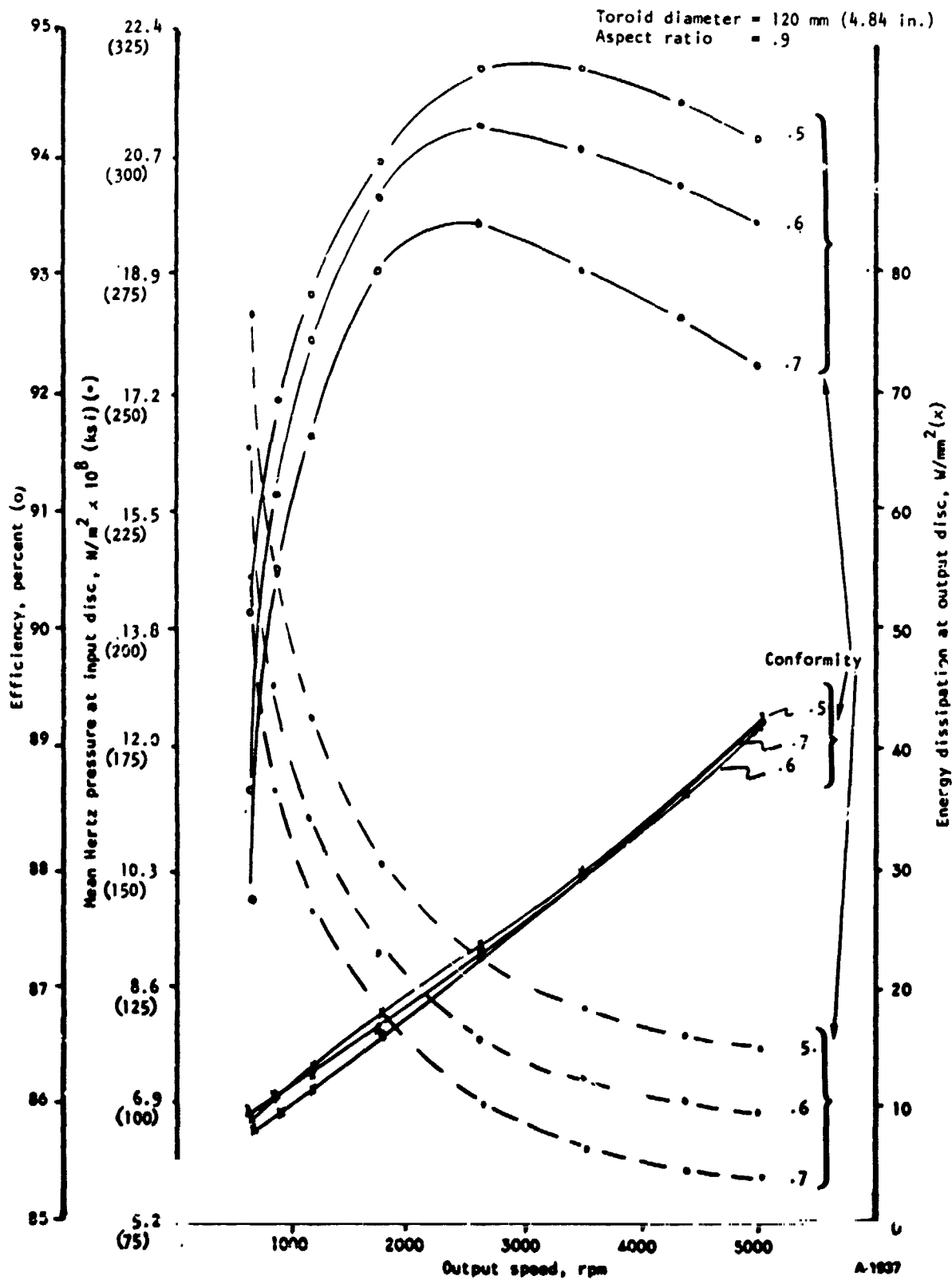


Figure 71.--Overall CVT efficiency, mean Hertz pressure, and energy dissipation vs output speed.

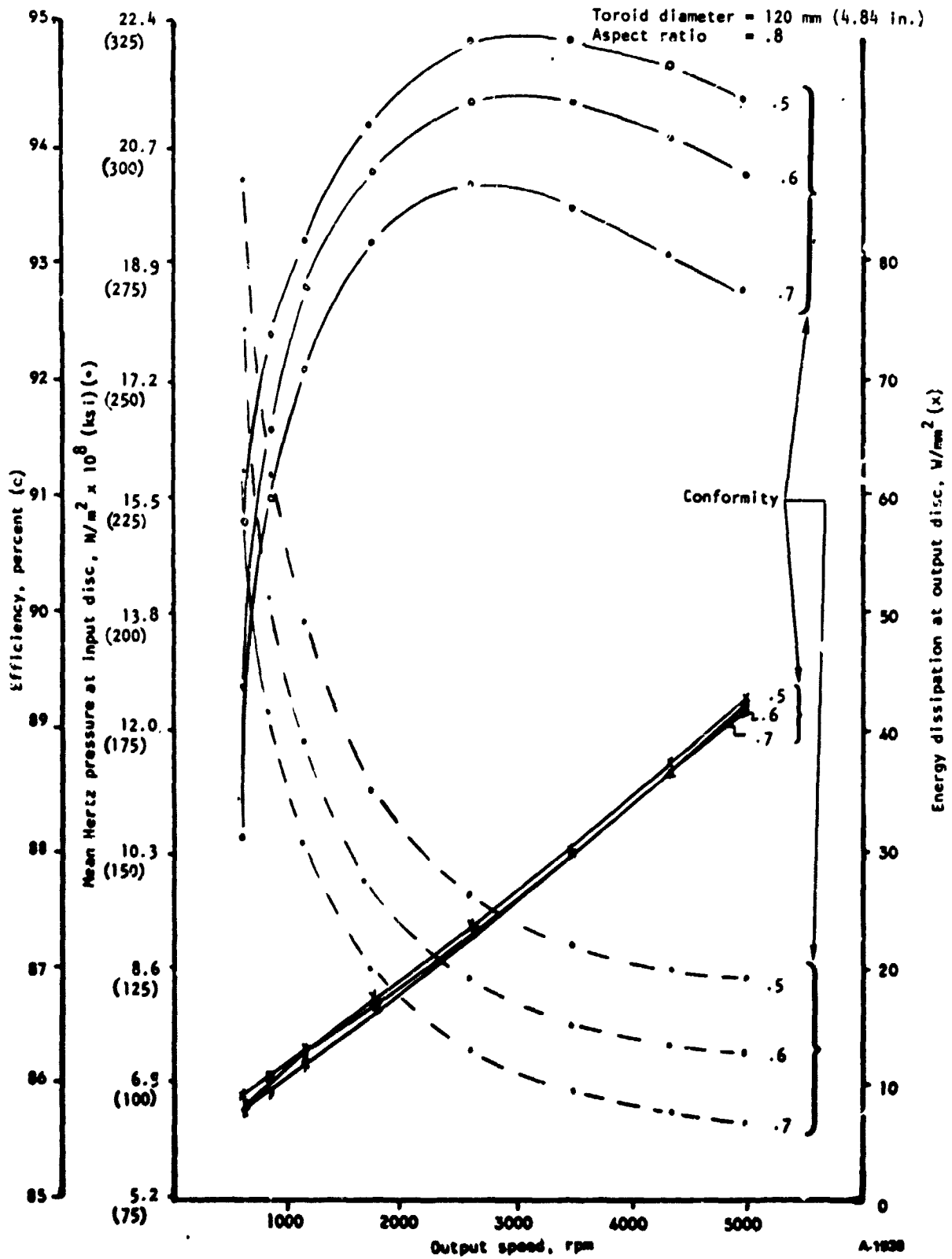


Figure 72.--Overall CVT efficiency, mean Hertz pressure, and energy dissipation vs output speed.

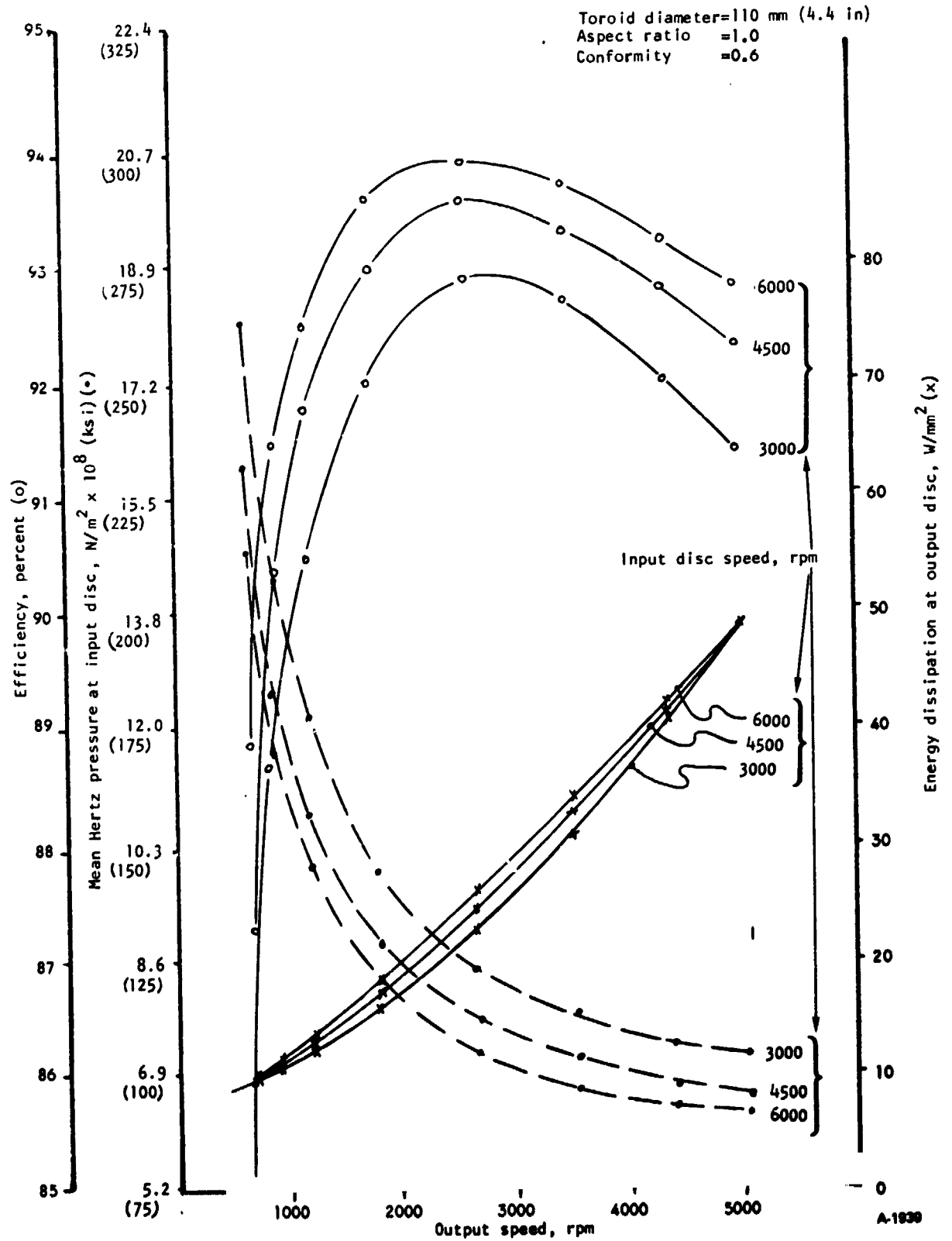


Figure 73.--Overall CVT efficiency, mean Hertz pressure, and energy dissipation vs output speed.

TABLE 10.--PERCENT CHANGE IN EFFICIENCY WITH CHANGE IN TOROID DIAMETER

Change in toroid diameter, mm (in.)	Aspect ratio	Conformity	Output speed, rpm (toroid cavity ratio)							
			625 (2.80:1)	875 (2.00:1)	1167 (1.50:1)	1750 (1.00:1)	2612 (0.67:1)	3500 (0.50:1)	4375 (0.40:1)	5000 (0.35:1)
			Change in efficiency, percent							
100 to 112 (3.96 to 4.40)	0.8	0.5	+0.5	+0.4	+0.4	+0.4	+0.5	+0.8	+1.1	+1.3
		0.6	+1.0	+0.7	+0.4	+0.7	+0.7	+1.1	+1.4	+1.5
		0.7	+2.0	+1.1	+0.7	+0.6	+0.7	+0.9	+1.5	+2.1
	0.9	0.5	+0.7	+0.5	+0.3	+0.3	+0.5	+0.8	+1.1	+1.2
		0.6	+1.0	+0.6	+0.4	+0.4	+0.6	+0.8	+1.2	+1.6
		0.7	+2.3	+1.0	+0.5	+0.5	+0.6	+0.8	+1.2	+1.4
1.0	0.5	+0.7	+0.4	+0.2	+0.2	+0.5	+0.7	+1.0	+1.3	
	0.6	+1.3	+0.6	+0.5	+0.4	+0.6	+0.6	+0.9	+1.1	
	0.7	+2.9	+0.8	+0.4	+0.6	+0.6	+0.5	+1.1	+1.4	
112 to 123 (4.40 to 4.84)	0.8	0.5	+0.4	+0.3	+0.1	+0.2	+0.4	+0.5	+0.7	+0.8
		0.6	+0.6	+0.4	+0.3	+0.3	+0.4	+0.6	+0.9	+1.2
		0.7	+1.3	+0.7	+0.4	+0.4	+0.5	+0.6	+0.7	+0.9
	0.9	0.5	+0.3	+0.2	+0.1	+0.2	+0.4	+0.5	+0.7	+0.9
		0.6	+0.7	+0.3	+0.3	+0.3	+0.4	+0.4	+0.6	+0.8
		0.7	+1.7	+0.6	+0.3	+0.5	+0.4	+0.3	+0.6	+1.0
1.0	0.5	+0.4	0	+0.2	+0.4	+0.3	+0.4	+0.4	+0.7	
	0.6	+0.7	+0.4	+0.2	+0.4	+0.3	+0.4	+0.5	+0.6	
	0.7	+1.2	+0.4	+0.4	+0.5	+0.4	+0.4	+0.5	+0.7	

TABLE 11.--PERCENT CHANGE IN HERTZ PRESSURE WITH CHANGE IN TOROID DIAMETER

Change in toroid diameter, mm (in.)	Aspect ratio	Conformity	Output speed, rpm (toroid cavity ratio,										
			625 (2.80:1)	875 (2.00:1)	1167 (1.50:1)	1750 (1.00:1)	2612 (0.67:1)	3500 (0.50:1)	4375 (0.40:1)	5000 (0.35:1)			
100 to 112 (3.96 to 4.40)	0.8	0.5	-6.8	-6.7	-6.7	-6.7	-6.7	-6.7	-6.8	-6.8	-6.8	-6.8	
		0.6	-6.8	-6.6	-6.7	-6.8	-6.8	-6.8	-6.8	-6.8	-6.8	-6.8	-6.8
		0.7	-6.8	-6.5	-6.6	-6.7	-6.7	-6.7	-6.7	-6.7	-6.8	-6.8	-6.8
	0.9	0.5	-6.8	-6.6	-6.7	-6.7	-6.7	-6.7	-6.7	-6.8	-6.8	-6.8	-6.8
		0.6	-6.8	-6.6	-6.7	-6.7	-6.8	-6.8	-6.8	-6.8	-6.8	-6.8	-6.8
		0.7	-6.8	-6.6	-6.7	-6.7	-6.8	-6.8	-6.8	-6.8	-6.8	-6.8	-6.8
	1.0	0.5	-6.8	-6.6	-6.7	-6.7	-6.8	-6.8	-6.8	-6.8	-6.8	-6.8	-6.8
		0.6	-6.8	-6.6	-6.7	-6.8	-6.8	-6.8	-6.8	-6.8	-6.8	-6.8	-6.8
		0.7	-6.8	-6.7	-6.8	-6.7	-6.8	-6.8	-6.8	-6.8	-6.8	-6.8	-6.8
112 to 123 (4.40 to 4.84)	0.8	0.5	-6.2	-6.1	-6.1	-6.1	-6.1	-6.1	-6.1	-6.1	-6.1	-6.1	
		0.6	-6.1	-6.0	-6.1	-6.2	-6.2	-6.1	-6.2	-6.2	-6.2	-6.2	
		0.7	-6.1	-6.0	-6.1	-6.1	-6.1	-6.1	-6.1	-6.2	-6.2	-6.2	
	0.9	0.5	-6.2	-6.0	-6.1	-6.1	-6.1	-6.1	-6.1	-6.2	-6.2	-6.2	-6.2
		0.6	-6.2	-6.1	-6.1	-6.1	-6.1	-6.1	-6.2	-6.2	-6.2	-6.2	
		0.7	-6.2	-6.1	-6.1	-6.1	-6.1	-6.1	-6.2	-6.2	-6.2	-6.2	
	1.0	0.5	-6.1	-6.1	-6.1	-6.1	-6.1	-6.1	-6.1	-6.1	-6.2	-6.2	
		0.6	-6.2	-6.1	-6.1	-6.1	-6.1	-6.1	-6.2	-6.2	-6.2	-6.2	
		0.7	-6.2	-6.1	-6.1	-6.1	-6.1	-6.1	-6.2	-6.2	-6.2	-6.2	

TABLE 12.---PERCENT CHANGE IN ENERGY DISSIPATION WITH CHANGE IN TOROID DIAMETER

Change in toroid diameter, mm (in.)	Aspect ratio	Conformity	Output speed, rpm (toroid cavity ratio)							
			625 (2.80:1)	875 (2.00:1)	1167 (1.50:1)	1750 (1.00:1)	2612 (0.67:1)	3500 (0.50:1)	4375 (0.40:1)	5000 (0.35:1)
100 to 112 (3.96 to 4.40)	0.8	0.5	4.3	6.5	10.1	11.6	16.3	20.8	24.1	25.6
		0.6	4.0	6.5	8.7	12.7	18.5	24.8	27.6	27.0
		0.7	3.5	8.8	9.8	13.3	17.3	21.9	26.8	31.3
	0.9	0.5	5.3	8.1	9.7	10.6	15.8	20.3	24.0	24.6
		0.6	2.9	6.5	10.0	11.8	15.2	19.8	25.6	29.2
		0.7	2.3	11.4	10.7	12.4	15.0	19.4	24.3	25.0
	1.0	0.5	5.2	8.1	9.2	9.9	13.9	17.9	23.8	26.6
		0.6	4.7	8.9	12.8	11.7	14.9	17.5	21.4	23.4
		0.7	9.0	10.8	12.4	12.9	12.9	14.7	22.1	24.6
112 to 123 (4.40 to 4.84)	0.8	0.5	6.7	6.9	8.4	10.1	13.2	16.6	19.0	21.0
		0.6	4.2	6.9	8.0	10.3	13.8	17.2	22.8	25.3
		0.7	3.6	10.6	10.1	10.9	13.4	16.2	19.9	21.7
	0.9	0.5	4.4	7.0	7.9	9.8	11.5	15.7	19.6	22.7
		0.6	5.0	8.6	11.1	11.1	12.9	15.0	17.8	20.1
		0.7	10.6	10.9	12.0	11.9	11.7	13.1	17.8	21.0
	1.0	0.5	5.4	6.2	8.7	11.6	11.4	13.6	16.2	19.8
		0.6	3.9	12.4	10.8	11.5	11.8	13.5	16.0	18.3
		0.7	9.9	13.1	12.5	11.8	12.8	13.0	15.1	18.4

APPENDIX C
WEIGHT CALCULATIONS

This appendix contains the weight calculation sheets for the CVT shown in figure 74, including:

- (1) Toroid assembly
- (2) Gears and shafts
- (3) Housing and covers

WEIGHT CALCULATION SHEET

DRAWING NO.	DESCRIPTION	MAT'L	GAGE	NO. REQ	CALCULATIONS	WEIGHT	STATUS
(72)	COVER - SEAL	AL		1	$(3.75 \times 3.75 \times .28) - (3.398 \times .12)$ $+ (4.0 \times .30 \times .15) + (.46 \times .46 \times .55)$ $+ (\pi \times 1.65 \times .38 \times .4) / (.100)$.46	
(73)	HOUSINGS - OUTPUT			1	$(14.40 \times 5.10 \times .18) + (\pi \times 2.90 \times .88 \times .80)$ $+ (\pi \times 2.60 \times 1.25 \times .5) + (2.80 \times 4.0 \times .18)$ $+ (21.30 \times 1.60 \times .2) + (29.22 \times 2 \times .5)$ $+ (1.60 \times 8.8 \times .2) + (37.20 \times .75 \times .3) / (.10)$	5.32	
(74)	WEB - OUTPUT			1	$(29.22 \times .5 \times .20) + (8.0 \times 8.2 \times .2)$ $+ (10.20 \times .75 \times .35) + (30.9 \times .75 \times .35)$ $+ (\pi \times 2.30 \times .50 \times .22) + (\pi \times 2.75 \times .4 \times .30)$ $- (4.714 \times .2) - (3.464 \times .2) - (1.65 \times 2 \times 3)$ $- (1.10 \times 2 \times 3) / (.100)$	2.54	
(75)	HOUSING			1	$(7.50 \times 29.0 \times .20) + (24.90 \times 2.4 \times .20)$ $+ (16.30 \times 6.6 \times .20) + (4.40 \times 6.40 \times 2 \times 2)$ $+ (14.5 \times 8.8 \times .4 \times .2) / (.100)$	9.84	
(76)	WEB - INPUT			1	$(10.40 \times 4.0 \times 8.80) - (8.85 \times 8.0 \times .10)$ $- (3.142 \times .25) - (3.464 \times .25) - (.442 \times .25)$ $- (4.0 \times 2.60 \times .25) / (.100)$	2.56	
(77)	HOUSING - INPUT			1	$(23.10 \times .50 \times .25) + (3.40 \times 8.0 \times .20)$ $+ (6.20 \times 3.30 \times .2 \times 2) + (4.5 \times 8.0 \times .2)$ $+ (\pi \times 2.20 \times 1.1 \times .4) + (\pi \times 2.80 \times 1.0 \times 1.1) / (.10)$	3.64	
(78)	COVER - SEAL			1	SIMILAR TO ITEM 72	.50	
(81)	HOUSING - PISTON			4	$(12.57 \times 3) + (\pi \times 2.9 \times .65 \times .4) + (1.25 \times \pi^3) / (10 \times 4)$	2.80	
	MISC					1.34	
DATE	CUSTOMER	APPLICATION		TOTAL WEIGHT - DRY		LBS.	
12-12-77				29.00			
PROJ ENGR.	TITLE			TOTAL WEIGHT - WET		LBS.	
	Housings & Covers						
CALC. BY				NEXT ASSY.		PAGE	OF
C.P. GUERRERO				CHANGES		DWG. NO.	1

FORM 0108

WEIGHT CALCULATION SHEET

DRAWING NO.	DESCRIPTION	MAT'L	GAGE	NO. REQ	CALCULATIONS	WEIGHT	STATUS
(6)	BEARING	STL		1	$(\pi 1.55 \times .54 \times .60 \times .75) \times (.283)$.33	
(7)	JACKSHAFT			1	$[(5.726 \times .30) + (.785 \times 10.0)] \times (.283)$	2.71	
(8)	SPACER			1	$(\pi 1.10 \times 6.22 \times .10 \times .283)$.61	
(9)	SPACER			1	$(\pi 1.20 \times .18 \times .20 \times .283)$.04	
(10)	SPRING			1	$(\pi 1.70 \times .62 \times .10 \times .283)$.09	
(11)	FACE - CLUTCH & BALL			1	$(\pi 2.0 \times .85 \times .30 \times .283)$.45	
(12)	FRUSTION PAD			2	$(\pi 1.90 \times .85 \times .08 \times .100 \times 2)$.08	
(13)	GEAR			1	$[(\pi 4.64 \times .95 \times .26) + (\pi 3.36 \times .38 \times .24) + (\pi 4.0 \times .38 \times .24) + (\pi 4.68 \times .48 \times .25)] \times (.283)$	2.12	
(14)	GEAR & KEY			1	$[(\pi 1.26 \times .42 \times .25) + (\pi 1.20 \times .30 \times .18) + (\pi 3.30 \times 2.25 \times .30) + (\pi 5.90 \times .52 \times .32)] \times (.283)$	3.03	
(16)	BEARING			1	$(\pi 1.52 \times .52 \times .56 \times .75 \times .283)$.30	
(17)	LOCK NUT & SPACER			1	$(\pi 1.15 \times .45 \times .14 \times .283)$.06	
(18)	BEARING			4	$(.196 \times .50 \times .283 \times 4)$.11	
(19)	RETAINER	BRONZE		1	$[(\pi 2.64 \times 1.06) - (.196 \times 4)] \times (.32 \times .320)$.82	
(20)	LOADING CAM			1	$(\pi 2.60 \times .70 \times .3 \times .283)$.49	
(21)	GEAR	STL		1	$[(\pi 1.70 \times .30 \times .12) + (\pi 2.32 \times .78 \times .65) + (\pi 2.25 \times .62 \times .58) + (\pi 1.82 \times 1.06)] \times (.283)$	1.83	
(22)	BUSHINGS			2	$(\pi 1.64 \times .50 \times .06 \times .320 \times 2)$.10	
(23)	BEARING			1	$(\pi 3.20 \times .38 \times .48 \times .75 \times .283)$.39	
(24)	"			1	$(\pi 1.32 \times .38 \times .10 \times .75 \times .283)$.03	
(25)	SLEEVE			1	$(\pi 1.40 \times 4.88 \times .15 \times .283)$.91	
(26)	SPRING			1	$(\pi 1.50 \times .50 \times .10 \times .283)$.07	

DATE	12-12-79	CUSTOMER	APPLICATION	TOTAL WEIGHT - DRY	LBS.
PROJ. ENGR.		TITLE	GEARING & SHAFTS	TOTAL WEIGHT - WET	LBS.
CALC. BY	C. P. GUERRERO			NEXT ASSY.	PAGE / OF 4
				CHANGES	DWG. NO.

WEIGHT CALCULATION SHEET

DRAWING NO.	DESCRIPTION	MAT'L	GAGE	NO. REQ	CALCULATIONS	WEIGHT	STATUS
(27)	GEAR	STL		1	$(\pi \cdot 1.16 \times .5 \times .18) + (\pi \cdot 1.18 \times .25 \times .24) / (.283)$.16	
(28)	BEARINGS			1	$(\pi \cdot 1.55 \times .62 \times .25) + (\pi \cdot 1.90 \times .70 \times .20)$.35	
(29)	GEAR			1	$(\pi \cdot 1.15 \times .50 \times .18) + (\pi \cdot 1.90 \times .70 \times .20)$ $+ (\pi \cdot 2.76 \times .35 \times .25) / (.283)$.54	
(30)	LOCK NUT			1	$(\pi \cdot 1.10 \times .50 \times .20) / (.283)$.10	
(31)	RING GEAR			1	$(\pi \cdot 3.25 \times .95 \times .2) + (\pi \cdot 3.3 \times .45 \times .15) / (.283)$.75	
(32)	GEAR + BRG - PLANET			4	$(\pi \cdot 9.0 \times .42 \times .14) + (\pi \cdot 6.8 \times .35 \times .2) / (.283) \times 4$.27	
(33)	SHAFT			4	$(\pi \cdot 1.13 \times .6 \times .159 \times .42) - (.028 \times .75) / (.283) \times 4$.13	
(34)	BRAKE BAND ASSY			1	$(.62") + (2.50") ACTUATION$	3.15	
(35)	BEARING	STL		2	$(\pi \cdot 1.32 \times .54 \times .54) / (.283) \times 2$.51	
(36)	SPACER			1	$(\pi \cdot 1.72 \times .10 \times .12) / (.283)$.18	
(37)	"			1	$(\pi \cdot 8.4 \times .10 \times .07) / (.283)$.05	
(38)	SLINGER			1	$(\pi \cdot 9.4 \times .15 \times .12) + (\pi \cdot 1.30 \times .25 \times .05) / (.283)$.03	
(39)	LOCK - SPIRAL			1	$(\pi \cdot 8.5 \times .18 \times .07) / (.283)$.01	
(40)	SWAP RINGS			1	$(\pi \cdot 2.0 \times .18 \times .05) / (.283)$.02	
(41)	SEAL ASSY	CARBON		1	$(\pi \cdot 1.10 \times .50 \times .35) / (.080)$.05	
(42)	SHAFT - INPUT	STL		1	$(.478 \times 4.78) + (.636 \times .5) + (.785 \times .65) / (.283)$.88	
(43)	PLANET CARRIER ASSY			1	$(\pi \cdot 2.0 \times .70 \times .15) + (2.70 \times .65 \times .15)$ $+ (\pi \cdot 2.58 \times .30 \times .2) + (\pi \cdot 3.68 \times .78 \times .18) / (.283)$	1.32	
(44)	BEARING			1	$(\pi \cdot 6.5 \times .75 \times .12) / (.283)$.04	
(45)	GEAR - IDLER			1	$(\pi \cdot 1.96 \times .95) + (.385 \times .06) + (.113) \times (.10)$ $+ (\pi \cdot 4.2 \times .32 \times .22) / (.283)$.18	
(45A)	THRUST WASHER			1	$(\pi \cdot 6.0 \times .10 \times .06) / (.283)$		
(45B)	SWAP RING			1	$(\pi \cdot 6.0 \times .10 \times .02) / (.283)$		

DATE	12-12-79	CUSTOMER	APPLICATION
PROJ. ENGR.		TITLE	GEARING & SHAFTS
CALC. BY	C.P. GUERRERO	TOTAL WEIGHT - DRY	LBS.
		TOTAL WEIGHT - WET	LBS.
		NEXT ASSY.	PAGE 2 OF 4
		CHANGES	DWG. NO.

WEIGHT CALCULATION SHEET

DRAWING NO.	DESCRIPTION	MAT'L	GAGE	NO. REQ	CALCULATIONS	WEIGHT	STATUS
46	Oil Pump	STL		1	$(4.524 \times 2.60 \times .283) \times (.6)$	2.00	
47	GEAR			1	$(7.548 \times .25 \times .283)$.53	
48	PAN			1	$(9.0 \times .90) + (1.70 \times 6.0) + (12.90 \times 3.40) + (2.45 \times 5.40) + (14.12 \times .90 \times 2) + (0.60 \times .90) \times (.063 \times .283)$	2.93	
49	GASKET	PHENOLIC		1	$(47.85 \times .20 \times .03 \times .065)$.07	
50	SNAP RING	STL		1	$(7.145 \times .14 \times .06 \times .283)$.01	
51	BUSHING	BRONZE		2	$(7.18 \times 1.0 \times .06 \times .370 \times 2)$.14	
52	SNAP RING	STL		4	$(7.62 \times .18 \times .04 \times .283 \times 4)$.02	
53	BEARING			1	$(7.192 \times .54 \times .55 \times .75 \times .283)$.38	
54	SHAFT			1	$(6.568 \times .65) + (.785 \times 2.20 \times (.985 \times 1.05) + (1.039 \times 0.48) + (1.327 \times 1.8) + (2.061 \times 1.8) + (1.220 \times 2.0) + (1.131 \times 1.14) + (.785 \times .90) \times (.283)$	5.41	
55	BEARING			2	$(7.168 \times .48 \times .5 \times .75 \times .283 \times 2)$.54	
56	GEAR			1	$(7.21 \times .06 \times .06) + (\pi \times 2.36 \times 1.20 \times .18)$		
				1	$(\pi \times 3.15 \times .56 \times .38) + (\pi \times 4.0 \times .62 \times .26)$		
57	RING GEAR			1	$(\pi \times 3.92 \times .18 \times .22) + (\pi \times 4.1 \times .4 \times .35) \times (.283)$	2.78	
58	SNAP RING			1	$(7.485 \times .94 \times .32) + (\pi \times 5 \times .38 \times .16) \times (.283)$	1.57	
59	" "			1	$(\pi \times 2.08 \times .18 \times .06 \times .283)$.02	
60	" "			1	$(\pi \times 1.30 \times .18 \times .06 \times .283)$.01	
61	BEARING			2	$(\pi \times 1.55 \times .52 \times .58 \times .75 \times .283 \times 2)$.62	
62	SPACER			1	$(\pi \times 1.92 \times 1.0 \times .12 \times .283)$.20	
				1	$(\pi \times 1.08 \times 1.0 \times .06 \times .283)$.06	

DATE	CUSTOMER	APPLICATION	TOTAL WEIGHT - DRY	LBS.
PROJ. ENGR.	TITLE		TOTAL WEIGHT - WET	LBS.
CALC. BY			NEXT ASSY. CHANGES	PAGE 3 OF 4 DWG. NO.

FORM 8788		WEIGHT CALCULATION SHEET						
DRAWING NO.	DESCRIPTION	MAT'L	GAGE	NO. REQ	CALCULATIONS	WEIGHT	STATUS	
(63)	SLINGER	STL		1	$(\pi \cdot 1.14 \cdot .15 \cdot .12) + (\pi \cdot 1.50 \cdot .2 \cdot .06) / (.283)$.03		
(64)	SNAP RING	"		1	$(\pi \cdot 1.12 \cdot .22 \cdot .07 \cdot .283)$.02		
(65)	OIL SEAL	CARBON		1	$(\pi \cdot 1.15 \cdot .28 \cdot .30 \cdot .080)$.02		
(66)	SHAFT OUTPUT	STL		1	$(.567 \cdot 1.95) + (.785 \cdot 1.10) + (.665 \cdot .06) + (.785 \cdot 1.32) + (.720 \cdot .25) - (.402 \cdot .25) - (.049 \cdot .12) / (.283)$	1.48		
(67)	CARRIER			1	$(.02 \cdot .57 \cdot .15) + (.30 \cdot 1.0 \cdot .15) - (.767 \cdot .15) - (.503 \cdot .3 \cdot .15) / (.283)$.52		
(68)	SHAFT-PLANET			3	$(\pi \cdot 2.65 \cdot 1.15 \cdot .15 \cdot .283 \cdot 3)$.30		
(69)	BEARING			3	$(\pi \cdot .94 \cdot .75 \cdot .12 \cdot .283 \cdot 3)$.17		
(70)	GEAR-PLANET			3	$(\pi \cdot 1.54 \cdot .45 \cdot .25 \cdot 4) + (\pi \cdot 1.18 \cdot .64 \cdot .12) / (.283 \cdot 3)$.70		
(71)	PLUG			3	$(.01 \cdot 3)$.03		
(72)	PIN-OIL FEED & O-RING	AL		2	$(.528 \cdot .22 \cdot 4) + (.113 \cdot .78) - (\pi \cdot .32 \cdot .7 \cdot .06) - (.018 \cdot 1.0) / (.100 \cdot 2)$.04		
(73)	O-RING	RUBBER		4	$(.001 \cdot 4)$	N		
(74)	SPIDER	AL		2	$(.478 \cdot 5.40) + (\pi \cdot 1.50 \cdot 1.0 \cdot .30) + (1.5 \cdot .38 \cdot .80 \cdot 4) - (.113 \cdot .48)$			
(75)	PIN	STL		2	$(.002 \cdot 4.0) - (.113 \cdot .62) / (.100 \cdot 2)$	1.09		
(76)	HOUSING-PISTON	AL		4	$(.503 \cdot .25) + (.113 \cdot 1.0) / (.283 \cdot 2) + (2.138 \cdot .75) - (.113 \cdot .35) - (.176 \cdot .18) - (.528 \cdot .22) / (.100 \cdot 4)$.57		
	MISC					2.31		
DATE	12-12-77	CUSTOMER	APPLICATION		TOTAL WEIGHT - DRY	LBS.		
PROJ. ENGR.		TITLE	SHAFTS & GEARS		TOTAL WEIGHT - WET	LBS.		
CALC. BY	C. P. GUERRERO	CHANGES				PAGE	4 OF 4	
						DWG. NO.		

FORM 1000

WEIGHT CALCULATION SHEET

BORING NO.	DESCRIPTION	MAT'L	QTY	NO. REQ	CALCULATIONS	WEIGHT	STATUS
(5)	PIN - PIVOT	STL		2	$(.196 \times 1.54) + (.442 \times .18) / (.283 \times 2)$.22	
(6)	BEARINGS			2	$(.785 \times .85) - (.196 \times .85) / (.283 \times 2)$.28	
(7)	BEARINGS			2	$(\pi \times 1.12 \times .75 \times .12 \times .75 \times .283 \times 2)$.13	
(8)	ROLLER			2	$(\pi \times 1.28 \times .75 \times .13) + (\pi \times 2.70 \times 1.20 \times .5) / (.283 \times 2)$	3.10	
(9)	TRUNION			2	$(.4 \times .5 \times 1.70 \times .50) + (\pi \times .80 \times 1.40 \times .14) + (\pi \times 1.42 \times 1.3 \times .55) + (\pi \times 1.30 \times .36 \times .16)$		
(10)	SWAP RIMS				$(.1 \times .50 \times .36 \times 1.16 \times 2) / (.283 \times 2)$	4.50	
(11)	BUSHINGS	BRONZE		4	$(\pi \times 2.3 \times 1.16 \times .06 \times .283 \times 4)$.05	
(12)	O-RINGS & CAP SEAL	CARBON		4	$(\pi \times 2.18 \times .54 \times .18 \times .320 \times 4)$.85	
(13)	CAM FOLLOWER	STL		4	$(\pi \times 1.90 \times 1.10 \times .08 \times .050 \times 4)$.01	
(14)	PIN - DOWEL	"		2	$(.75 \times .25 \times .25) - (.049 \times .25) / (.283 \times 4)$.04	
(15)	PISTON	AL		2	$(2 \times .31 \times .049 \times .283 \times 2)$.06	
(16)	PISTON	AL		2	$(\pi \times 1.90 \times .80 \times .30) + (3 \times .142 \times .42) + (\pi \times 1.80 \times .28 \times .20) - (\pi \times 1.30 \times .32 \times .24)$		
(17)	RACEWAY	STL		2	$(\pi \times 1.90 \times 1.18 \times .11) - (.049 \times .3) / (.283 \times 2)$.52	
(18)	BEARINGS	"		2	$(3 \times .142 \times .72) - (.1 \times .887 \times .25) - (\pi \times 1.9 \times .18 \times .11) + (.100 \times 2)$.34	
(19)	DISC - INPUT	"		2	$(2 \times .405 \times 1.10) + (.196 \times .10) + (.785 \times .05) / (.283 \times 2)$.17	
(20)	BEARINGS	"		2	$(\pi \times 1.32 \times .32 \times 1.10 \times .75 \times .283 \times 2)$.06	
(21)	DISC - INPUT	"		1	$(\pi \times 1.80 \times .60 \times .15) + (\pi \times 2.60 \times .53 \times .50) + (\pi \times 4 \times .20 \times 2.50 \times .47) + (\pi \times 4.32 \times .30 \times .18) + (\pi \times 7.20 \times 1.36 \times .50) / (.283)$	9.55	
"	SPLINE - INPUT DISC	"		1	$(\pi \times 1.50 \times 1.23 \times 2.0 \times .283)$.33	
DATE	12-12-77	CUSTOMER	APPLICATION		TOTAL WEIGHT - DRY	LBS.	
PROJ. ENGR.		TITLE	TOROID ASSY		TOTAL WEIGHT - WET	LBS.	
DRW. BY	C.P. GUERRELO				NET ASSEMBLY	PAGE 1 OF 2	
					CHANGES	DWG. NO.	

ORIGINAL PAGE IS OF POOR QUALITY

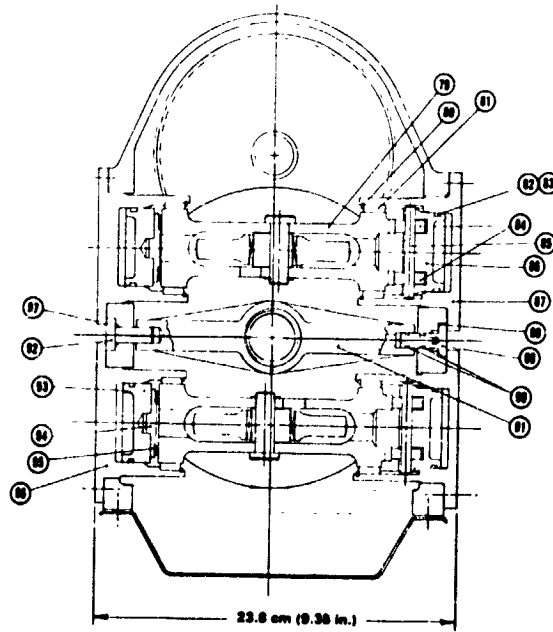
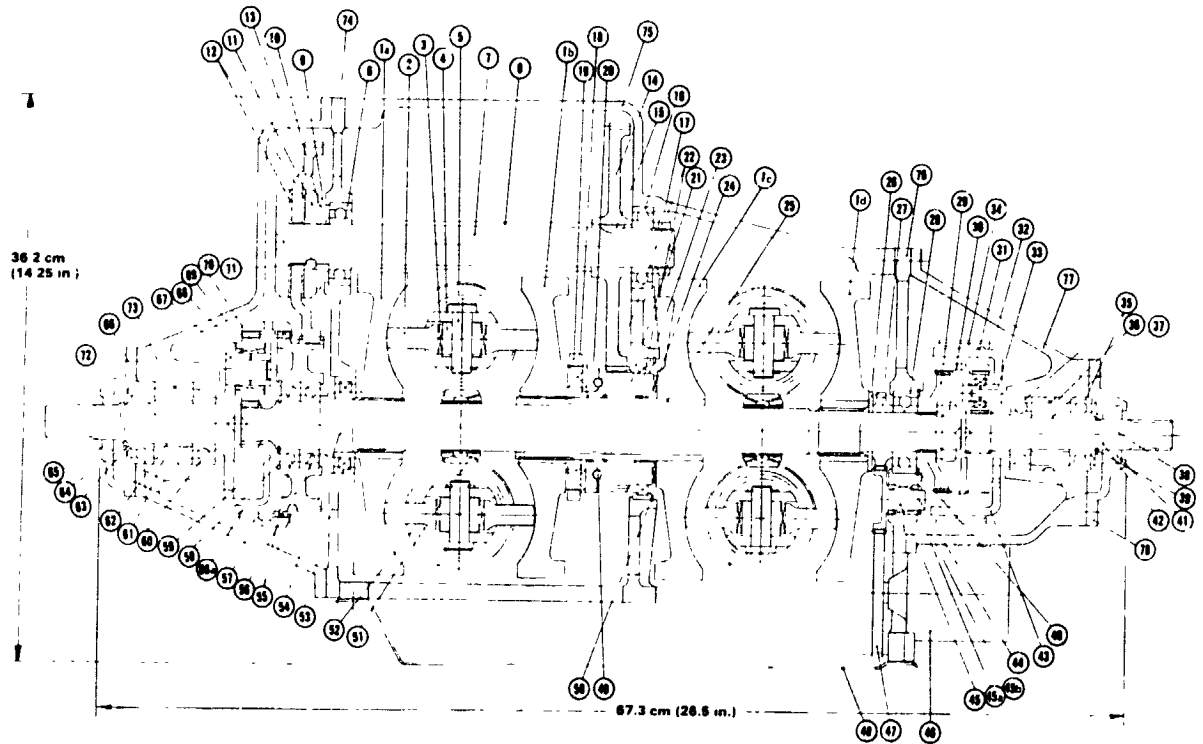
WEIGHT CALCULATION SHEET

DRAWING NO.	DESCRIPTION	MAT'L	GAGE	NO. REQ	CALCULATIONS	WEIGHT	STATUS
(8)	DISC - OUTPUT	STL		1	$(\pi 2.52 \times .70 \times .12) + (\pi 2.56 \times .57 \times .58)$ $+ (\pi 4.30 \times 2.46 \times .5) + (\pi 6.23 \times .35 \times .13)$ $+ (\pi 7.15 \times 1.22 \times .45) / (.283)$	9.48	
	SPRINE - OUTPUT DISC	"		1	$(\pi 1.68 \times 1.22 \times .10 \times .283)$.18	
	MISC TOROID ASSY					1.53	
						(31.40)	
(9)	DISC - INPUT	STL		1	$(\pi 1.85 \times .30 \times .15) + (\pi 1.75 \times .62 \times .18)$ $+ (\pi 4.10 \times 2.56 \times .45) + (\pi 2.60 \times .55 \times .50)$ $+ (\pi 6.3 \times .32 \times .2) + (\pi 7.15 \times 1.26 \times .45) / (.283)$	9.05	
	SPRINE - INPUT DISC	STL		1	$(\pi 1.36 \times 1.22 \times .20 \times .283)$.30	
(9)	DISC - OUTPUT	STL		1	$(\pi 1.25 \times .70 \times .15) + (\pi 2.60 \times .57 \times .56)$ $+ (\pi 4.4 \times 2.60 \times .46) + (\pi 1.10 \times .70 \times .14)$ $+ (\pi 6.40 \times .28 \times .16) + (\pi 2.15 \times 1.20 \times .45) / (.283)$	9.11	
	TOROIDAL ASSY				ITEMS PER SMT 1	10.33	
	MISC TOROID ASSY					1.51	
						(30.30)	
					TOTAL WEIGHT - DRY	61.70	LBS.
					TOTAL WEIGHT - WET		LBS.
DATE	CUSTOMER	APPLICATION		NEXT ASSY.		PAGE 2 OF 2	
12-12-79	TOROID ASSY			CHANGES		DWG. NO.	
PROJ. ENGR.							
CALC. BY							
C.P. GUERRERO							

APPENDIX D

CVT DRAWING AND PARTS LIST

This appendix presents a drawing of the CVT in figure 74 and lists its parts in table 13.



54792

Figure 74.--Continuously variable transmission cross section drawing.

TABLE 13.--CVT Parts List

Item	Quantity	Name	Material	Formed	Remarks
1a	1	Disc-input 1	52100 RC60-62	Close Die Forged	Sleeve brazed in during heat treatments with spline.
1b	1	Disc-output 1	52100 RC60-62	Close Die Forged	
1c	1	Disc-output 2	52100 RC60-62	Close Die Forged	
1d	1	Disc-input 2	52100 RC60-62	Close Die Forged	
2	4	Roller	52100 RC62-64	Close Die Forged	Torrington no. JH-1612
3	4	Bearing			
4	4	Excentric	52100 RC60-62	Machine from bar	Carburize 205 size
5	4	Pivot pin	1018/1020		
6	1	Bearing			Cold head formed and turned
7	1	Transfer shaft	4340	Tube	
8	1	Spacer	1018	Tube	Carburize Carburize
9	1	Spacer	1018	Tube	
10	1	Belleville spring			205 size 7/8 in. light series 1/2 in. by 1/2 in.
11	1	Face-clutch	1018	Stamped	
12	2	Friction pads			Carburize Carburize
13	1	Gear	8620		
14	1	Gear	8620		205 size 7/8 in. light series 1/2 in. by 1/2 in.
15	1	Woodruff key			
16	1	Bearing			Carburize
17	1	Lock nut			
18	4	Bearing rollers	52100	Stamped	Carburize
19	1	Retainer	Bronze	Contour, cut, and grind	
20	1	Loading cam	52100 RC60-62		Rollway No. 61913 L-U Torrington No. FNT-5070 Braze into disc 1c
21	1	Gear	8620	1 9/16 in. by	
22	2	Bushings	Bronze	1 11/16 in. by 1/2 in.	
23	1	Bearing			Spline and Grind OD
24	1	Bearing			
25	1	Sleeve	1018/1020 tube		
26	1	Belleville spring			

TAPLE 13.---(Continued)

Item	Quantity	Name	Material	Formed	Remarks
27	1	Gear	8620		Carburize
28	1	Bearing			205 size
29	1	Gear	8620		Carburize
30	1	Lock nut			7/8 in. heavy series
31	1	Ring gear	8620		Carburize
32	4	Planet gear	8620		Includes integral roller bearing
33	4	Shaft	52100 RC60-62	Turn from bar	
34	1	Brake band assembly			
35	2	Bearings			204, Grade 5 to 28 000 rpm
36	1	Spacer	1018 tube		
37	1	Spacer	1C.8 tube		
38	1	Slinger	1010	Stamped	
39	1	Spiral lock			20 mm shaft
40	1	Snap ring			IRR no. 3000-X206
41	1	Seal assembly	Carbon		
42	1	Shaft-input	8620		Carburize-integral spline and gear 2-piece
43	1	Planet carrier assembly	1040	Stamped and welded	
44	1	Bearing			Torrington no. JH-812
45	1	Gear-idler	8620		Carburize
45a	1	Thrust washer	1018/1020	Stamped and ground	Carburized
45b	1	Snap ring			IRR no. 3101-50
46	1	Oil pump assembly			Cerotor Type
47	1	Gear	8620		0.4 gal/1000 rpm
48	1	Pan	1010		Carburize
48a	1	Gasket		Stamped	
49	2	Ball 7/32 in. dia	52100		
50	1	Snap ring			IRR no. 3000-X354

TABLE 13.--(Continued)

Item	Quantity	Name	Material	Formed	Remarks
51	2	Bushing	Bronze	1 1/8 in. by 1 1/4 in. by 1 in.	IRR no. 3101-50 Rollway no. 61007 Nitrided Duplex angle contact, no. 7106, grade 5 to 17 000 rpm Carburized Carburized IRR no. 3000-X218 IRR no. 4100-118 205 size
52	4	Snap ring			
53	1	Bearing			
54	1	Shaft	4130	Roll formed	
55	2	Bearing			
56	1	Gear	8620		
57	1	Ring gear	8620		
58	1	Snap ring			
59	1	Snap ring			
60	2	Bearing			
61	1	Spacer	1018 tube		
62	1	Spacer	1018 tube	stamped	
63	1	Slinger	1010		
64	1	Snap ring			
65	1	Oil seal			
66	1	Shaft-output	4130	Cold head formed	IRR no. 3100-98
66a	1	Carrier	1040	Stamped	CR no. 8665 Nitrided
67	3	Shaft-planet	52100 RC60-62	Turned from bar	
68	3	Bearing			
69	3	Gear-planet	8620		Torrington no. FJ-2020 Carburize
70	3	Plug	101C	Stamped	
71	1	Ball 1/4 in. dia	52100		
72	1	Cover-seal	Al 356-T6	Cast	
73	1	Housing-output	Al 356-T6	Cast	
74	1	Web-output	Al 356-T6	Cast	
75	1	Housing	Al 356-T6	Cast	
76	1	Web-input	Al 356-T6	Cast	
77	1	Housing-input	Al 356-T6	Cast	
78	1	Cover-seal	Al 356-T6	Cast	
79	4	Trunion	1018/1020	Forged	Carburize IRR no. 4000-237
80	8	Snap ring			

TABLE 13.--(Continued)

Item	Quantity	Name	Material	Formed	Remarks
81	8	Bushing	Bronze	2 in. by 2 3/8 in. by 1/2 in.	
82	8	O-ring	Teflon		
83	8	Cap seal	1/4 in. by		
84	8	Cam follower	3/4 in. by 1/4 in.		
85	4	Dowel pin	1/4 in. by 2 5/16 in.		
86	4	Pistons	Al 7075-T6	Turned from bar	
87	4	Housing-piston	Al 356-T6	Cast	
88	2	O-ring			
89	2	Pin-oil feed	Al 7075-T6	Turned from bar	
90	4	O-ring			
91	2	Spider-oil feed	Al 356-T6	Cast	
92	2	Pin	Al 7075-T6	Turned from bar	
93	4	Pistons	Al 7075-T6	Turned from bar	
94	4	Raceway	Al 7075-T6	Turned from bar	
95	4	Bearing	1018/1020	Stamped	
96	4	Housing-piston	Al 356-T6	Cast	
97	2	O-ring			
	1	Hydraulic cylinder brake band control			Carburize Torrington NTA-162

REFERENCES

1. Roark, R.J.: Formulas for Stress and Strain. Fourth ed., McGraw-Hill Book Co., Inc., 1965.
2. Harris, T.A.: Rolling Bearing Analysis. John Wiley & Sons, Inc., 1966.
3. Dowson, D.; and Higginson, G.R.: Elasto-Hydrodynamic Lubrication. SI Edition, Pergamon Press, 1977.
4. Lundberg, G.; and Palmgren, A.: Dyanmic Capacity of Rolling Bearings: Acta Polytechnica, Mechanical Engineering Series, vol. 1, no. 3, 1947; and vol. 2, no. 4, 1952.
5. Anon.: Life Adjustment Factors for Ball and Roller Bearings. ASME, 1971.
6. Dudley, Darle W.: Gear Handbook. McGraw-Hill Book Co., Inc., 1962.
7. Anon: Estimated Weights and Manufacturing Costs, Automobiles, Vehicles, Systems, and Parts. Rath and Strong, Inc., Mar. 1976.

BIBLIOGRAPHY

- Daniels, B.K.: Non-Newtonian Thermo-Viscoelastic EHD Traction from Combined Slip and Spin. Presented at the American Society of Lubrication Engineers Conference, 1978.
- Dowson, D.; and Higginson, G.R.: Elasto-Hydrodynamic Lubrication. SI Edition, Pergamon Press, 1977.
- Fitzgibbons, R.G.; and Lindgren, L.H.: Estimated Weights and Manufacturing Costs: Automobiles, Vehicles, Systems and Parts. Prepared for U.S. Dept. of Transportation by Rath and Strong, Inc., Lexington, Mass., 1976.
- Gaggermeier, H.: Investigations of Tractive Force Transmission in Variable Traction Drives in the Area of Elastohydrodynamic Lubrication. Ph.D. Thesis, Technical University of Munich, 1977.
- Harris, T.A.: Rolling Bearing Analysis. John Wiley & Sons, Inc., 1966.
- Johnson, K.L.; and Cameron, R.: Shear Behavior of Elastohydrodynamic Oil Films at High Rolling Contact Pressures. Institute of Mechanical Engineers, Cambridge, England, 1967.
- Kannel, J.W.; and Walowit, J.A.: Simplified Analysis for Traction Between Rolling Sliding Elastohydrodynamic Contacts: Journal of Lubrication Technology. vol. 93, no. 1, Jan. 1971.
- Kraus, C.E.: Rolling Traction Analysis and Design. Excelsomatic, Inc., Austin, Texas, 1977.
- Liui, J.Y.; Tallian, T.E.; and McCool, J.I.: Dependence of Bearing Fatigue Life on Film Thickness to Surface Roughness Ratio. ASLE Preprint No. 74AM-7B-1, 1974.
- Lundberg, G.; and Palmgren, A.: Dynamic Capacity of Roller Bearings: Acta Polytechnica, Mechanical Engineering Series. vol. 1, no. 3, 1947; and vol. 2, no. 4, 1952.
- McCool, J.I.: Load Ratings and Fatigue Life Prediction for Ball and Roller Bearings: Journal of Lubrication Technology. vol. 92, no. 1, Jan. 1970.
- Palmgren, A.: Ball and Roller Bearing Engineering. SKF Industries, Inc., 1959.
- Plint, M.A.: Traction in Elastohydrodynamic Contacts. Ph.D. Thesis, University of London, 1967.
- Roark, R.J.: Formulas for Stress and Strain. Fourth ed., McGraw-Hill Book Co., Inc., 1965.
- Tevaarwerk, J.L.: Traction Drive Performance Prediction for the Johnson and Tevaarwerk Traction Model. NASA TP-1530, 1979.